ASD-TDR-63-604

WIDE BAND COHERENT LIGHT MODULATOR

TECHNICAL DOCUMENTARY REPORT No. ASD-TDR-63-604

SEPTEMBER 1963

AF AVIONICS LABORATORY
RESEARCH AND TECHNOLOGY DIVISION
AIR FORCE SYSTEMS COMMAND
WRIGHT-PATTERSON AIR FORCE BASE, OHIO

Project No. 4335, Task No. 433513

(Prepared under Contract No. AF 33(657)-9209
By Baird-Atomic, Inc., Cambridge, Massachusetts

NOTICES

When Government drawings, specifications, or other data are used for any purpose other than in connection with a definitely related Government procurement operation, the United States Government thereby incurs no responsibility nor any obligation whatsoever; and the fact that the Government may have formulated, furnished, or in any way supplied the said drawings, specifications, or other data, is not to be regarded by implication or otherwise as in any manner licensing the holder or any other person or corporation, or conveying any rights or permission to manufacture, use, or sell any patented invention that may in any way be related thereto.

Qualified requesters may obtain copies of this report from the Armed Services Technical Information Agency, (ASTIA), Arlington Hall Station, Arlington 12, Virginia.

This report has been released to the Office of Technical Services, U.S. Department of Commerce, Washington 25, D.C., in stock quantities for sale to the general public.

Copies of this report should not be returned to the Aeronautical Systems Division unless return is required by security considerations, contractual obligations, or notice on a specific document.

200 - October 1963 - 162-12-202

FOREWORD

This report was prepared by Baird-Atomic, Inc., Cambridge, Massachusetts on Air Force contract AF33(657)-9209 under Task No. 433513 of Project No. 4335, "Wide Band Coherent Light Modulator". The work was administered under the direction of AF Avionics Laboratory, Aeronautical Systems Division. Mr. Matulka was Project Engineer for the Laboratory.

The studies presented began in July 1962, were concluded in June 1963, and represent effort of the Research and Engineering Department of Baird-Atomic, Inc. Sture R. Blom was the engineer responsible for the research activity of Baird-Atomic, Inc.

Although the studies were a group effort, the chief contributors and their fields of interest were: V. del Piano and H. Raterink, optics; A. Quesada, mathematics; S. Marcus, electronics; and S. Schiller, mechanical design.

This report is the final report and it concludes the work on contract AF33(657)-9209. The contractor's report number is 4067/Final.

ABSTRACT

A thorough analysis is made of the theoretical factors affecting Fabry-Perot interferometers containing electro-optical crystals as phase-shifting elements and used as wideband modulators of coherent light. Bandwidth, modulation percentage and distortion, optical transmission, the effect of optical imperfections and modulator amplifier characteristics are discussed. Descriptions of two experimental modulators based on the results of this analysis are included. The design of a wideband distributed amplifier to drive the final modulator is discussed. The characteristics of this modulator were investigated at low frequencies with a mercury vapor light source and at frequencies up to 30 megacycles with a continuous gas laser operating at 6328Å. Results of final tests indicate a modulation sensitivity one third of that expected, but a flat pass band out to 30 megacycles. It is suggested that direct experimental verification of the transmission functions and maximum modulation frequencies be made.

RONALD G. STIMMEL
Actg. Assoc. Director/Electronic Warfare
AF Avionics Laboratory

TABLE OF CONTENTS

TABLE OF CONTENTS (Con't)

TABLE OF CONTENTS (con't)

TABLE OF CONTENTS (Con't)

LIST OF ILLUSTRATIONS

LIST OF ILLUSTRATIONS

INTRODUCTION

The design of wideband light modulators is complicated by two characteristics of electro-optic materials. These materials require high voltages to obtain the desired optical effects and they present essentially reactive loads to electronic driving circuits, since their equivalent shunt resistive component, at least up to high microwave frequencies, is negligibly small when compared to the reactive component.

To overcome the high voltages required, the interaction length between the applied electric fields and the optical electro-magnetic fields must be large. The modulator configuration studied during this program produced a large interaction length by the multi-reflection of a light ray within a resonant optical cavity, consisting of an electro-optic material partially filling the volume between two highly reflective surfaces. At each surface part of the light is transmitted while most is reflected back through the electro-optic material. This resonant cavity is essentially a Fabry-Perot interferometer in which the effective path length between the reflecting surfaces is varied by the change in the refractive index caused by the modulating voltage impressed on the electro-optic material in the cavity.

Manuscript released by the author 2 August 1963 for publication as an ASD Technical Documentary Report.

1.0 THEORETICAL CALCULATIONS

1.1 Basic Theory

1.1.1 Description of Fabry-Perot Interferometer

A Fabry-Perot Interferometer consists essentially of two plates of glass (Mirror 1 and Mirror 2 in figure 1-1) whose surfaces are flat to a small fraction of a wavelength of the light from source S. The inner surfaces of the plates are held accurately parallel a distance p apart and are coated on their inner surfaces to form mirrors with high reflectivity for the light from the source. When light from the source enters the interferometer at an angle ζ from the normal, a number of beams of light leave mirror 2 as the original beam is multiply reflected between the two inner surfaces. These transmitted beams have a definite phase relationship which depends on the optical path length np (where n is the index of refraction of the material between the mirrors), the wavelength of the light from the source S and the angle ζ.

For a given wavelength and mirror spacing there are a series of values of ϕ for which the transmitted beams add in phase and form an image at a point on a screen when focused by lens L_2. Since there is cylindrical symmetry about the optical axis, a ring is formed on the screen with radius r_1 corresponding to the angle ζ_1 for the first in-phase condition. In the same manner a series of sharp concentric rings are formed on the screen at radial distances r_2, r_3, ..., r_i corresponding to the series of values of ζ_i for the in-phase addition of the multiply reflected-transmitted beams.

1.1.2 Transmission of Light Through a Fabry-Perot Interferometer

It can be shown that the transmission of light through a lossless Fabry-Perot interferometer for equal to zero is:[1]

$$\frac{I_t}{I_i} = \frac{1}{1 + F \sin^2 \frac{\theta}{2}} \qquad (1.1\text{-}1)$$

[1] Jenkins and White, Fundamentals of Optics, Third Edition, McGraw-Hill, p. 274.

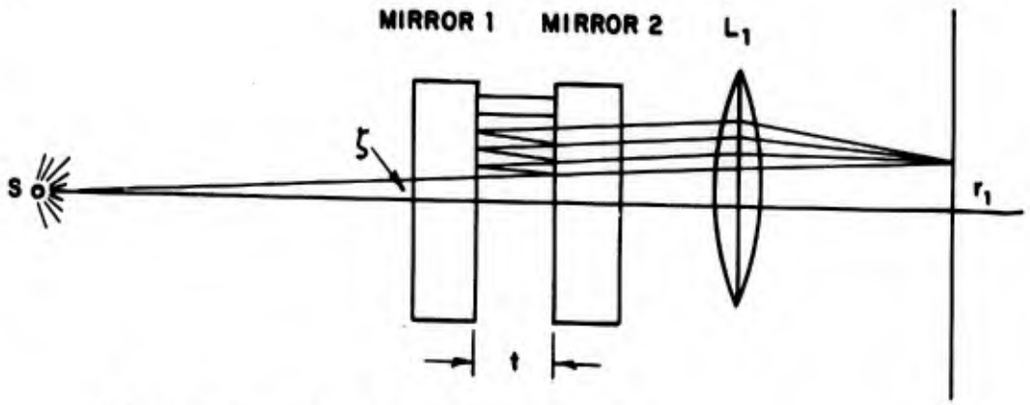

Figure 1-1. Fabry-Perot Interferometer

where:

$\frac{I_t}{I_i}$ = the ratio of the transmitted light intensity to the input light intensity

$F = \frac{4R}{(1 - R)^2}$ (the finesse)

R = reflectivity of the mirrors

θ = phase difference between consecutive reflections of a beam at a mirror.

The phase difference θ depends linearly on the equivalent optical path length p' between the mirrors and depends inversely on the wavelength λ. This is expressed as follows:

$$\theta = \frac{4\pi p'}{\lambda} \qquad (1.1\text{-}2)$$

The factor F is determined solely by the quality of the mirror surfaces and can be made independent of wavelength in the regions of interest. Some representative transmission curves are shown in figure 1-2. These curves show that for large values of F the transmission of a Fabry-Perot Interferometer is a very sensitive function of the phase angle.

In a practical Fabry-Perot interferometer, energy passing through the reflecting surfaces suffers an absorption loss. It can be shown that the ratio of transmitted light intensity I_t to input light intensity I_i is:

$$\frac{I_t}{I_i} = \frac{T^2}{(1 - R)^2} \left[\frac{1}{(1 + F \sin^2 \frac{\theta}{2})} \right]^2 \qquad (1.1\text{-}3)$$

where T is the transmission of either mirror, both being assumed identical. The absorption of the mirror is related to T and R by the energy balance equation,

$$1 = T + R + A$$

---

[2] Jenkins and White, Fundamentals of Optics, Third Edition, McGraw-Hill, p. 275

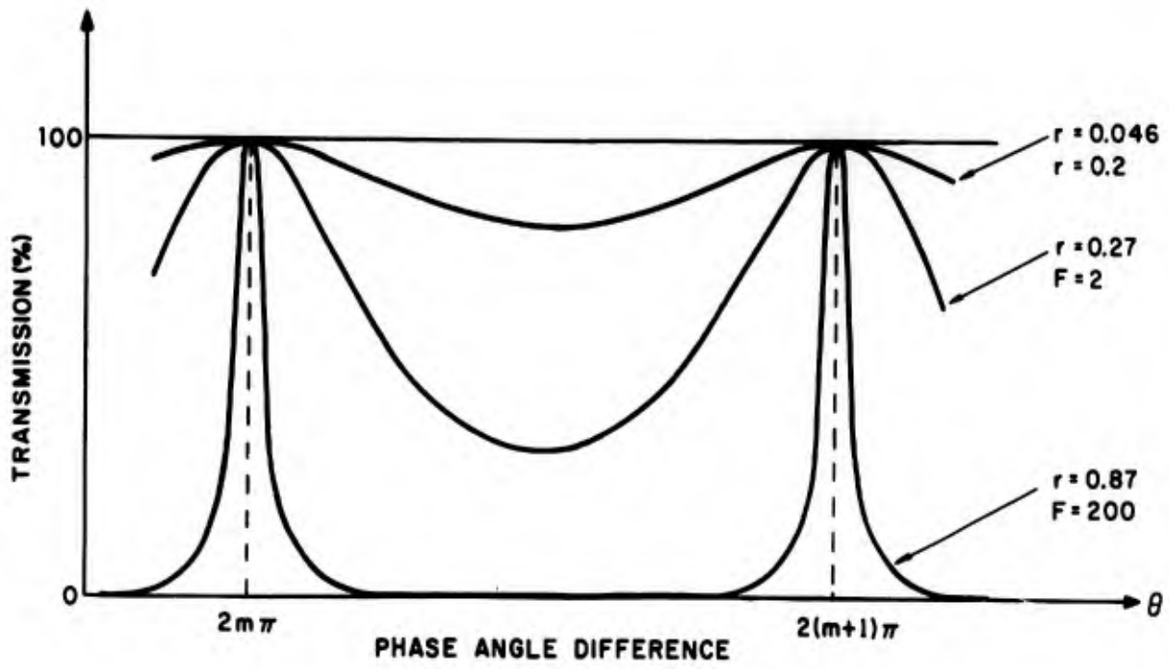

C381-06

Figure 1-2. Representative Interferometer Transmission Curves.

Using the above relation, the total transmission through a Fabry-Perot interferometer can be rewritten to include the effects of absorption:

$$\frac{I_t}{I_i} = \frac{T^2}{(T + A)^2} \quad \frac{}{(1 + F \sin^2 \frac{\theta}{2})} \tag{1.1-4}$$

The above relations for a "lossy" interferometer show that absorption in the reflecting surfaces does not change the shape of the transmission curve, and thus its sensitivity to phase angle, but merely reduces peak transmission. To achieve high modulation sensitivity it is desirable that the mirrors be highly reflective with resulting interferometer transmissions of 10% or less. Even small amounts of absorption in the mirrors or in the cavity can thus produce disproportionate changes in transmission through the device.

When absorption within the cavity is taken into account, it can be shown (see Appendix A) that the transmission of the interferometer can be written in the standard form by suitable definitions of terms:

$$\frac{I_t}{I_i} = \left(\frac{T'}{1 - R'} \right) \quad \frac{1}{(1 + F_{eff} \sin^2 \frac{\theta}{2})} \tag{1.1-5}$$

where T' and R' are now the transmission and reflectivity of the combination of the mirrors and the absorbing medium. The effective finesse F_{eff} is still defined by reflectivity:

$$F_{eff} = \frac{4 R'}{(1 - R'^2)^2}$$

Since the cavity absorption makes R' less than R, F_{eff} is always less than the value of F determined by measurement of the mirrors above. We can see that absorption within the cavity will affect the modulation sensitivity as well as the total transmission. Absorption in the cavity includes losses in the bulk material as well as scattering losses due to scratches, veils and so forth on the optical surfaces and reflection losses at the interfaces within the cavity. It is

assumed that reflections between surfaces inside the cavity do not contribute to the modulation but represent energy lost.

1.1.3 Electro-Optic Materials and Characteristics

When a class $\bar{4}2m$ crystal is inserted between the plates, the transmission becomes a function of the electro-optic properties of the crystal for a fixed wavelength of light. Assuming a beam of polarized light parallel to the Z-axis with the plane of polarization parallel to either the x' or y' induced axis, the expression for the magnitude of change in the index of refraction of a Z-cut crystal is:

$$\Delta n = \frac{1}{2} n_o^3 r_{63} E_Z \qquad (1.1\text{-}6)$$

where

n_o = the ordinary index of refraction of the crystal

E_Z = the electric field in the Z direction

r_{63} = a constant, describing Pockel's effect[1].

Note that the equivalent optical path length can be written as:

$$p' = n\,p$$

where

p = the spacing of the mirrors

n = the index of refraction of the material between the mirrors.

This information, together with equations 1.1-2 and 1.1-3, indicates that the application of an electric field to the crystal can produce large changes in the transmission through the Fabry-Perot structure.

---

[1] Billings, B.H., The Electro-Optic Effect in Uniaxial Crystals of the Type XH_2PO_4. I. Theoretical, Journal of Optical Society of America, Vol. 39, No. 10, 797-808.

In the longitudinal mode of operation, both the electric field and the direction of light propagation are parallel to the Z axis of a uniaxial crystal.. There is also a transverse effect that can be used in the Fabry-Perot modulator. This can best be explained by referring to figure 1-3. In this figure, the light beam enters the crystal in the plane formed by the x and z axes at an angle of incidence i to the z axis. It has been shown[2] that light polarized perpendicular to the plane of incidence (parallel to the y axis in this figure) has an index of refraction β' that is related to the electric field in the z direction by:

$$\beta' = n_o \left(1 - \frac{1}{2} n_o^2 r_{63} E_Z\right) \qquad (1.1\text{-}7)$$

Two properties of this expression are worth noting:

1. For this direction of polarization, the index of refraction is <u>not</u> a function of the angle of incidence.

2. For this direction of polarization, the index of refraction is a <u>linear</u> function of the field E_Z.

If the component is polarized parallel to the plane of incidence, the index of refraction γ' is:

$$\gamma' = \frac{n_\epsilon n_o}{\sqrt{n_\epsilon^2 \cos^2 i + n_o^2 \sin^2 i}} \left\{ 1 + \frac{1}{2} \left(\frac{n_\epsilon^2 n_o^2 \cos^2 i}{n_\epsilon^2 \cos^2 i + n_o^2 \sin^2 i} \right) r_{63} E_Z \right\} \qquad (1.1\text{-}8)$$

where:

n_ϵ = the extraordinary index of refraction.

---

[2] Baird-Atomic Internal Memorandum from Antonio Quesada to Ralph McDonough concerning KDP Crystal Parameters of Significance in Design of Light Phase Modulator, dated 11 December 1961.

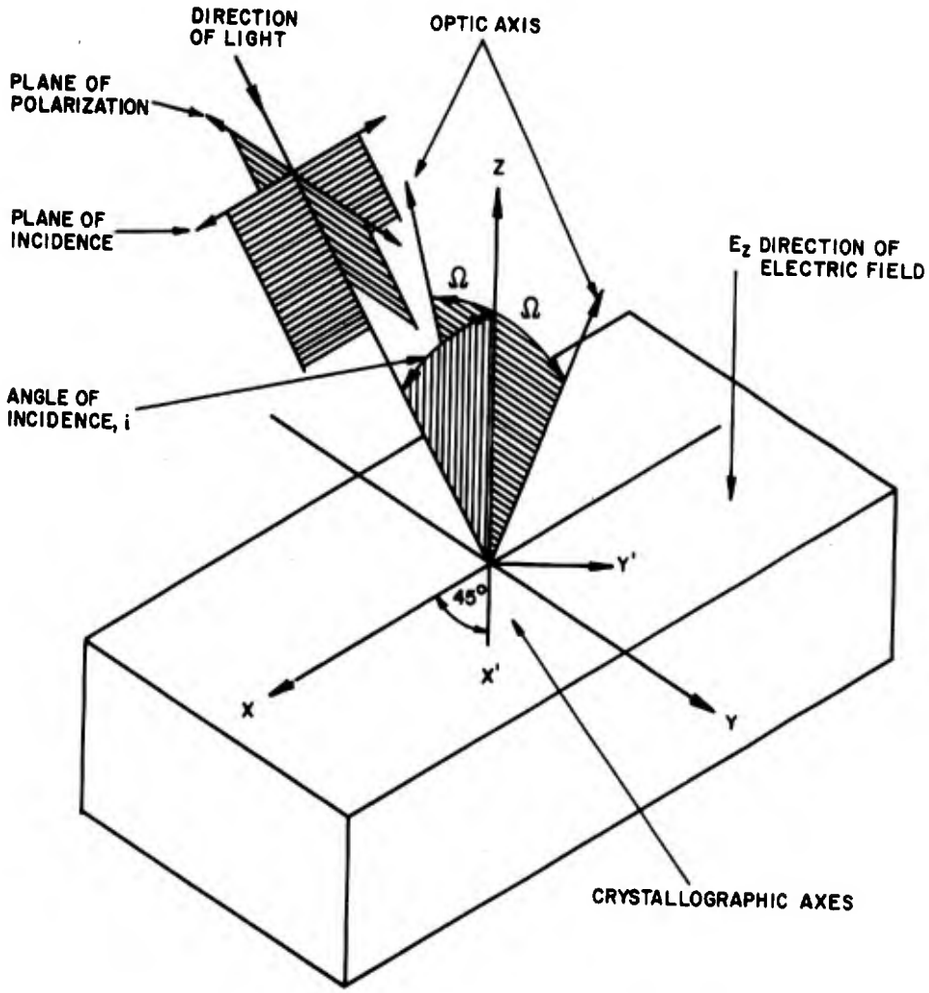

Figure 1-3. Analysis of Relevant Crystal and Light Beam Parameters

For the crystal shown in figure 1-3, the plane of incidence contains the x and z axes and is normal to the plane determined by the optic axes. An equally acceptable configuration is one in which the plane of incidence contains the y and z axes and so coincides with the plane of the optic axes. It can be shown that so far as the modulator is concerned, this configuration is fully equivalent to that of figure 1-3 and that for light polarized perpendicular to the plane of the optic axes the expression for the index of refraction is similar to that given in equation (1. 1-7) with the negative sign changed to a plus sign.

When the angle of incidence is $\frac{\pi}{2}$ radians, γ' reduces to n_ϵ and is independent of the applied electric field, as would be expected for a uniaxial crystal. The index of refraction for the perpendicular component is independent of the angle of incidence. It can be seen from equation (1. 1-7) that light propagated in the x direction and polarized perpendicular to the x-z axis encounters changes in the index of refraction of the crystal which are identical to the changes in the longitudinal configuration, as expressed in equation (1. 1-6).

If the z dimension is h and the mirror separation is p (assuming that the crystal essentially fills the space between the mirrors) the expression for the magnitude of change in the index of refraction $\Delta\beta$ is

$$\Delta\beta = \frac{1}{2} n_o^3 r_{63} E_Z \frac{p}{h} \qquad (1.1\text{-}9)$$

When this expression is compared with equation 1. 3, it can be seen that for a given change in the index of refraction E_Z can be reduced by making p greater than h. Limitations imposed by the aperture (which is determined by h) and available crystal configurations prevent reductions greater than three or four fold in E_Z over the z-axis mode of operation. Twofold reductions are typical of available crystals.

Many crystals of the $\bar{4}2m$ class exhibit electro-cptic effects but the three with large values of Pockel's constants are ammonium dihydrogen phosphate (ADP), potassium dihydrogen phosphate (KDP) and potassium dideuterium phosphate (DKDP).

Some pertinent constants of these materials are shown in table 1.1-1. For this class of crystals it has been found that the total electro-optic effect is the sum of two effects, a direct effect involving interaction between electron clouds and the applied field and an effect related to mechanical strain in the crystal. Since the direct effect should not exhibit resonance below infrared wavelengths, it can be considered inertialess well up into microwave frequencies. Measurements of Pockel's constant have been reported at 9.2 Kmc/s[3], and an unreported measurement has been taken at 25 Kmc/s[4]. In the region of 25 Kmc/s the crystal loss tangent increases due to the absorption of microwave energy by entrapped water molecules. In KDP the direct effect is approximately 90% of the low frequency (i.e., d. c.) Pockel's constant, while for ADP it is only 60%. No measurement of the ratio of direct to photoelastic effect has been made for DKDP but it is assumed by workers in the field that the direct effect is about 90% of the total since deuteration of KDP is equivalent to moving the Curie point of the crystal closer to room temperature.

The larger value of r_{63} for DKDP is equivalent to operating KDP at a lower temperature closer to its Curie point. The cross-over between low frequency and high frequency Pockel's constant is determined by the physical dimensions of the crystal and occurs in the 10 Kc/s to 100 Kc/s frequency region for crystals with one inch edge dimensions. Because of this the high frequency Pockel's constant is pertinent to wideband or microwave modulators using these materials.

---

[3] I.P. Kaminow, to be published.

[4] B.H. Billings, private communication.

TABLE 1.1-1. PERTINENT CONSTANTS OF ELECTRO-OPTIC MATERIALS

		KDP	DKDP	ADP
Pockel's constant r_{63}(cm/volt)	Low freq.	1.05×10^{-9} [2]	2.64×10^{-9} [5]	0.85×10^{-9} [2]
	High freq.	0.97×10^{-9} [3]	assumed 90% of LF value [5]	0.49×10^{-9} [2]
Loss tangent tan (in VHF range)		less than 5×10^{-4} [1]	7×10^{-4} [6]	60×10^{-4} [1]
Index of refraction (at 5560 Å)	N_o	1.5100 [2]	Data not available but similar to KDP [5]	1.524 [2]
	N_1	1.4684 [2]		1.4798 [2]
Half wave voltage $V_{1/2}$ (at low frequency) kilovolts		7.7 [4]	Approx. 3.4 [5]	8.5 [4]
Relative dielectric constant ϵ_r (along C axis, at 1 mc/s)		20.2 [1]	85 [6]	14.3 [1]

[1] A. Von Hippel, Editor, "Dielectric Materials and Applications", The Technology Press of MIT and John Wiley and Sons, Inc., New York, p. 301.

[2] R. Carpenter, "The Electro-Optic Effect in Uniaxial Crystals of the Dihydrogen Phosphate Type III Measurements of Coefficients", Journal of the Optical Society of America, Vol. 40, No. 4, April 1950, p. 225-229.

[3] B. H. Billings, "The Electro-Optic Effect in Crystals and Its Possible Application to Distant Measure"; Optics in Meterology, Pergamon Press, 1960, p. 119.

[4] Baird-Atomic, Inc., Technical Data RD-501-1.

[5] Private communication, Clevite Corporation

[6] Measured at Baird-Atomic, Inc., on 100% Deuterated Sample.

One advantage of these materials over some newer materials is that fairly large crystals of excellent optical quality can be obtained. ADP can be grown with 2 inch x and y axes and with z axes 2 to 3 inches long. KDP seems to be limited to 1 inch x and y axes and 3/4 inch z axes. Longer z axes can be had but the probability of getting good optical and electrical quality decreases rapidly. It is estimated that DKDP could with great difficulty be grown in 1/2 inch cubes. Since one of the goals of this study was to develop a modulator with a large optical aperture for use with high power continuous lasers (when they become available) crystal size became an important parameter in the program.

To demonstrate the feasibility of this type of modulator, KDP was chosen as a compromise between the large sizes but lower high frequency Pockel's constant of ADP and the smaller sizes but larger Pockel's constant of DKDP. Because of the large photoelastic effect in ADP, the high frequency Pockel's constant is only 1/2 of the KDP value. The loss tangent of ADP is also slightly greater than that of KDP over the frequency range of interest.

The technology of DKDP crystal growing has not progressed to the stage where large crystals of high deuterium to hydrogen ratios can be obtained. In addition, the relative dielectric constant of DKDP is approximately four times as large as KDP. This highly capacitive load presented to the modulating electronics introduces additional circuitry problems that are not pertinent to the feasibility of the modulator. Data on the low frequency loss tangent of DKDP could not be found in the published literature, so it was measured up to 50 mc/s on a highly deuterated sample of DKDP. As shown in section 2 3 the power dissipated in the material (causing internal heating) is dependent not only on r_{63} and the loss tangent but on the relative dielectric constant as well. A comparison of the figure of merit for KDP and DKDP show that internal heating is approximately the same for both materials.

1.1.4 Estimation of Modulation Voltage

To estimate the modulation sensitivity of a Fabry-Perot Interferometer modulator, consider the configuration shown in figure 1-4. The modulator consists of electro-optic material placed between highly reflective parallel mirrors perpendicular to a

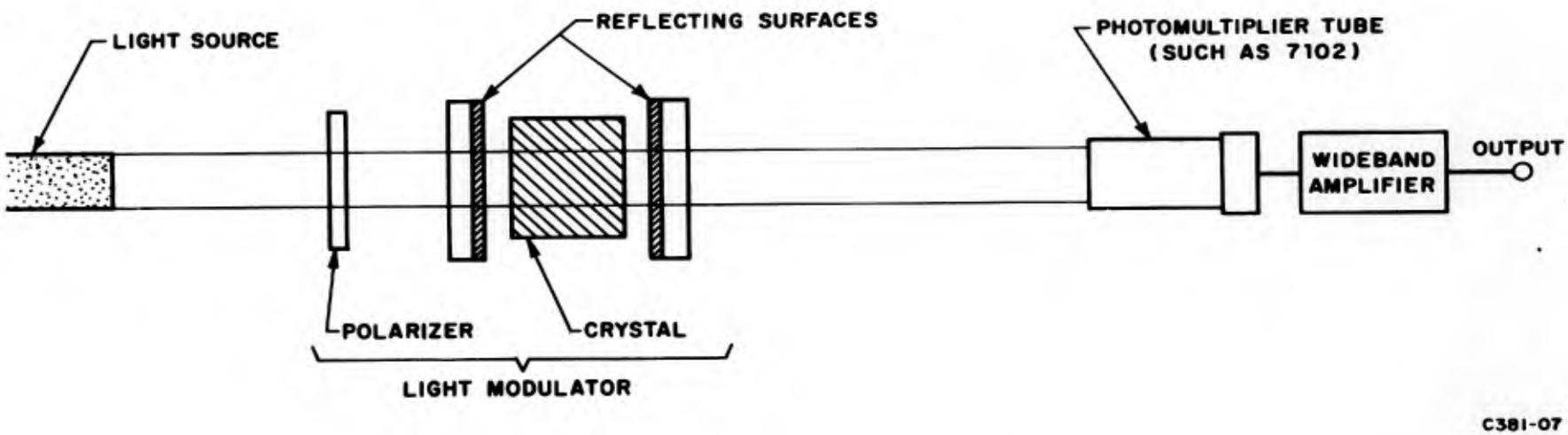

Figure 1-4. Interferometer Modulator Assembly

collimated, monochromatic light beam that passes through them and is polarized parallel to one of the sensitive axis of crystal. Assume the crystal is used in the longitudinal configuration, with the optic axis (z axis) parallel to the propagation of the light. For this configuration, the polarization must be parallel to the induced axes, x' or y'. The spacing of the mirrors is adjusted to give 50% transmission. Application of voltage V_Z changes the optical path within the cavity, thus varying the intensity of the output about the center value. The modulation sensitivity is approximated by the slope of the transmission curve as a function of p when evaluated at the 50-percent transmission point. As a first order approximation, this slope is independent of the spacing of the plates and can be expressed as:

$$\frac{\Delta I_i}{\Delta p} = -\frac{\pi\sqrt{F}}{\lambda} \quad (\text{for } \sqrt{F} >> 1) \tag{1.1-10}$$

(See appendix B for derivation)

By letting the differential represent incremental changes, the change in transmitted intensity is

$$\Delta I_t = \frac{\pi\sqrt{F}}{\lambda} I_i \Delta p' = \frac{\pi\sqrt{F}}{\lambda} \frac{1}{2} I_i n_o^3 r_{63} E_Z p = \frac{\pi\sqrt{F}\, n_o^3\, r_{63}\, V_Z\, I_i}{2\lambda} \tag{1.1-11}$$

where

V_Z = the total voltage applied to the crystal in the Z direction.

Define the intensity modulation index m as the ratio of the change in intensity upon the application of voltage to the quiescent intensity I_o:

$$m = \frac{\Delta I_t}{I_o}$$

For the quiescent point set at 50% transmission, $I_o = \frac{1}{2} I_i$, and

$$m = \frac{2\Delta I_t}{I_i} = \frac{\pi n_o^3 \sqrt{F}\, r_{63}\, E_Z}{\lambda}$$

For KDP the parameters have the following values

$$r_{63} = 3.15 \times 10^{-7} \text{ cm/stat. volt} = 1.05 \times 10^{-9} \text{cm/volt}$$

$$n_o = 1.51$$

For 90% reflecting mirrors $\sqrt{F} = \sqrt{360}$ and for a helium-neon gas maser operating at 6328 Å, the modulation index is

$$m = 3.42 \times 10^{-3} E_Z$$

For 25% modulation, the voltage required at low frequencies will be 73 volts. For operation at 1.15 micron wavelength, the voltage increases by the ratio

$\frac{1.15}{0.6328}$, or 132 volts for the same modulation index.

1.2 Influence of Surface Imperfections on the Transmission Curve $I_{(\xi)}$ of a Fabry-Perot Interferometer

1.2.1 Introduction

A general formula (the Airy formula) was derived in the preceding section for the transmission of light through a Fabry-Perot interferometer:

$$I_{(\xi)} = \frac{T^2}{(1 - R)^2} \left[1 + \frac{4R}{(1 - R)^2} \sin^2 \xi/2 \right]^{-1/2} \qquad (1.2\text{-}1)$$

where:

T = the transmission coefficient of each mirror surface;

R = the coefficient of reflection of each mirror surface = $1 - T$;

ξ = the phase different between 2 successive output components for one incident light ray = $4 n p \cos i/\lambda$;

n = the refractive index for the medium between the mirrors;

p = the mirror distance

i = the angle of incidence

λ = the wavelength of the incident light

Formula (1.2-1) is valid only if the reflecting surfaces are perfectly plane and parallel, which means that p must be constant over the aperture of the incident light beam.

When a crystal is placed between the plates, formula (1.2-1) can only be used if the crystal surfaces are perfectly plane and parallel and if the crystal is perfectly homogeneous. The optical pathlength n times p will then still be constant.

In practice the surfaces of the interferometer and the crystal cannot be made perfectly plane, the interferometer plates cannot be perfectly adjusted, the crystal surfaces will not be parallel and the crystal will not be homogeneous. As a consequence the optical pathlength n times p will always vary over the aperture of the interferometer. This means that the $I_{(\xi)}$ curves, when plotted as functions of ξ do not coincide for all surface elements dS.

There will be a shift along the ζ axis for these $I_{(\zeta)}$ curves which will result in fringe broadening and a decrease in peak-transmission. The effect of the variations in n x p has been discussed by Dufour and Picca[1] and Chabbal[2]. They have shown that as $R \rightarrow 1$, the effective finesse F approaches a limit which is a function of surface imperfections. The value of this limit is determined by the form and magnitude of the departure from plane parallelism. An increase in reflectivity beyond this limit will only reduce peak-transmission.

Absorption in the mirrors and crystal will not affect the shape of the $I_{(\zeta)}$ curve, only the peak-transmission will be decreased.

The influence of the crystal surface defects can be eliminated by replacing the air between the plates with a homogeneous medium of the same refractive index as the crystal.

If the crystal surfaces are plane but not parallel, and if the mirror surfaces are plane, the effect of the lack of parallelism of the crystal faces can be eliminated by making the mirror surfaces perpendicular to light rays emergent from the crystal. With non-parallel faces the crystal acts as a prism, so light rays passing through it will be diverted from a straight line, and the mirrors will not be parallel to each other when finally adjusted.

The Fabry-Perot modulator described in this report was designed to modulate a light beam with a diameter of about 1/4 inch. This large diameter requires an analysis of the influence of surface imperfections before the shape of the transmission curve can be calculated as function of the form and magnitude of the departure of the mirror faces from plane parallelism. These curves can be used with the crystal characteristics to determine the voltage needed on the crystal for 25% modulation.

---

[1] C. Dufour and R. Picca, Revue d' Optique 24, 1945, 19.

[2] R. Chabbal: J. Rech. Ant. Nat. Rech. Sci., Lab. Bellevue (Paris) No. 24, 1953 Journal de Physique et le Radium, t. 19, 1958, 295.

1.2.2 Probability Distribution Curves f(Δ)

It is impossible to devise a probability curve for surface defects that covers all practical cases. As already mentioned, the following imperfections must be taken in consideration:

a. a lack in parallelism of the mirror and crystal surfaces
b. irregular surface imperfections on the mirror and crystal
c. spherical mirror and crystal surfaces
d. crystal inhomogenities.

To simplify the calculations all irregularities are assumed to be on one mirror as shown in figure 1-5 while the other mirror is assumed to have perfect surface conditions.

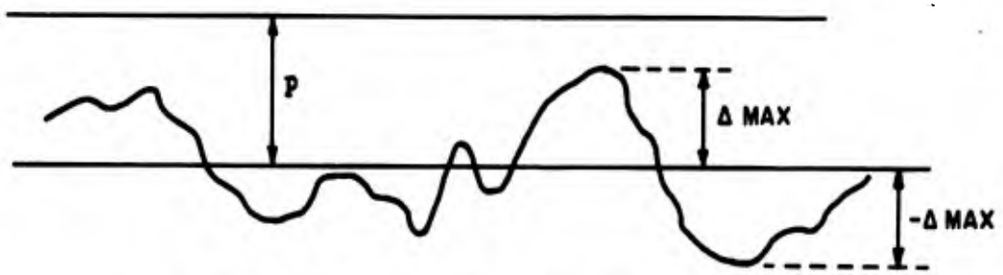

Figure 1-5. Irregularities on One Mirror Surface

p is the mean distance between the mirrors and

Δ_M is the maximum amplitude of the irregularities.

Mirror 2 is split up into very small surface elements which, to a close approximation, will be parallel to mirror 1.

If the distribution of a deviation Δ over the surface of mirror 2 is given by f(Δ), the total surface of mirror 2 which is at a distance p + Δ and p + Δ + dΔ from mirror 1 is given by the formula:

$$dS = f(\Delta)\, d\Delta.$$

In figure 1-6 some examples of possible probability distributions f(Δ) are given.

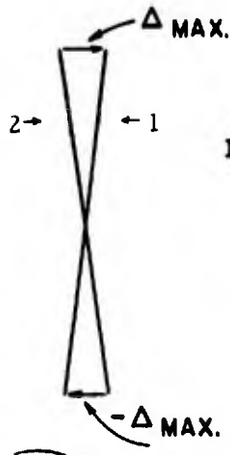

Figure 1-6a

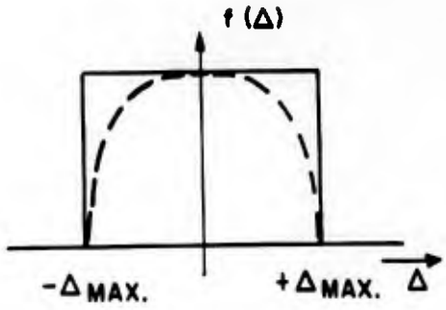

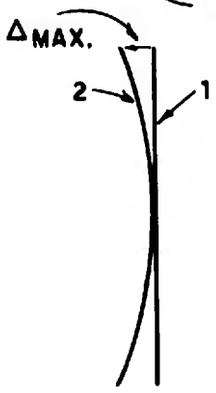

Figure 1-6b

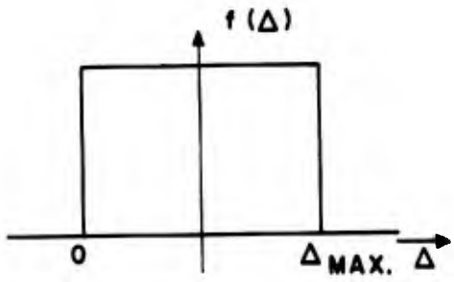

Figure 1-6c

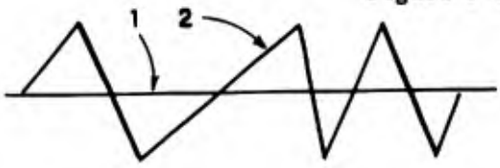

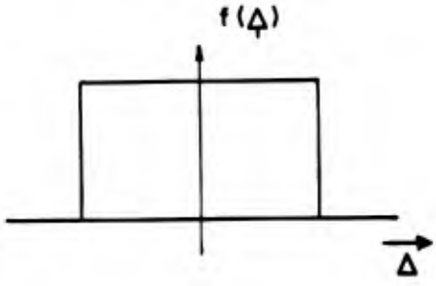

Figure 1-6d

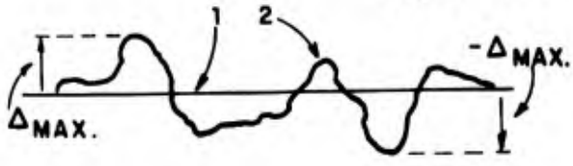

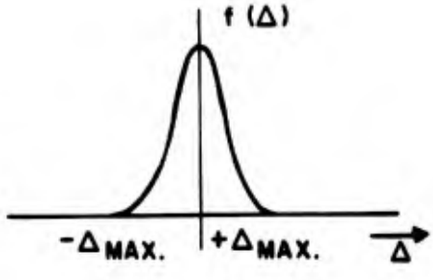

Figure 1-6. Possible Probability Distributions

Figure 1-6-a shows that a lack of parallelism between the mirrors results in a rectangular distribution f(Δ) when a rectangular aperture is used. This means that the total surface, which corresponds to a deviation between Δ and Δ + dΔ, is constant for $-\Delta_{max} < \Delta < \Delta_{max}$.

If mirror 2 is spherical instead of plane, the probability distribution will be rectangular too if R >> r where R is the radius of the mirror 2 and r is the radius of the circular aperture. Refer to figure 1-6-b and appendix C.

Figure 1-6-c shows that a rectangular distribution will exist for this special form of mirror.

A Gaussian probability distribution is shown in figure 1-6-d.

If a circular aperture is used, the probability distribution will be somewhat different. Given non-parallel mirrors, the resultant probability curve is shown in dotted lines in figure 1-6-a.

The rectangular and Gaussian probability distributions are amenable to calculations, but these calculations can only be performed for normal incidence. The transmission curves can be plotted as functions of Δ_{max} or $\sqrt{\Delta^2}$ (fig. 1-10) and with aid of these curves the ΔV for 25% modulation can be calculated. (Table 1.2-3).

1.2.3 Formula for the Rectangular Probability Distribution and the Gaussian Distribution

If the distribution of a deviation Δ on the surface (figure 1-5) is given by f(Δ), the surface dS, which is at a distance p + Δ and p + Δ + dΔ from the mirror, is given by formula

$$dS = f(\Delta)d\Delta$$

Distance Δ corresponds with phase difference δζ:

$$\delta\zeta = \frac{4\pi\Delta \cos i}{\lambda}$$

This proves that the problem can only be solved for normal incidence. For an ideal Fabry-Perot interferometer, the illumination E, at a point on a fringe, is given by:

$$E = kx\, I(\xi)\, x\, S,$$

in which K is a constant.

If $I(\xi)$ is not constant over the aperture, we find:

$$E = k \int_S I(\xi)\, dS = k\, J(\xi)\, dS.$$

$J(\xi)$ is the deformed transmission curve and ξ is defined on page 17.

$$J(\xi) = \frac{1}{S} \int I(\xi)\, dS.$$

For the calculation we take $\delta\xi$ as variable instead of Δ.

$$dS = f(\Delta)d\Delta = g(\delta\xi)\, d(\delta\xi).$$

For the rectangular case the following formula for $J(\xi)$ can be derived as shown in Appendix D.

$$J(\xi) = \frac{1}{\sqrt{4h+1}\ \delta\xi_M} \left[\arctan\left(\sqrt{4h+1}\ \tan \frac{\xi + \delta\xi_M}{2} \right) - \arctan\left(\sqrt{4h+1}\ \tan \frac{\xi - \delta\xi_M}{2} \right) \right] \qquad (1.2\text{-}2)$$

$$J(0) = \frac{\arctan\left(\sqrt{h}\ \delta\xi_M\right)}{\sqrt{h}.\ \delta\xi_M} \qquad (1.2\text{-}3)$$

in which

$$\begin{cases} h = \dfrac{R}{(1-R)^2} \\ \delta\xi_M = 21.766\ \dfrac{\sqrt{\Delta 2}}{\lambda} \end{cases}$$

Formulas (1.2-2) and (1.2-3) have been programmed for a computer and calculations have been performed for different values of R and $\sqrt{\bar{\Delta}^2}/\lambda$.

The mathematical analysis of Gaussian probability distribution is shown in Appendix E. The following expression for the deformed transmission curve $J(\zeta)$ has been derived:

$$J(\zeta) = \frac{1 - R}{1 + R}\left[1 + 2\sum_{-\infty}^{+\infty} R^n \cos n\zeta\, e^{-n^2/4\alpha}\right] \qquad (1.2\text{-}4)$$

As shown in Appendix E, α is a function of the standard deviation of the Gaussian distribution. If $\sqrt{\bar{\Delta}^2}/\lambda$ is defined as the standard deviation, $\bar{\Delta}^2$ can be determined by measuring Δ over the surfaces. For rectangular distribution, $\delta\zeta_M$ is determined $\delta\zeta_M = 21.766 \times \sqrt{\bar{\Delta}^2}/\lambda$.

For a Guassian distribution the standard deviation of $\delta\zeta_s$ is determined by $\delta\zeta_s = 4\pi \times \sqrt{\bar{\Delta}^2}/\lambda$. In formula (1.2-4)

$$\alpha = \frac{1}{\delta\zeta_s^2} \rightarrow \alpha = \frac{1}{32\,\pi^2} \times \frac{1}{\bar{\Delta}^2/\lambda^2}$$

A useful approximate formula for J(0) is:

$$J(0) = \sqrt{\frac{1}{1 + 0.4621\, h\, \delta\zeta_s^2}} \qquad (1.2\text{-}5)$$

The influence of a Doppler effect in the light source on $J(\zeta)$ can be compared with a Gaussian distribution of surface imperfections on $I(\zeta)$.

Burger and van Cittert[3] have made calculations of fringe broadening where the Doppler effect occurs. The results of the calculations are given in Appendix E.

With the aid of a computer $J(\zeta)$ in formula (1.2-4) and J(0) in formula (1.2-5) have been calculated for different values of R and $\sqrt{\bar{\Delta}^2}/\lambda$. The results show that there is very good correspondence between J(0), calculated by using formula (1.2-4) and J(0) calculated by using formula (1.2-5).

---

[3] Zeitschrif for Physik 1928, Vol. 51, p. 638; Vol. 79, p. 722; Vol. 81, p. 428.

1.2.4 Calculation of Deformed Transmission Curves

A computer was used in the calculation of the rectangular and Gaussian distributions of surface imperfections as function of R and $\sqrt{\overline{\Delta^2}}/2$.

The calculated peak transmission value J(0) and the finesse $F = 2\pi/\zeta_1$ $\left[J(\zeta_1) = J(0)/2\right]$ are given in table 1.2-1. The upper number at each position in the table is J(0) while the lower number is the finesse F.

J(0) and F are given for both the rectangular and Gaussian distributions for R = 0.85, 0.90 and 0.95. It can be seen from table 1.2-1 that the difference between the J(0) values for the rectangular and for the Gaussian cases increases with increasing $\sqrt{\overline{\Delta^2}}/\lambda$ and also with increasing R. F increases in the same manner.

Figure 1-7 shows a plot of $J(\zeta)$ as a function of ζ for rectangular distribution. R is made equal to 0.80, and for the four curves, $\sqrt{\overline{\Delta^2}}/\lambda$ = 1/500 λ, 1/100 λ, 2/100 λ, and 4/100 λ. ζ' is the difference in phase from $k \cdot 2\pi$.

Figure 1-8 is the same as figure 1-7 with R made equal to 0.90,

Figure 1-9 is the same as figure 1-7 with R made equal to 0.99.

Figures 1-7, 1-8 and 1-9 illustrate clearly that both fringe broadening and the rate of decrease in peak transmission increase with increasing values of R and $\sqrt{\overline{\Delta^2}}/\lambda$.

Fringe broadening is illustrated in figure 1-10 in which J(0) has been plotted for the rectangular and Gaussian distribution with R set equal to 0.90 and with all curves normalized to J(0) equal to 1.

1.2.5. The Influence of Surface Imperfections on the Modulating Voltage

For light polarized parallel to the x'-axis of a z-cut KDP crystal and transmitted along the z-axis, a change Δn in the index of refraction is expressed by:

$$\Delta n_{x'} = \frac{1}{2}\ \omega^3\ r_{63}\ E_{z'} \qquad (1.2\text{-}6)$$

TABLE 1.2-1. PEAK TRANSMISSION J(0) AND FINESSE F AS FUNCTIONS OF THE REFLECTIVITY AND THE DISTRIBUTION OF IRREGULARITIES

$\sqrt{\bar{\Delta}^2}$	R = 0.7	R = 0.8	R = 0.85		R = 0.9		R = 0.95		R = 0.99
	Rect.	Rect.	Rect.	Gauss.	Rect.	Gauss.	Rect.	Gauss.	Rect.
1/500 λ	0.995 8.9	0.99 13.8	0.98 18.2	0.98 18.4	0.95 27.2	0.95 27.4	0.85 47.0	0.85 47.04	0.30 53.0
1/100 λ	0.90 6.9	0.79 10.0	0.69 11.6	0.75 12.3	0.54 13.0	0.60 14.7	0.32 13.4	0.38 17.7	0.07 13.6
2/100 λ	0.73 5.5	0.56 6.4	0.45 6.7	0.52 8.0	0.32 7.0	0.39 8.8	0.17 7.2	0.22 9.3	0.04 7.3
4/100 λ	0.49 3.0	0.34 3.5	0.26 3.6	0.32 4.6	0.18 3.6	0.22 4.8	0.09 3.6	0.12 5.0	0.02 3.65
$F_{(ideal)}$	9.0	14.0	19.0		30.0		61.0		312

The upper number at each position in the table is J(0) while the lower number is the finesse F.

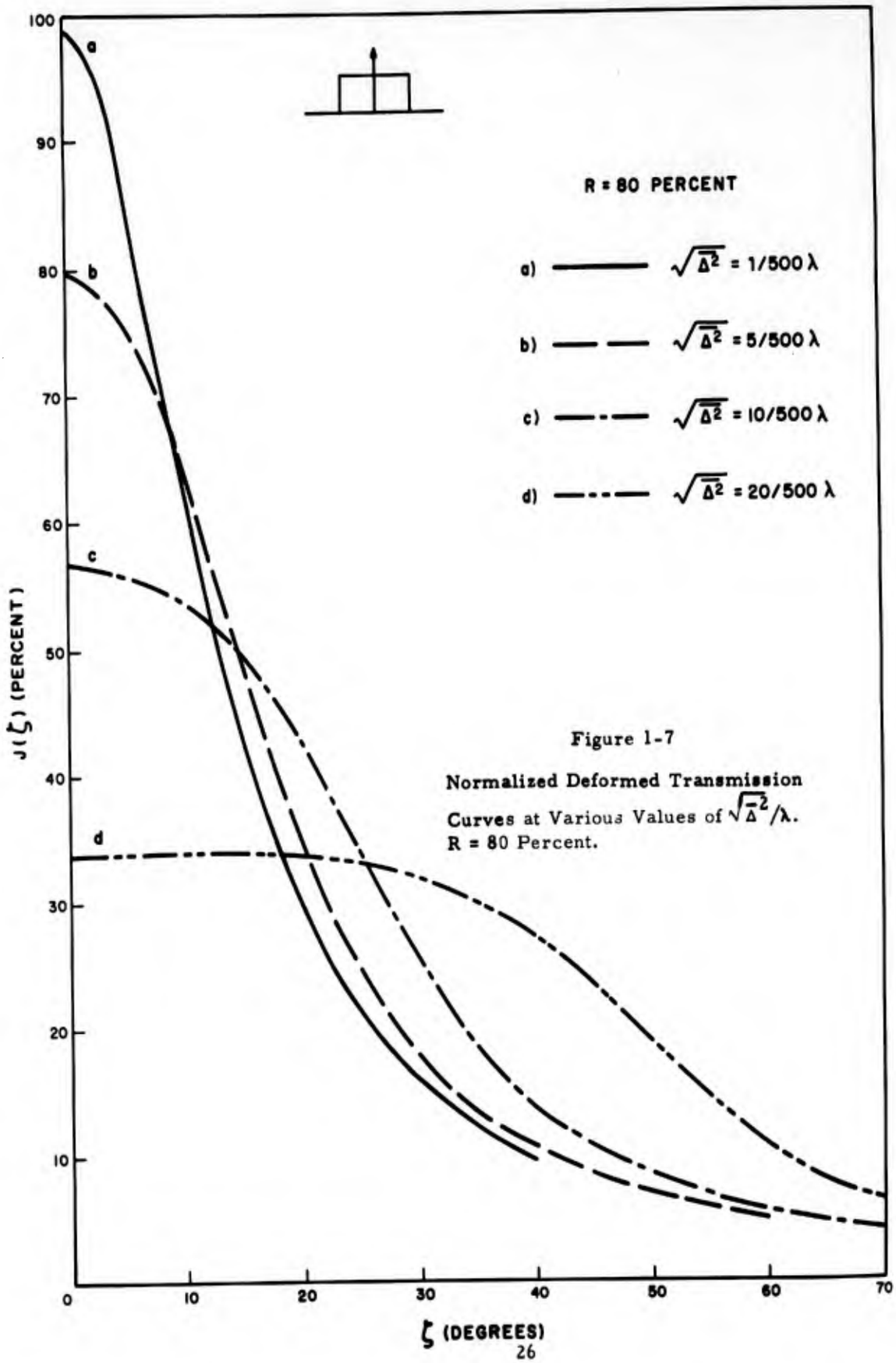

Figure 1-7

Normalized Deformed Transmission Curves at Various Values of $\sqrt{\overline{\Delta^2}}/\lambda$. R = 80 Percent.

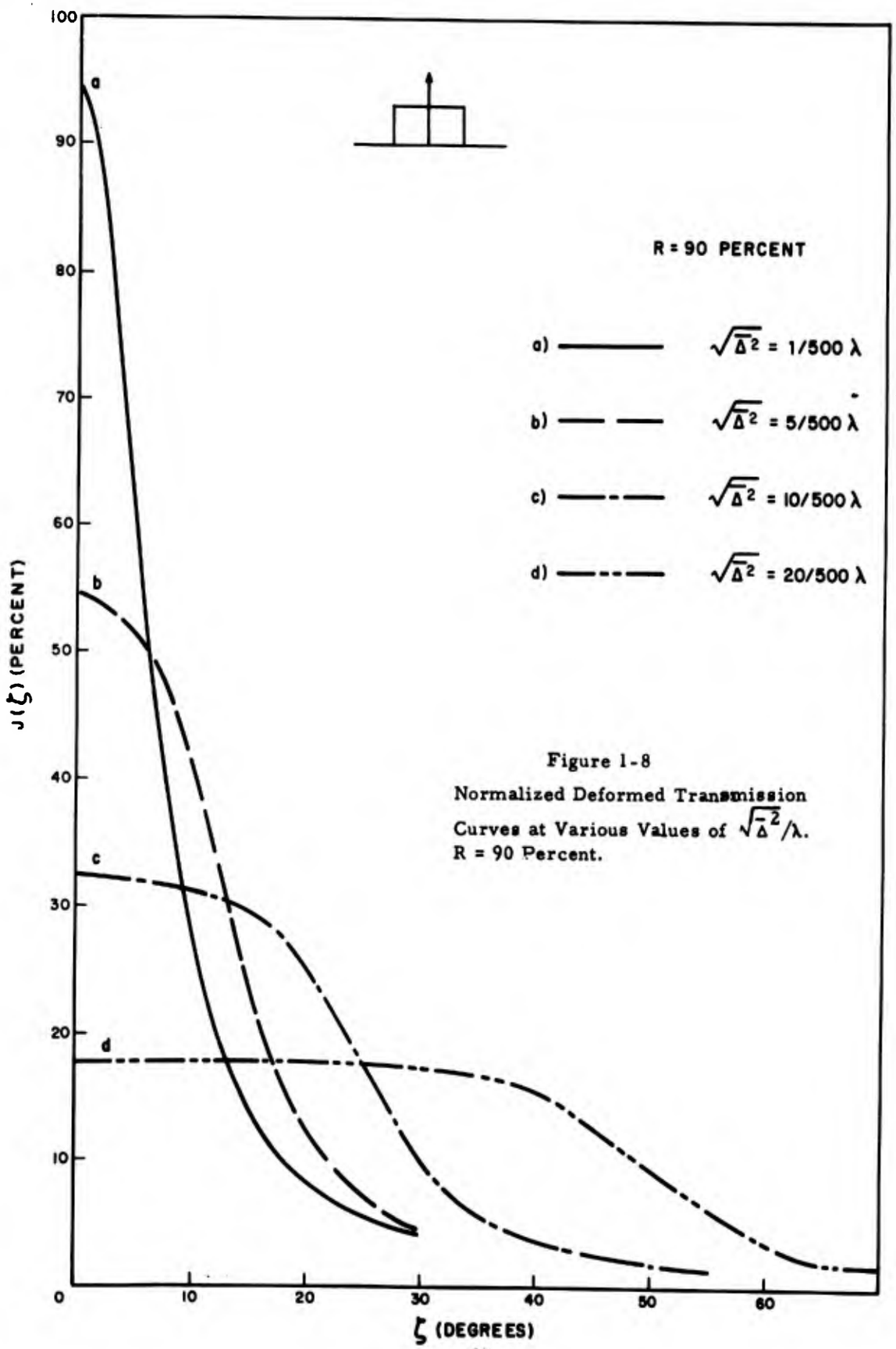

Figure 1-8
Normalized Deformed Transmission Curves at Various Values of $\sqrt{\overline{\Delta^2}}/\lambda$. R = 90 Percent.

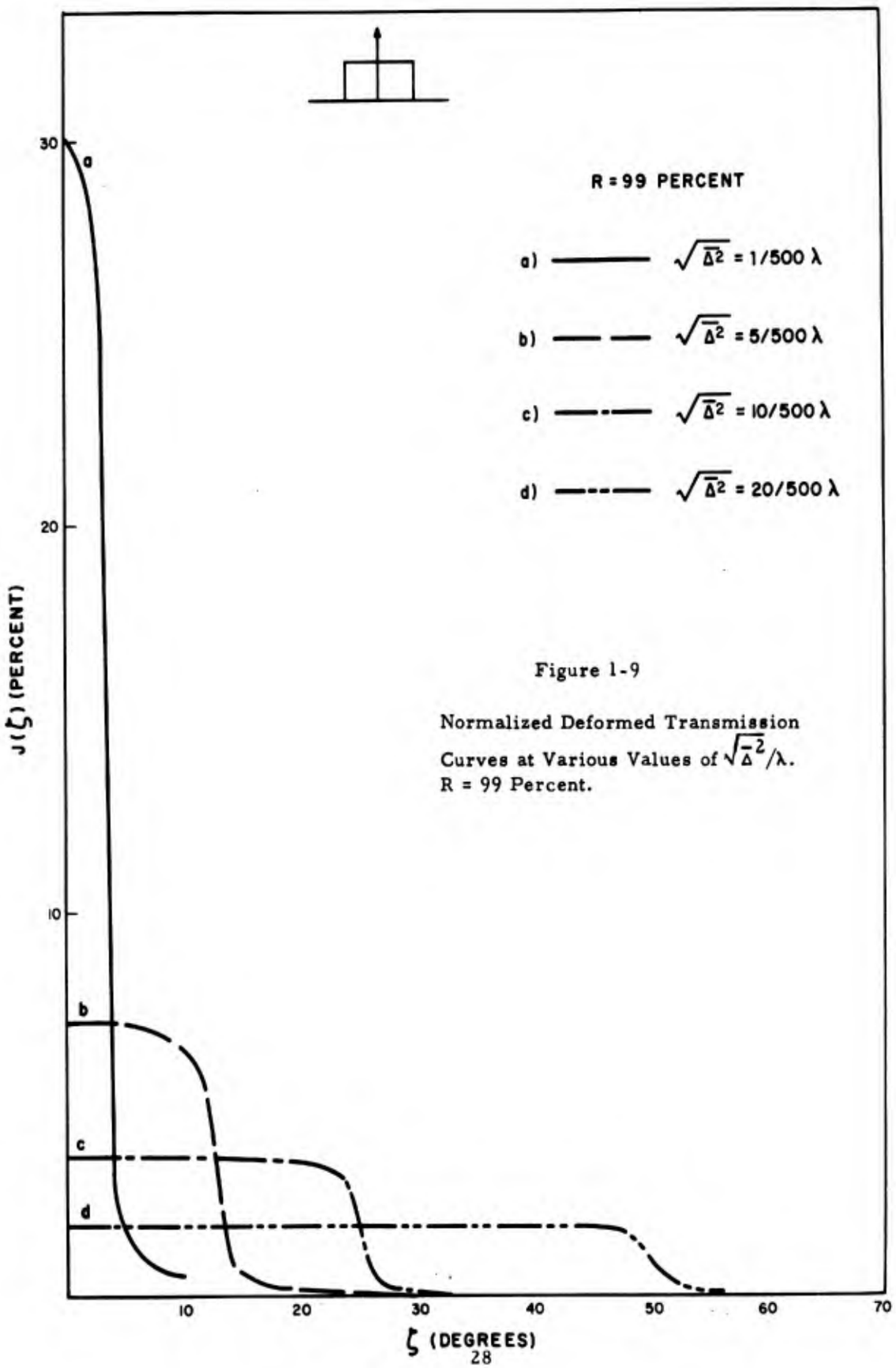

Figure 1-9

Normalized Deformed Transmission Curves at Various Values of $\sqrt{\overline{\Delta^2}}/\lambda$. R = 99 Percent.

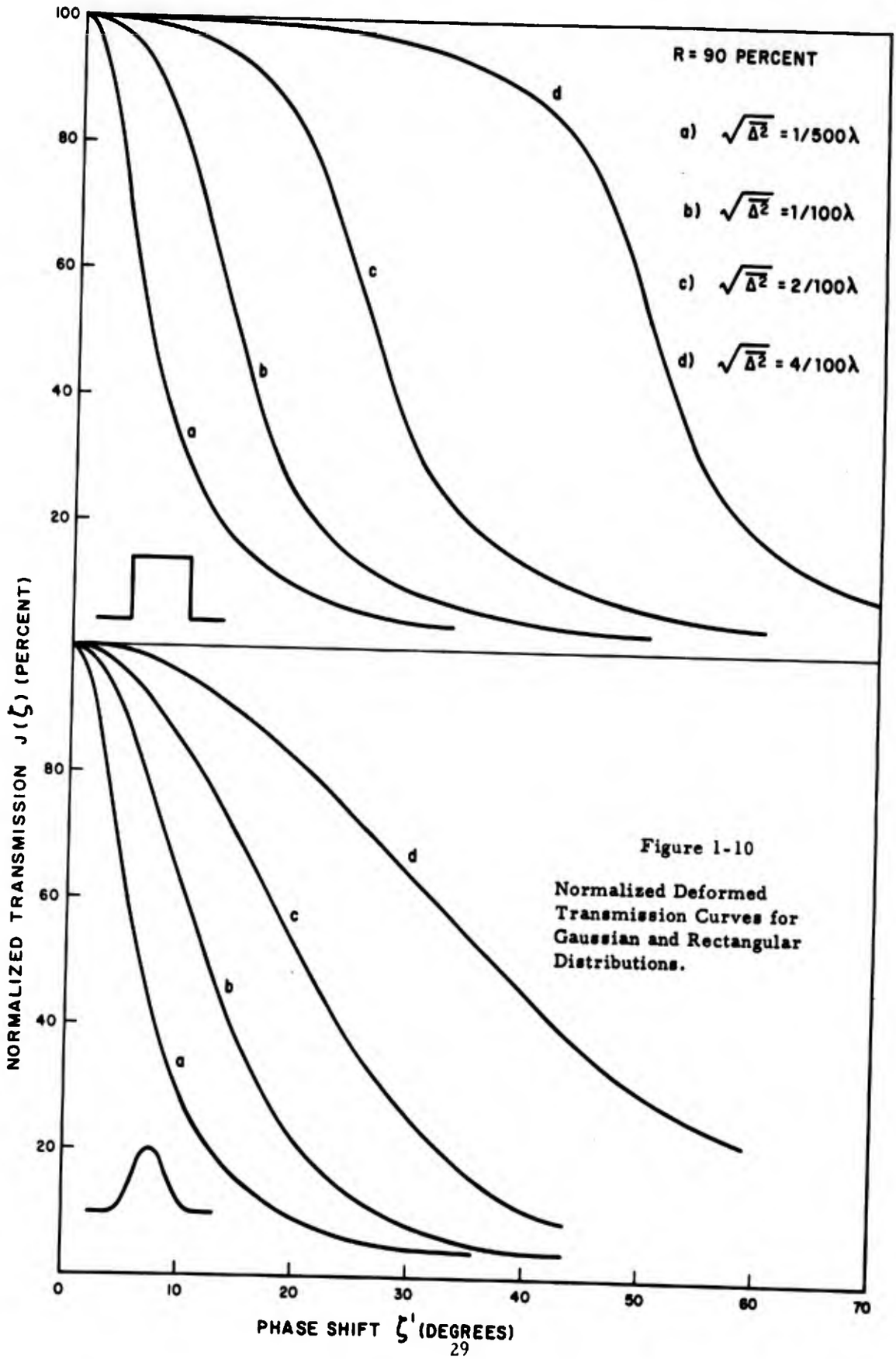

Figure 1-10

Normalized Deformed Transmission Curves for Gaussian and Rectangular Distributions.

Where: E_Z = the electric field applied along the z-axis

ω = the index of refraction for the incident ray

r_{63} = the electro-optic coefficient.

The electrically induced phase-retardation brought about by the change of refraction is equal to $\frac{2\pi \Delta n\, p}{\lambda}$, in which p is the thickness of the crystal and λ is the wavelength of the incident light.

With reference to the formulas in section 1.2.3 $\Delta\zeta$ is defined for normal incidence by:

$$\Delta\zeta = \frac{4\pi\, \Delta n\, p}{\lambda} \qquad (1.2\text{-}7)$$

For KDP

$$r_{63} = 3.2 \times 10^{-7}$$

$$\omega^3 = 3.17$$

If $\lambda = 0.5 \times 10^{-4}$ cm

$$\Delta\zeta = \frac{4\pi}{\lambda} \cdot \frac{1}{2}\, \omega^3\, r_{63} \cdot E_Z\, dp = 2\pi .\ 0.205 .\ 10^{-2}\ V \qquad (1.2\text{-}8)$$

Where

V = applied crystal voltage in stat. volt (1 stat. volt = 300 volts).

It can be seen from formula (1.2-8) that $\Delta\zeta$ = one degree for every 36.1 volts applied to the crystal. It should be pointed out that one degree corresponds to 0.5 degree phase shift in the crystal.

By using the calculated transmission curves for the rectangular and Gaussian distribution of surface imperfections, the voltage for 25-percent modulation can be graphically determined, starting from the 50-percent transmission point.

$$J(\phi_1) = \frac{1}{2}\ J(0)$$

Section 1.3.5 shows that the theoretical calculated modulation voltage for a z-cut KDP crystal must be multiplied by a factor of about 1.2 introduced by the circular electrode configuration. ΔV^{peak} for 25% modulation must then be calculated by using:

$$\Delta V^{peak} = 43.3 \times \Delta \xi \text{ (in degrees) volts.} \qquad (1.2\text{-}9)$$

The modulation sensitivity for an ideal Fabry-Perot interferometer is approximated by the slope of the transmission curve as a function of (np) when evaluated at the 50-percent transmission point.

The slope is, to a first approximation, independent of the spacing of the plates and can be expressed as:

$$\frac{dI}{d(np)} = -\frac{\pi\sqrt{F}}{\lambda} \text{ (for } F >> 1)$$

Letting the differential represent incremental changes and using the factor 1.2, ΔV^{peak}_{ideal} can be calculated for 25-percent modulation and with $\lambda = 0.5 \times 10^{-4}$ cm:

$$\Delta V^{peak}_{ideal} \text{ (stat. volt)} = \frac{4.7}{F} \text{ or:}$$

$$\Delta V^{peak}_{ideal} \text{ (Volt)} = \frac{1410}{F} \qquad (1.2\text{-}10)$$

Table 1.2-2 lists ΔV^{peak}_{ideal} as a function of R.

Table 1.2-3 lists the results of the calculation of ΔV^{peak} for 25% modulation with $J(\phi_1) = \frac{J(0)}{2}$ and as a function of R and $\frac{\sqrt{\Delta^2}}{\lambda}$ for the rectangular and the Gaussian distribution. All calculations have been for $\lambda = 0.5\mu$.

The accuracy of the values for ΔV^{peak} is about 10%. In many cases the 50-percent transmission point was not found to be the most suitable quiescent value.

Figure 1-11 shows ΔV^{peak} from table 1.2-3 plotted as a function of R for the rectangular distribution.

TABLE 1.2-2
ΔV as a Function of R

	R = 0.7	R = 0.8	R = 0.85	R = 0.90	R = 0.95	R = 0.99
$\sqrt{F}$	31	80	151	300	1520	39600
ΔV^{peak}_{ideal} (Volts)	253	157	115	74	36	7

TABLE 1.2-3
ΔV for 25% Modulation as a Function of R

	R = 0.8	R = 0.85		R = 0.90		R = 0.95		R = 0.99
	Rect.	Rect.	Gaus.	Rect.	Gauss.	Rect.	Gauss.	Rect.
$\frac{\sqrt{\overline{\Delta^2}}}{\lambda}$ $\frac{1}{500}$	146	106	107	70	70	35	40	15
$\frac{1}{50}$	180	136	197	94	173	49	170	17
$\frac{2}{50}$	202	173	320	102	313	55	207	23

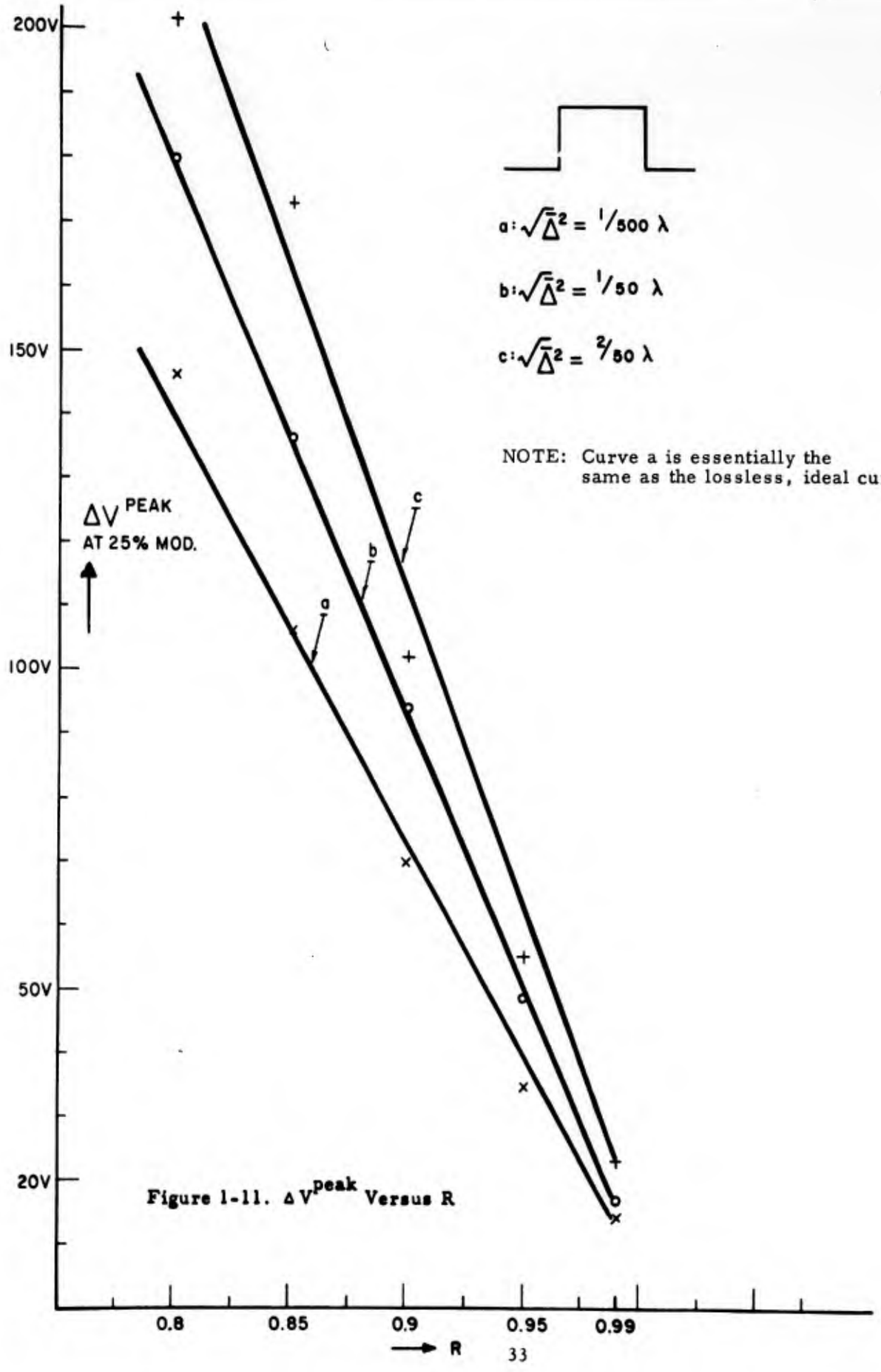

Figure 1-11. ΔV^{peak} Versus R

1.3 Frequency Response of the Fabry-Perot Modulator

1.3.1 Introduction

The intensity of the light transmitted by a Fabry-Perot interferometer, illuminated by monochromatic parallel rays normal to its surface, can be altered by changing either the separation between the plates or the index of refraction of the medium between them. We shall investigate the second possibility for an interferometer in which the spacer layer is KDP crystal oriented with its z-axis normal to the reflecting surfaces.

1.3.2 Harmonic Analysis

When an alternating electric field is applied in the z-direction, the crystal is periodically changed from uniaxial to biaxial, with an index of refraction for plane polarized light of the proper orientation given by the expression

$$n = n_o (1 + \epsilon \cos\omega_M t) \qquad (1.3\text{-}1)$$

where

n_o = index of refraction in the z-direction with no field.

ω_M = angular frequency of the applied voltage.

and

$$\epsilon = \left[\frac{r_{63} n_o^2}{2p}\right] V \qquad (1.3\text{-}2)$$

In equation (1.3-2) p is the geometrical thickness of the crystal and V the amplitude of the voltage applied to its faces.

For a medium characterized by an index of refraction which varies according to equation (1.3-1), the instantaneous speed of propagation of a wavefront is

$$v(t) = c/n \qquad (1.3\text{-}3)$$

where c is the speed of light in vacuum.

In a time dt the wavefront advances a distance ds = c dt/n. Thus, after a time $t - t_o$ the total distance traveled is

$$s = C \int_{t_o}^{t} \frac{dt}{n_o [1 + \epsilon \cos \omega_M t]} \qquad (1.3\text{-}4)$$

As shown in appendix F, the integration of equation (1.3-4) can be carried out without undue difficulties. For all cases of immediate interest, ϵ is a quantity of the order of 10^{-7}. This circumstance allows the replacement of the exact expression arising from equation (1.3-4) by an expression which is far simpler and does not sacrifice numerical accuracy.

The result is

$$s = \frac{2c}{n_o \omega_M} \left\{ \frac{\omega_M}{2} (t - t_o) + \frac{\epsilon}{2} [\sin \omega_M t_o - \sin \omega_M t] \right\} \qquad (1.3\text{-}5)$$

Equation (1.3-5) can be written in a slightly different form which permits the immediate calculation of the phase difference between the wavefront that has traveled a distance s = (2k-1)d and the wavefront that has gone only as far as s = d. Letting this phase difference be ϕ_k we have:

$$\phi_k = 2(k-1)\, \phi_o + \delta_k \qquad (1.3\text{-}6)$$

where

$$\phi_o = \frac{2\pi n_o p}{\lambda} \qquad (1.3\text{-}7a)$$

and

$$\delta_k = \alpha \left\{ \sin [\psi + 2 (k-1) \Omega] - \sin \psi \right\} \qquad (1.3\text{-}7b)$$

$$\alpha = \epsilon \left(\frac{\omega}{\omega_M}\right), \quad (\omega \text{ is the angular frequency of the incident light}).$$

$$\Omega = \left(\frac{\omega_M}{\omega}\right) \phi_o$$

$$\psi = \omega_M t_o + \Omega$$

If we define $|r^2|$ and $|t^2|$ as the reflection and transmission coefficients of the interferometer end surfaces, the resultant amplitude can be written in the form

$$A = t^2 [1 + r^2 e^{i(2\phi_o + \delta_2)} + r^4 e^{i(4\phi_o + \delta_3)} + \ldots .] \qquad (1.3\text{-}8)$$

which by virtue of the relation

$$e^{i\delta_k} = e^{-i\alpha \sin \psi} \sum_{-\infty}^{\infty} J_n(\alpha)\, e^{in[\psi + 2(k-1)\Omega]}$$

can be written in the equivalent form

$$A = t^2 e^{-i\alpha \sin \psi} \sum_{-\infty}^{\infty} \frac{J_n(\alpha)\, e^{in\psi}}{1 - r^2 e^{i2(\delta + n\Omega)}} \qquad (1.3\text{-}9)$$

where δ is the fractional order of the interferometer in the absence of an applied field, that is,

$$\delta = \phi_o - K\pi \quad , \quad K = \text{integer}$$

To find the intensity of the emergent beam it is only necessary to multiply equation (1.3-9) by its complex conjugate. As shown in appendix F, it is an easy matter after this is done to pick out the various order harmonics in the transmitted beam. If I_m is the intensity of the m-th harmonic, we have

$$I_m = 2\left|t^4\right| \sum_{n=-\infty}^{\infty} \left[\frac{J_n(\alpha)\, J_{n+m}(\alpha)}{\sqrt{\Delta_n\, \Delta_{n+m}}}\right] \cos\left[m\psi + \zeta_n^m\right] \qquad (1.3\text{-}10)$$

where

$$\tan \zeta_n^m = \frac{2\left|r\right|^2 \sin m\Omega \cos\left[(2n+m)\Omega + 2\delta\right] - \left|r\right|^4 \sin 2m\Omega}{1 - 2\left|r\right|^2 \cos m\Omega \cos\left[(2n+m)\Omega + 2\delta\right] + \left|r\right|^4 \cos 2m\Omega}$$

and

$$\Delta_n = 1 - 2\left|r^2\right| \cos 2(\delta + n\Omega) + \left|r^4\right|$$

Although equation (1.3-10) appears at first sight to be rather involved, it is actually quite manageable. The reason for this is to be found in the behaviour of the Bessel functions. The higher values of Ω, which in our case correspond to frequencies above 10 megacycles, are associated with small values of α, the common argument of the Bessel functions in equation (1.3-10). For low values of this common argument, Bessel functions of increasing order decrease very rapidly, and it is not necessary to extend the summation beyond the first few terms in order to obtain accurate results.

Equation (1.3-10) was programmed for the computer and values for the amplitude of the first harmonic calculated as a function of the non-dimensional frequency Ω.

Figure 1-12 shows normalized first harmonic amplitudes for various reflectivities, with voltages adjusted to furnish approximately a 25 percent modulation index.

1.3.3 Frequency Response of the Modulator

Although previous calculations indicated that 73 volts would be sufficient to produce 25 percent intensity modulation at 90 percent reflectivity, a trial indicated that 100 volts was a more practical value. The frequency response curve for 90 percent mirrors was therefore calculated assuming 100 volts peak modulating signal. Voltages for other mirror reflectivities were determined by multiplying 100 volts by the square root of the inverse ratio of the coefficients of finesse F:

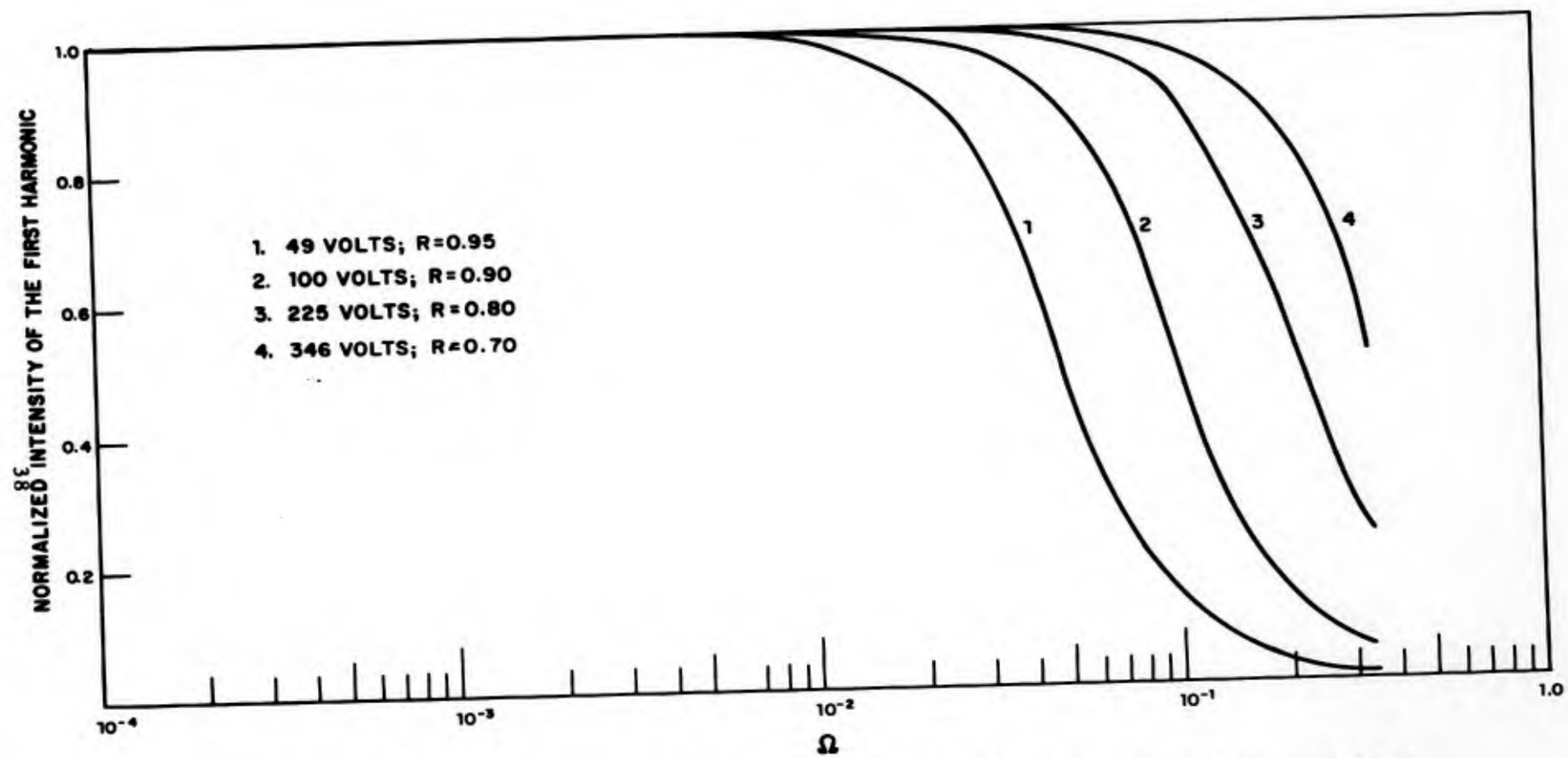

Figure 1-12. First Harmonic Distortion as a Function of Frequency at 25 Percent Modulation

$$V_{95\%} = 100 \sqrt{\frac{F_{95\%}}{F_{90\%}}} \quad .$$

Since the modulator is essentially a time varying medium it would be expected that the high frequency cutoff would be dependent on the magnitude of the modulating voltage. Although not presented in this report, initial calculations of the frequency response were done with a peak voltage of 100 volts for all values of reflectivity. Comparison of these curves with the curves of figure 1-12 shows that the change in high frequency response is only a second order function of the applied voltage so that the values of modulating voltage used in the calculations were not critical.

A more convenient form of the non-dimensional frequency Ω can be obtained by substituting ϕ.

$$\Omega = \left(\frac{\omega_M}{\omega}\right) \phi_o = \frac{f_m}{f} \quad \frac{2\pi n_o p}{\lambda}$$

where λ is the wavelength of the light frequency f. By using the relation between free space wavelength and velocity

$$C = f\lambda$$

the non-dimensional frequency can be written as

$$\Omega = \frac{2\pi n_o p}{\lambda_m}$$

where λ_m is the free space wavelength of the modulating frequency. The non-dimensional frequency is than a constant times the ratio of mirror spacing to free space modulating wavelength. Defining the high frequency cutoff as the frequency at which the intensity of the first harmonic is down to 0.707 of its low frequency value, 90 percent reflectivity gives a cutoff point for the normalized frequency Ω_C of 7.5×10^{-2}, corresponding to a minimum modulating wavelength $\lambda_m\big]_C$, of

$$\lambda_m\big]_C = 126\, p$$

for a medium with $n_o = 1.51$ (i.e. KDP). The response for a mirror spacing of 1 cm is shown in figure 1.13.

1.3.4 Frequency Response as a Function of Crystal Thickness

Inspection of figure 1-5 shows that for reflectivities of interest (R = 0.80 to R = 0.95) the cutoff modulating wavelength is on the order of 100 times the crystal thickness. Thus for a 1,000 mc/s cutoff frequency, a crystal thickness on the order of 0.3 cm would be required. At the start of this investigation it was assumed that the cutoff wavelength would be about ten times the crystal thickness so that 3 cm crystals would suffice. The reduction to 0.3 cm thick crystals indicated by the above derivation introduces a problem related to the linear aperture of the modulator. This problem is discussed in the next section.

1.3.5 Electrode Configuration and Optical Aperture

At this point the electrode structure must be considered. For the longitudinal (or z-cut) crystal configuration, the field is applied parallel to the direction of propagation of light. Transparent conducting electrodes introduce excessive electrode resistance so that the low pass filter formed by the crystal shunt capacity and the series electrode resistance limits the high frequency response to well below one mc/s. The use of a set of circular ring electrodes of high conductivity does not limit the high frequency response. Fringing in the dielectric medium extends the electric field into the optical path through the crystal. Previous calculations have shown that approximately 20 percent more voltage is required to produce a given modulation when the inside diameter of the circular electrode is equal to the crystal thickness. This relationship between electrode size and crystal thickness represents an upper limit to the diameter of the ring electrodes.

For the transverse (or x-cut) crystal configuration it was shown in section 1.1 that the change in index of refraction is proportional to $\frac{p}{h} V_z$, where h is the dimension of the crystal's z-axis. To keep the modulating voltage low h should be equal to or less than p. Assuming a circular beam of light, the maximum diameter of the linear aperture should be no greater than the crystal thickness. Thus for either configuration the linear aperture will be limited to diameters approximately equal to the crystal thickness.

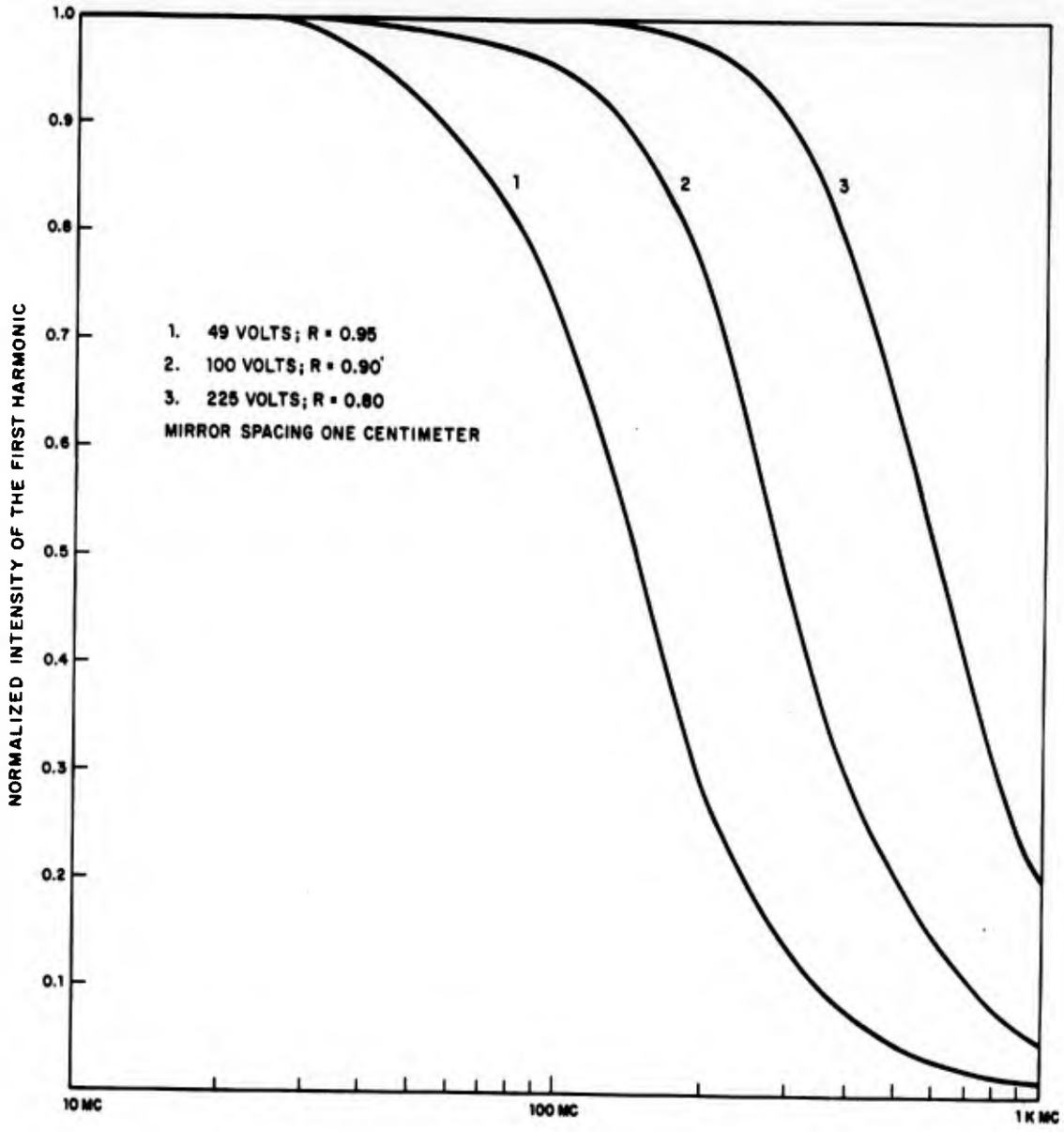

Figure 1-13. Frequency Response at 25 Percent Modulation

One of the goals of this program is to keep the aperture as large as possible to allow for eventual high powered light sources. For sources available now absorption of light within the crystal is no problem but with source powers on the order of tens of watts and with small crystal dimensions, the problem of crystal heating by the absorption of light energy will become important.

1.3.6 Demonstration of Modulation at 1,000 Megacycles

Our intent during this investigation was the demonstration of the high frequency capabilities of the modulator by sinusoidal modulation at 1,000 mc/s. When the small thickness of the crystal needed for 1,000 mc/s modulation was made evident by the analysis, insufficient time was available in the contract to obtain and polish these thinner crystals and modify the modulator structure to accept them and the associate circuitry. In addition, the small optical apertures required by the thinner crystals did not make this avenue of investigation appear to be a fruitful one. Since the crystals used in the final modulator are about 1.3 cm thick, it is estimated that a high frequency cutoff of just under 200 mc/s could be obtained.

1.3.7 Method for High Frequency Modulation

To cope with the problems presented by the limitations on aperture and power dissipation at high frequencies, we have postulated a different system of modulation which also permits modulation at kilomegacycle frequencies. This system uses bandpass modulation, or modulation of the crystal by some high frequency which in turn is modulated by the frequencies of interest. For this method, the crystal is placed in some broadly resonant microwave structure and the information is used to modulate the microwave carrier. The length of the crystal can then be some integral number of guided half wavelengths. No theoretical limitation is placed on the cross-section of the crystal by the cavity except that the introduction of too large a dielectric into a cavity might disturb its mode structure and resonant frequency. These crystals are low loss dielectrics at low microwave frequencies so the perturbation in the cavity can be estimated.

1.3.8 Modulation Index for Low Frequencies

The derivation of equation (1.3-10) was carried out in a general enough way to make it valid for all frequencies of interest. To find a closed expression for the modulation index, it is necessary to use the limiting form of this equation (or equation (1.3-9) which displays all harmonics at once) for low frequencies. In appendix F it is shown that the limiting form of equation (1.3-9) after multiplication by its complex conjugate is

$$\frac{I}{I_o} = \frac{1}{1 + \dfrac{4|r^2|}{(1-|r^2|)^2} \sin^2 [\delta + \epsilon\phi_o \cos \omega_M t]} \qquad (1.3\text{-}11)$$

Letting $r^2 = q$ we have,

$$\frac{I}{I_o} = \frac{(1-q)^2}{1-q^2} \left\{ 1 + 2q \cos 2(\delta + \epsilon\phi_o \cos \omega_M t) + 2q^2 \cos 4(\delta + \epsilon\phi_o \cos \omega_M t) + \ldots \right\}$$

$$= \left(\frac{1-q}{1+q}\right) \Big\{ 1 + 2q\, J_o(2\epsilon\phi_o) \cos 2\delta + 2q^2 J_o(4\epsilon\phi_o) \cos 4\delta + \ldots$$

$$- 4 \cos \omega_M t \,[q\, J_1(2\epsilon\phi_o) \sin 2\delta + q^2 J_1(4\epsilon\phi_o) \sin 4\delta + \ldots$$

$$- 4 \cos 2\omega_M t \,[q\, J_2(2\epsilon\phi_o) \cos 2\delta + q^2 J_2(4\epsilon\phi_o) \cos 4\delta + \ldots$$

$$+ \ldots \Big\} \qquad (1.3\text{-}12)$$

Now, the product $2\epsilon\phi_o$ is generally a small number. Recall that ϵ for KDP is of the order of 10^{-6} cm/Kv. whereas for a crystal 1 cm thick and a wavelength of 1 micron ϕ_o is about 10^5. We can then write, very approximately,

$$\sum_1^\infty q^n \sin 2n\delta \, J_1(2n\epsilon\phi_o) \approx (2\epsilon\phi_o) \sum_1^\infty n\, q^n \sin 2n\delta \qquad (1.3\text{-}13)$$

The series on the right is closely related to the geometrical series and can be summed without any difficulty. The amplitude of the first harmonic can then be shown to be

$$\frac{A_1}{I_o} = \left(\frac{8\epsilon\phi_o q}{(1-q)^2}\right) \frac{\sin\delta\cos\delta}{\left[1 + \frac{4q}{(1-q)^2}\sin^2\delta\right]^2} \qquad (1.3\text{-}14)$$

If the intensity of the beam is varied about the 50 percent point $\sin\delta = \frac{1-q}{2\sqrt{q}}$ and A_1/I_o becomes

$$\frac{A_1}{I_o} = \epsilon\phi_o \sqrt{\frac{4q}{(1-q)^2} - 1} = (r_{63} V)\left(\frac{\pi n_o^3}{2\lambda}\right)\sqrt{F-1} \qquad (1.3\text{-}15)$$

where

$$F = \frac{4|r^2|}{(1-|r^2|)^2}$$

is the so-called coefficient of finesse. Since within the same order of approximation A_o/I_o is one-half, the intensity modulation index can be written as

$$m = \frac{\pi r_{63} V n_o^3}{\lambda}\sqrt{F-1}\,.$$

This expression differs from the one derived in section 1.1 by the factor $\frac{\sqrt{F}}{F-1}$. For large F's the factor approaches one. This difference can be attributed to approximations used in the first derivation.

1.4 Total Harmonic Distortion

1.4.1 Summation of Harmonic Terms

Figure 1-14 is a plot in which calculated values of second, third, fourth and fifth harminic amplitudes are combined into a single rms term and compared with the first harmonic amplitude. The resultant expression, defined as the harmonic distortion, is shown as a function of the non-dimensional frequency Ω for the various reflectivities and voltages previously used. In all cases shown in the figures it is assumed that the no-voltage transmission of the interferometer is one half the peak transmission. The total harmonic distortion is shown to be less than 10 percent over the frequency range of interest.

1.4.2 Low Frequency Distortion as a Function of Operating Point

A quasi-static distortion analysis produced a first approximation of the harmonic content of the modulated signal. Since the result was to be an approximation, the ideal theoretical transmission characteristic of the Fabry-Perot interferometer was used. The transmission characteristic function can be expanded in a Taylor series and the operating points can be substituted directly into the series.

$$I(\phi) = I(\phi_1) + I'(\phi_1)\,\Delta\phi \sin \omega t + I''(\phi_1)\,\Delta\phi^2 \sin^2 \omega t + \ldots.$$

ϕ_1 is chosen to give the desired d-c operating point and $\Delta\phi(t)$ is of sufficient magnitude to produce 25 percent modulation at that operating point. The following expression can be derived for $I(\phi)$ =

$$I(\phi) = I(\phi_1) + I'(\phi_1) - \frac{3}{24}\,\Delta\phi^2\, I'''(\phi_1) \quad \sin \omega t +$$

$$\frac{\Delta\phi}{4}\, I''(\phi_1) \cos 2\,\omega t + \frac{\Delta\phi^2}{24}\, I'''(\phi_1) \sin 3\,\omega t + \ldots..$$

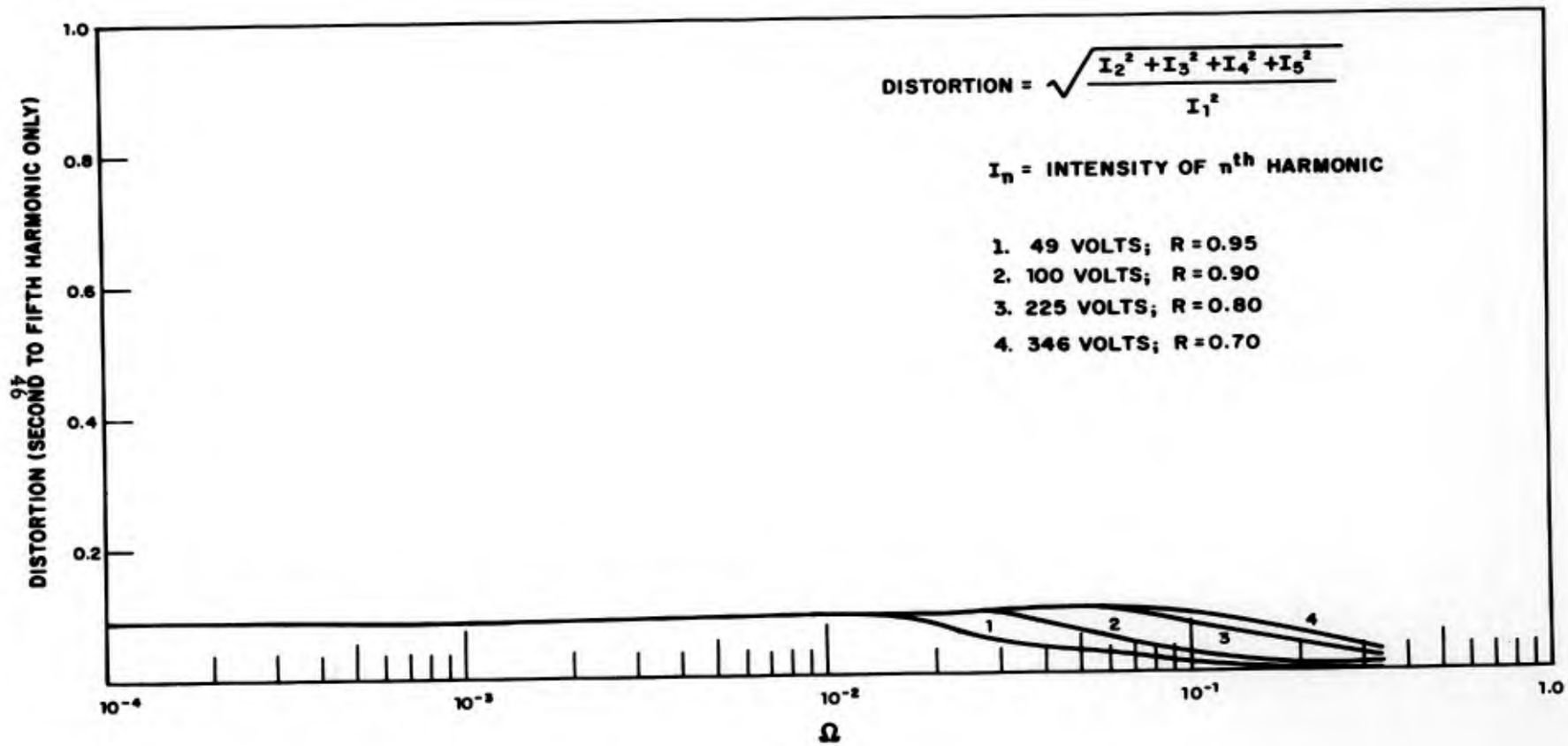

Figure 1-14. Harmonic Distortion as a Function of Frequency at Various Voltages and Frequencies

Distortion is defined in this analysis as the ratio of power in the 2nd and 3rd harmonics to the power in the fundamental.

$$D^2 = \frac{\left|A_2^2\right| + \left|A_3^2\right|}{\left|A_1^2\right|}$$

and since the transmission function is

$$I(\phi) = [A(\phi)]^2 = \frac{I}{I + F \sin^2 [\phi \pm \Delta\phi(t)]}$$

we have

$$D^2 = \frac{\left|I_2\right| + \left|I_3\right|}{\left|I_1\right|}$$

This represents the harmonic distortion in the modulated output of the interferometer. The intensities were squared again, for they were expressed as current outputs from the photomultiplier used as a detector. The current output of a photomultiplier is proportional to the square root of the light intensity at the photocathode.

The harmonic distortion in the photomultiplier output is thus:

$$D^2 = \frac{\left|I_2^2\right| + \left|I_3^2\right|}{\left|I_1^2\right|}$$

Figure 1-14 is a plot of the calculated harmonic distortion against the indicated values of the operating point $I\phi$. Minimum distortion is seen graphically to occur at $I\phi = 0.75$. An independent calculation confirmed 0.75 as the inflection point.

The inflection is independent of λ and can be shown to occur at $I\phi = 0.75$ regardless of the cavity Q. The result of this approximation is the calculation that the harmonic distortion at $I\phi = 0.50$ and 25 percent modulation is 7.5 percent. This figure is recalculated in sections 1.3 and 1.4.1 for the high frequency response characteristics of the modulator.

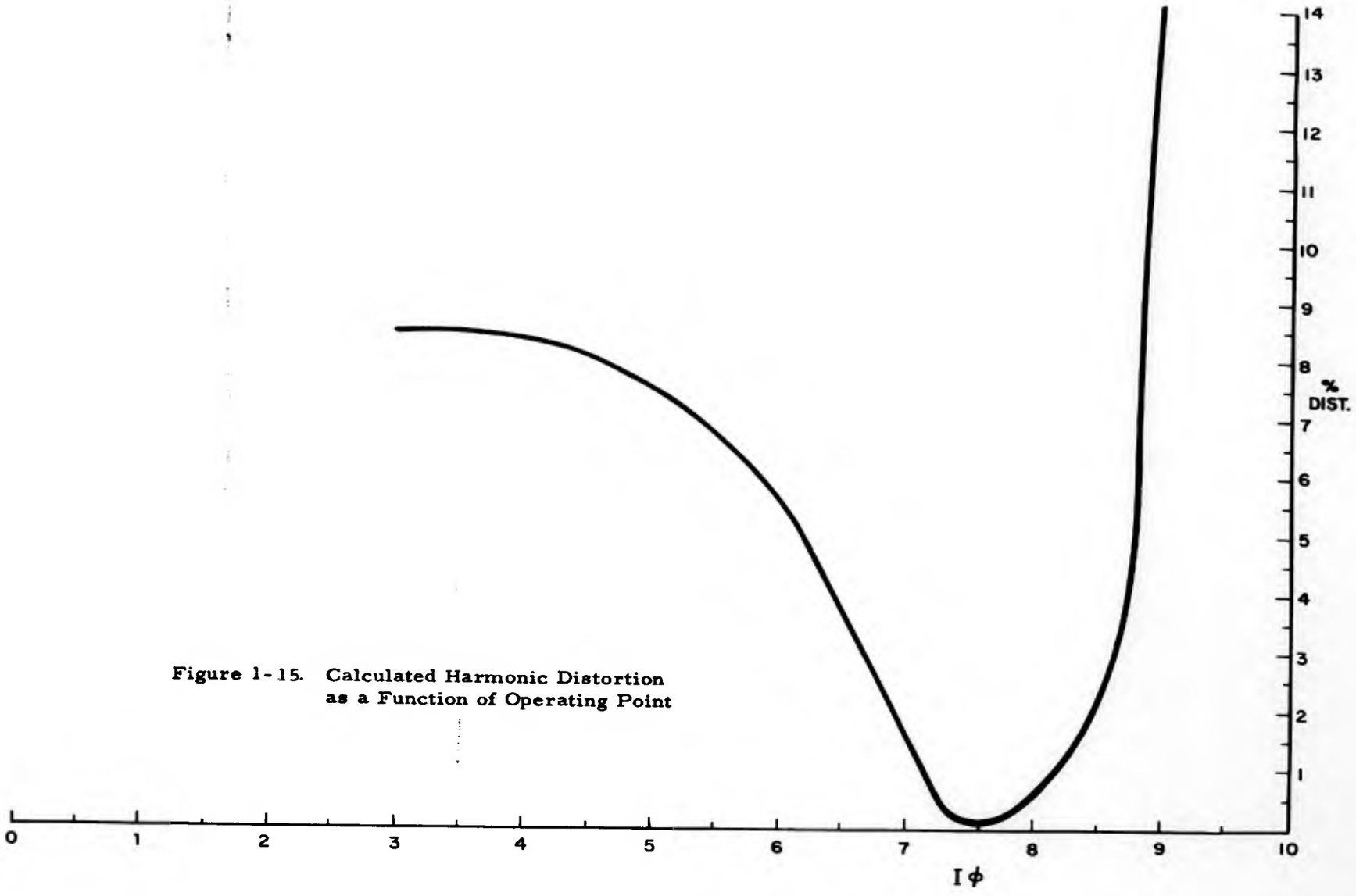

Figure 1-15. Calculated Harmonic Distortion as a Function of Operating Point

Distortion is defined in this analysis as the ratio of power in the 2nd and 3rd harmonics to the power in the fundamental.

$$D^2 = \frac{\left(A_2^2\right) + \left(A_3^2\right)}{\left(A_1^2\right)}$$

and since the transmission function is

$$I(\phi) = [A(\phi)]^2 = \frac{1}{1 + F \sin^2 [\phi \pm \Delta\phi(t)]}$$

we have

$$D^2 = \frac{\left(I_2\right) + \left(I_3\right)}{\left(I_1\right)}$$

This represents the harmonic distortion in the modulated output of the interferometer. The intensities were squared again, for they were expressed as current outputs from the photomultiplier used as a detector. The current output of a photomultiplier is proportional to the square root of the light intensity at the photocathode.

The harmonic distortion in the photomultiplier output is thus:

$$D^2 = \frac{\left(I_2^2\right) + \left(I_3^2\right)}{\left(I_1^2\right)}$$

Figure 1-14 is a plot of the calculated harmonic distortion against the indicated values of the operating point $I\phi$. Minimum distortion is seen graphically to occur at $I\phi = 0.75$. An independent calculation confirmed 0.75 as the inflection point.

The inflection is independent of λ and can be shown to occur at $I\phi = 0.75$ regardless of the cavity Q. The result of this approximation is the calculation that the harmonic distortion at $I\phi = 0.50$ and 25 percent modulation is 7.5 percent. This figure is re-calculated in sections 1.3 and 1.4.1 for the high frequency response characteristics of the modulator.

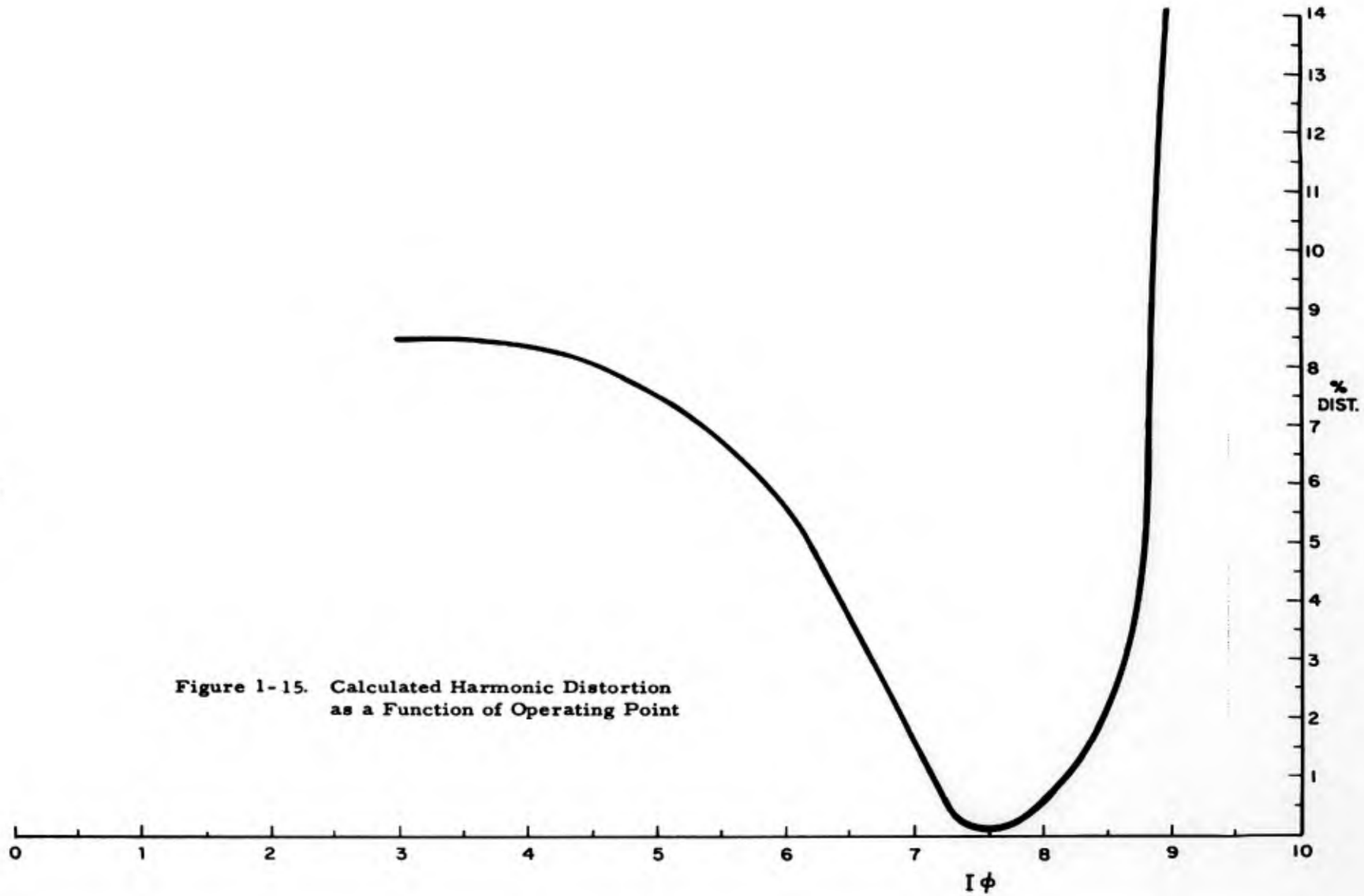

Figure 1-15. Calculated Harmonic Distortion as a Function of Operating Point

1.5 Modulator Electronics

1.5.1 Electronics Requirements

The voltage swing needed for 25 percent modulation with a KDP crystal has been found to be 100 volts rms (282 volts peak to peak) in a bandpass of 100 cycles to 30 megacycles. The modulating signal is assumed to be about 3 volts peak to peak, so a modulator amplifier with a voltage gain of 100 is needed.

The load to be driven by the amplifier is the 10pf crystal capacitance and an additional 20pf in the connecting cable. The use of a matched load technique eliminates the effect of the cable capacitance but is limited by the standard values of coaxial cable impedances, the highest of which is 200 ohms.

The current and power requirements for various load configurations were calculated. The current needed to drive a 200 ohm matched load is $100/200 = 0.5$ amp rms or a swing of about 1.5 amp. An unmatched reactive load of 30pf at a half power (3db) point of 30mc requires $100 \times 2\pi \times 30 \times 10^6 \times 30 \times 10^{-12}/\sqrt{2} = 0.40$ amp rms or a swing of about 1.2 amp. The power required for a matched load of 200 ohms is $(100)^2/200 = 50$ watts, while the minimum power for an unmatched load of 30pf is $(0.4)^2 \times 175 = 28$ watts.

1.5.2 Distributed Amplifier Discussion

Receiving tubes with gain-bandwidth products suitable for this application cannot supply the currents or power required even in differential modes. Normal practice in this case is to parallel tubes, but at high frequencies this is not practical since input and output capacities in parallel are additive.

The distributed amplifier technique of paralleling tubes increases power output while not degrading frequency response. In distributed amplifiers paralleled tubes have their input grids and their plates connected to tapped delay lines, with the plate delay line terminated by the load. The tube input and output capacities are used as components in the respective lumped delay lines. The high frequency limitation of a distributed amplifier is determined by the cutoff frequency of the lumped delay line, which can usually be made quite high relative to the desired amplifier bandwidth. A detailed description of distributed amplifiers is found in appendix G.

The distributed amplifier that has been designed for this application uses 14 vacuum tubes, two of which are used in a phase splitter. As an alternative to this design, a frequency multiplexed amplifier was postulated with a view toward reducing the complexity of the overall amplifier. A reasonable configuration would consist of three 10mc bandpass amplifiers centered at 25mc, 15mc and 5mc with the necessary associated cross-over networks.

Reducing the bandwidth to 10mc allows the output impedance to be tripled thus reducing the output current by 1/3. Assume the use of a tube that can swing 100ma with a reasonably high gain-bandwidth factor such as the Amperex type 8233. Using two of these tubes in the differential mode with shunt peaking to increase the bandwidth would just about produce 100v rms output.

A phase splitter and a gain stage would require two more tubes so that one now has conservatively 4 tubes per bandpass amplifier, or a total of 12 tubes. This is comparable to the 14 tubes in the distributed amplifier configuration.

Since complex crossover networks are needed with this multiplex technique it appears that the final amplifier design would not be less complex than the distributed amplifier design which was chosen.

1.5.3 Determination of Amplifier Parameters

The large voltage swing required across the load dictates the use of a differential output with both sides of the crystal isolated from ground. Since the wide band width required makes the use of an output coupling transformer impractical, the loads must be driven from an output impedance of less than 250 ohms to get a 3db response at 30mc. A voltage swing of ≈ 150 volts from each of the differential output stages requires a maximum current swing:

$$I_T = \frac{V}{R} = \frac{150}{250} = 600 \text{ ma} \qquad (1.5\text{-}1)$$

The use of a tube with a wide current swing and good high frequency characteristics minimizes the number of tubes needed in the amplifier. The best tube for this application was found to be the Amperex type 8233 which has a maximum current swing of 100ma and a g_m of 45,000 μmhos.

From these specifications it can be seen that six 8233 tubes are required for each half of the amplifier. This number can be verified in the following way. Consider an ideal transconductance:

$$i_{out} = g_m V_{in} \tag{1.5-2}$$

and

$$G = \frac{V_{out}}{V_{in}} = g_m \frac{V_{out}}{i_{out}} \tag{1.5-3}$$

But from equation (G-15) in appendix G

$$G = \frac{n g_m R_p}{2} \tag{1.5-4}$$

so

$$n = 2 \frac{V_o}{i_o R_p} \tag{1.5-5}$$

Consider V_o as the maximum voltage swing required across R_p, and i_o as the maximum current swing per tube. Since the line is loaded at both ends with R_p, the output impedance is $R_p/2 = 250$ ohms, or $R_p = 500$ ohms. Then,

$$n = 2 \frac{V_{o\,max}}{i_{o\,max} R_p} = \frac{2 \times 150}{0.1 \times 500} = 6 \text{ tubes} \tag{1.5-6}$$

It is interesting to note in equation (1.5-6) that there is a direct relationship between the design parameters of an amplifier of this type where:

n = number of tubes

R_p = maximum load resistance for a required bandwidth across a capacitive load C_1, $f_c = 1/2\pi R_p C_1$

V_o max = maximum voltage swing across the load

i_o max = maximum current swing per tube.

$$G = \frac{6 \times 0.045 \times 500}{2} = 67.5 \qquad (1.5\text{-}7)$$

The crystal driver is thus a differential amplifier made up of two six-tube distributed amplifier stages. The voltage gain of the differential amplifier is 67.5.

Two signals 180° out of phase are used to drive the halves of the differential amplifier. These signals are supplied by a driving stage which accepts the single-ended input and presents equal driving impedances to the grid lines.

The grid line impedances were made 100 ohms, so the paraphase amplifier used as a driving stage has a 100 ohm resistor in each plate circuit for a match. A paraphase amplifier is made up of two tubes with one common cathode resistor. The amplifier input is to one grid while the other grid is grounded. Outputs E_{01} and E_{02} are of opposite phase and are taken from the plates, while equal value resistors (100 ohms in this case) are used as plate loads.

The gain of this circuit is $g_m R_2/2$ and the output impedance at E_{01} and E_{02} is the plate load 100 ohms so the voltage gain is

$$G = \frac{g_m R_1}{2} \times \frac{1}{2} = \frac{0.045 \times 100}{4} = 1.125$$

A block diagram of the complete amplifier appears in figure 1-15. The calculated values for the grid and plate line parameters were:

$Z_p = R_p = 500$ ohms

$Z_g = R_g = 100$ ohms

$C_p = 7$ pf

$C_g = 35$ pf

$L_p = 1.75$ μh

$L_g = 0.35$ μh

m-derived sections were used for the lumped lines and for the terminations using the values given above. Details and calculations of these sections are found in appendix H.

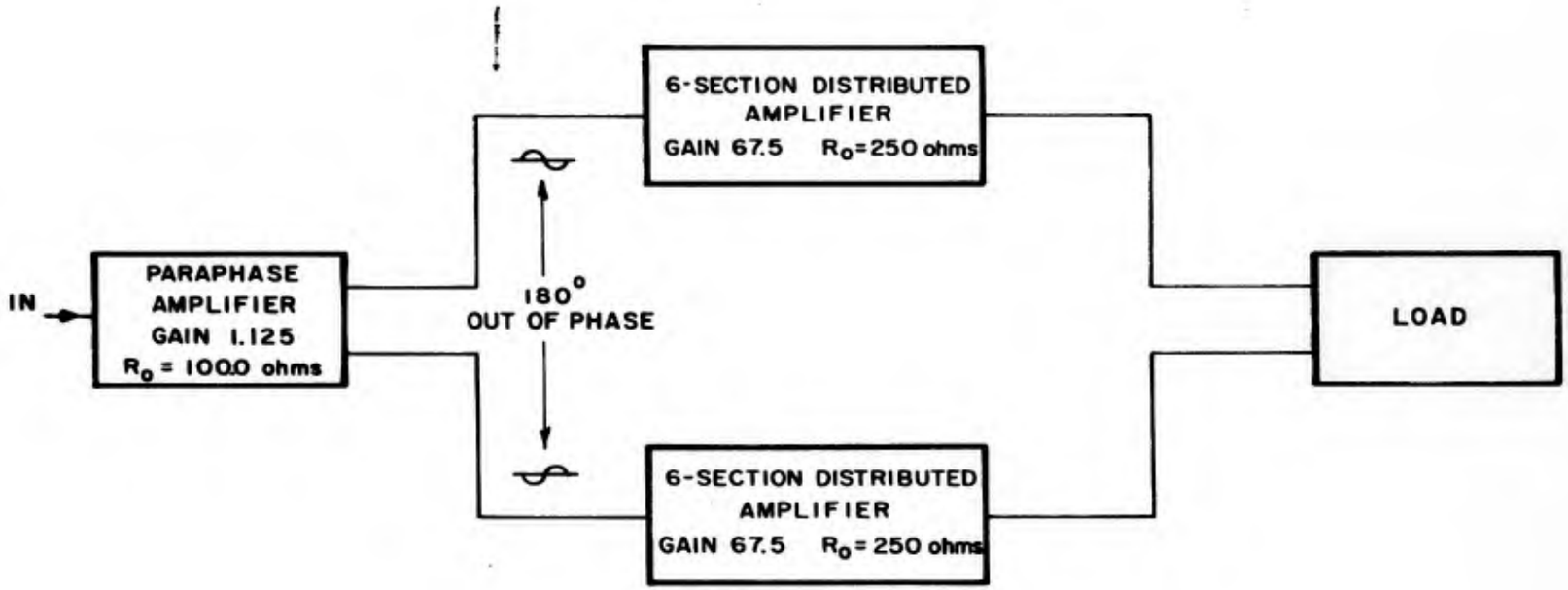

Figure 1-16 Block Diagram 30 Megacycle Modulator Amplifier

2.0 EXPERIMENTS AND MEASUREMENTS

2.1 System Quality Factor

2.1.1 Mirror Flatness

The flatness of a plate that has a spherical shape is usually expressed in units of the number of wavelengths of green light. A plate characterized as being flat to $\lambda/20$ is one in which the saggita of the arc is $\left|\lambda/20\right|$.

When the saggita is small (radius of curvature large) the saggita to a good approximation is directly proportional to the chord length. If we have a 2 inch plate that is polished flat to $\lambda/20$ and only use a 1/2 inch aperture in the center of the plate, this aperture will be flat to $\lambda/80$.

An optical flat can also be described in terms of the surface smoothness. Small scale imperfections such as polishing scratches that appear as rms deviations about the mean spherical surface will determine the smoothness. Optical glass that has been fire polished will generally be free from local micro-structure but mechanically polished flats will have a local micro-structure determined by the physical dimensions of the polishing grit.

When a parallel beam of monochromatic light passes through two flats that have a slight wedge angle between them, fringes of equal displacement are formed. These fringes are intensity maxima that appear along all contours that are separated by a multiple of $\lambda/2$ wavelengths.

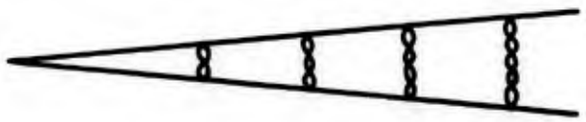

If the plates are flat the fringe contours appear as straight lines that run parallel to the intersection of the planes of the plates. If the surfaces are slightly spherical the fringe contours appear as sections of circles and represent the contour of all points on the surface that lie $n\lambda/2$ above the reference plane.

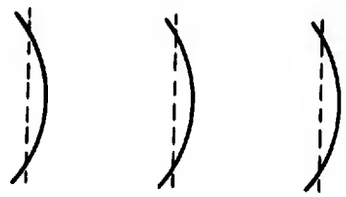

The flatness figure is found by drawing a cord through one or more of these fringe contours and measuring the saggita. Since it is known that the separation of two maxima represents a change in elevation of $\lambda/2$, the saggita can readily be determined in fractions of a wavelength by taking the ratio of its linear dimension to the linear separation of two fringes. Thus if the saggita is 1/10 of the separation between fringes the plate is flat to $\lambda/20$. This represents the total optical path length change across the aperture determined by the chord and consists of contributions from each plate. Since we are only interested in the total optical path difference across the aperture there is no need to designate one or the other of the plates as a reference. The sensitivity of this measurement is seen to depend on the width of the fringe maxima relative to the fringe separation. If the plates are highly reflective, the Airy-derivation for multiple beam interference becomes applicable and the fringe width can be orders of magnitude less than the fringe separation.

Photographs were made of the fringe contours obtained with two such plates spaced 1.5 mm apart with 90 percent reflectivity. ($\lambda = 5461\text{Å}$.) The theoretical fringe width should have been about 1/30 of the separation, but was found to be actually about 1/10 because of the source bandwidth. Thus a shift of the maxima of 1/2 of its width was readily detectable. The flatness figure for these two plates was $\lambda/40$ across a 1.5 inch aperture, or $\lambda/240$ across a 1/4 inch aperture. With this reflectivity and plate separation it was not possible to detect a local microstructure of a magnitude less than about $\lambda/40$ with any accuracy.

2.1.2 Crystal Polishing

At the start of this investigation we felt that the crystal surfaces would probably be difficult to prepare and that the crystal surface quality might limit the system flatness. Fortunately our crystal polisher has been able to polish the z-cut crystals at least as flat as the probable interferometer plate adjustment.

2.1.2.1 KDP Crystals, Z-Face Polishing

KDP crystals are difficult to polish because they are soft, brittle and hygroscopic. Their compressibility and large temperature coefficient contribute to the difficulty. These factors make it almost impossible to eliminate the surface microstructure caused by the abrasive material and the hairline scratches resulting from dust, KDP chips and lap impurities. The z-cut crystals used in the modulator were polished in a dust-free chamber with 0.05 micron aluminum oxide on a beeswax lap. Before any polishing was attempted, all of the edges of the crystals were beveled to reduce chipping and the resultant contamination of the abrasive. Since the final flatness of any surface being optically polished will be highly dependent on the area of the polished surface, 25 one inch square crystals were polished at once.

2.1.2.2 KDP Crystals, X-Face Polishing

An attempt was made to polish z-cut crystals on their x-axis faces, for the electrodes are not in the optical path when the path is parallel to the x-axis. Unfortunately only about three square inches of crystal were available for polishing and in spite of the best efforts of the crystal polisher crystals suitable for use in the modulator could not be made. The crystals could be polished well with surfaces that were not flat, or with flat surfaces that had excessive scratches. Polishing x-axis faces should not be more difficult than z-axis faces when enough crystals are available.

2.1.3 Crystal Flatness

Since it was desirable to determine a flatness figure for the plates together with the crystal in the modulator configuration the crystal was placed in the cavity and the procedure described in 2.1.1 was repeated. We found that the crystal was flat to only 2λ from corner to corner but that the central portion was about λ/10. This is the flatness figure of the system used for the first experiment.

The experiment was performed again with the final modulator configuration. The plates were coated to be 95 percent reflective at 6328Å and the visible laser source was used. The crystal has a 3/8 inch aperture and is anti-reflection coated. The theoretical sensitivity of this measurement is λ/500 since the fringe width is 1/125 of the fringe separation and we can measure a deviation of about 1/2 fringe width. The practical sensitivity of the measurement turned out to be λ/300 which is attributable to the reduction of the cavity Q by the introduction of the crystal.

2.2 Cavity Q

2.2.1 Crystal Absorption and Mirror Reflectivity

Reduction of the cavity Q has been shown to be dependent on the loss in the cavity as expressed by

$$F_{eff.} = \frac{4R(1-a)}{\left[1-R(1-a)\right]^2}$$

The peak transmission reduction is expressed by

$$\frac{I}{I_o} = \left(\frac{T}{T+A+a}\right)^2 \quad , \text{ when } a \simeq A << 1$$

The following calculation was performed to find the absorbtion loss in KDP. Kaminow at Bell Labs has quoted the absorbtion length (that length of material necessary to reduce the transmission to 1/e) of KDP in the direction of the optical axis as 35 cm at 6328Å. Using the relation

$$\frac{I}{I_o} = e^{-\alpha t} = \frac{1}{e^{\alpha t}}$$

α = 0.0285 when t = 35 cm.

or if t = 1.25 cm (0.5")

$$\text{Ln}\frac{I}{I_o} = -(0.028)(1.25)$$

$$= -0.035$$

$$\frac{I}{I_o} = 0.965$$

and since

$$a = 1 - \frac{I}{I_o}$$

a = 3.5 percent for a 1/2" KDP crystal

We measured the absorbtion loss of KDP directly in the Fabry-Perot cavity and calculated its absorbtion length in the following way.

If the intensities of successive reflected rays are compared, the ratio of these intensities can be shown to be:

$$\frac{I_1}{I_n} = \frac{1}{R^{2(n-1)}}$$ (see figure below)

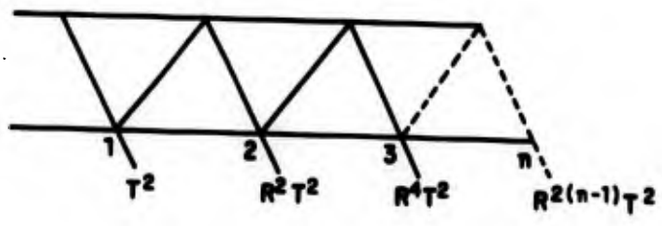

If n is large, the error in the calculated value of R can be much less than the measuring error of I_1 and I_n.

$$R = \left(\frac{I_1}{I_r}\right)^{\frac{1}{2(n-1)}}$$

$$\mathrm{Ln}R = \frac{1}{2(n-1)} \mathrm{Ln}\left(\frac{I_1}{I_r}\right)$$

$$\frac{dR}{R} = \frac{1}{2(n-1)} \frac{d\,(I_1/I_n)}{(I_1/I_n)} \propto \frac{1}{2(n-1)}$$

This technique is found to be most useful when the reflectivity is fairly high so that the intensities of the rays fall off slowly. A very well collimated beam of light was passed through the interferometer and the multiple reflections were scanned with a mechanically driven P.M. Nine reflections were scanned and the voltage output of the P.M. was read on a V.T.V.M. with 1 percent accuracy. The resulting error in the calculated R is

$$\text{error} = \frac{0.02}{16} = 0.00125$$

$$= 0.12 \text{ percent}$$

The true reflectivity of the plates is first calculated as above. If an absorbing medium such as DKP is placed between the plates, the equivalent reflectivity can be calculated since

$$\frac{I_1}{I_n} = \frac{1}{[R(1-a)]^{2(n-1)}} = \frac{1}{R'^{2(n-1)}}$$

a can be calculated by:

$$a = 1 - \frac{R'}{R}$$

a can be found to ± 0.2 percent accuracy if both R and R' are accurate to 0.1 percent.

The true reflectivity was calculated and found to be 0.907 ± 0.001. The equivalent reflectivity with the crystal in the cavity was found to be 0.799 ± 0.001 and the resulting total loss introduced by the crystal was calculated.

$$a = 1 - 0.88$$

$$= 0.120 \pm 0.002$$

The reflection loss at the air - KDP interface can be calculated and subtracted from the total loss giving

$$a = 0.036 \pm 0.002$$

Since the sample was 1.25 cm thick the absorption coefficient α is computed to be 0.0288 and the resulting absorbtion length is

$$t_{\alpha} = 34 \text{ cm}$$

This result was in good agreement with Kaminow's measurement of 35 cm.

2.2.2 Use of Anti-reflection Coatings on Crystals

Since the measurement corroborated the expected 8.4 percent loss due to reflection at the air - KDP interfaces the effects of anti-reflection coatings on the crystal were investigated. Anti-reflection coatings were applied to both faces of the crystal used in the absorbtion experiment and its transmission

was measured on a Cary spectrophotometer. This instrument indicated a total transmission loss of 4.5 percent indicating a reflection loss of 0.45 percent at each face. We decided that the mechanical complications involved in the use of index matching liquids were not warrented, since the additional reduction in reflection loss over the use of anti-reflection coatings could not exceed 0.5 percent total. Moreover, it is known that the use of properly deposited dielectric coatings with the correct index of refraction can produce the same reduction.

The reflectivity of all mirrors used as modulators was calculated so that the predicted modulation index could be compared with experimental results. The transmission of each was measured on the Cary so that it could be used together with the reflectivity to determine the dielectric absorbtion.

The dielectric absorption of the plates was found to be 1 percent so that the total cavity loss is 5.5 percent (4.5 percent transmission loss plus 1 percent dielectric absorption).

2.2.3 Measurement of Cavity Q

Photographs were taken to determine the reduction of cavity Q by the insertion of KDP crystals. As explained in section 1.4.1 the finesse value offers a direct means of measuring the effective Q of the cavity.

Although the photographs were not of sufficient quality for accurate measurements, it was determined that the finesse decreased at approximately the predicted rate.

Measured Finesse	Theoretical
12	15
10	11
6	9

The theoretical values were calculated from the known losses of the crystal.

2.3 Deuterated KDP Measurements

Deuterated KDP (KD_2PO_4) has been investigated as an alternative modulating element since it is well known that it displays a Pockel's coefficient 2.2 times greater than DKDP (KD_2PO_4) (i.e. the half-wave retardation voltage is 3.4 KV for DKDP v.s. 7.5 KV for KDP). We have made independent measurements of the loss tangent (tan δ) of DKDP and have also made a spectral transmission measurement. No measurement of the absorbtion length of this material was possible since we could not obtain a suitably polished sample of convenient dimensions.

2.3.1 Loss Tangent of DKDP and KDP

The loss tangent measurement was performed between 5 mc and 30 mc. It was found that the experiment was unsuccessful unless the sample was very carefully prepared and the experiment conducted in a controlled atmosphere. Atmospheric humidity has a first order effect on the crystal's effective loss tangent. Inspection of the equivalent circuit of the crystal will illustrate this:

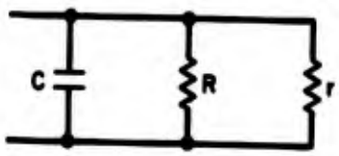

Where

C = crystal capacity

R = shunt resistance

r = leakage resistance

The leakage resistance is the resistance on the surface of the crystal while the shunt resistance is the resistance through the body of the crystal. Since the loss tangent is given by

$$\tan \delta = \frac{1}{\omega C R_{eqiv}}$$

It can be seen that the leak resistance must be much greater than the crystal's true shunt resistance if the material's loss tangent is to be represented accurately. Several attempts at the measurement have produced techniques that help to insure that $r >> R$. The crystal must be polished on its edges to eliminate saw cuts and moisture trapping scratches. The crystal should then be dried in an oven for 24 hours at 50°C and the experiment should be conducted in a dry atmosphere.

2.3.2 Figure of Merit of DKDP and KDP

On the basis of the measured loss tangent of our sample we derive a figure of merit for each of the two materials in the following manner.

The power dissipated in the crystal is given by:

$$P = E^2/R$$

and

$$E = \lambda \Gamma / n_o^3 r_{63}$$

where

Γ = retardation

λ = wavelength (optical)

n_o = index of refraction (z direction)

r_{63} = Pockel's coefficient

We can rewrite this

$$P = E^2/1/\omega \tan \delta \, c$$

or

$$P = E^2 \omega \tan \delta \, C$$

and since

$$C = \epsilon A/d$$

where

ϵ = dielectric constant

A = area

d = thickness

$$P = E^2 \omega \tan \delta \frac{\epsilon A}{d}$$

or

$$P = (\lambda / n_o^3 r_{63})^2 \omega \tan \delta \frac{\epsilon A}{d}$$

Now we can define the figures of merit for KDP and DKDP for equal retardation at a given optical wavelength:

$$P \propto \frac{\tan \delta \epsilon}{(n_o^3 r_{63})} \frac{A}{d}$$

$$P \propto K A/d$$

Figure 2.1 is a plot of the loss tangents for KDP and DKDP. The value for KDP is a maximum upper limit and was obtained from Von Hippels measurements at M.I.T.[1]

We purchased a 100 percent deuterated sample of DKDP. The following table compares the known constants for KDP and DKDP.[2]

Table 2.1 Constants of KDP and DKDP

Crystal	Pockels Coefficient	Half-wave Voltage	Symmetry	Dielectric Constant
KD_2PO_4	r_{63} = -79 Å/statvolt	3.4 KV	V_d	90
KH_2PO_4	r_{63} = -32 Å/statvolt	7.5 KV	V_d	20

[1] Dielectric Materials and Applications, A. Von Hippel, The Technology Press of M.I.T. - Wiley

[2] A.I.P. Handbook

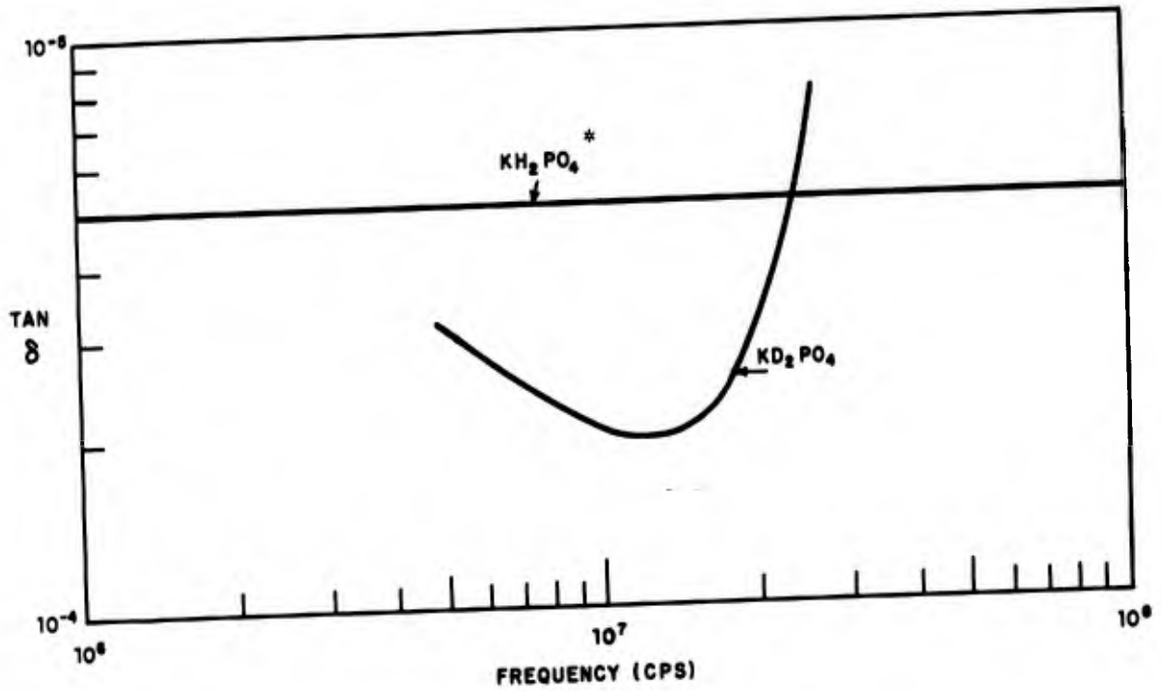

*Maximum upper limit

Figure 2.1 Loss Tangent of KDP and DKDP Versus Frequency

The Boonton Q meter with which the measurements were made is not highly accurate in the portion of its range that had to be used. Because of this the results can be in error by as much as 100 percent. The results indicate that the loss tangents of the two materials are approximately equal and are in the vicinity of 5×10^{-4}.

2.3.3 Power Dissipation of DKDP and KDP

The accumulated data and the derived expression for figure of merit allow the comparison of the power dissipation in the two materials for samples of similar dimensions (area and thickness) and for equal retardation.

$$\frac{P_1}{P_2} = \frac{(5 \times 10^{-4})(85)}{[(n_1)^3 (-79)]^2} \div \frac{(5 \times 10^{-4})\ 20}{[(n_2)^3 (-32)]^2}$$

where n_1 and n_2 are the indices of refraction of DKDP and KDP and

P_1 = Power dissipation in DKDP

P_2 = Power dissipation in KDP

Since

$$\left(\frac{n_1}{n_2}\right)^3 = 0.99$$

$$\frac{P_1}{P_2} = \frac{85}{20} \left[\frac{-32}{-79} \cdot \frac{1}{0.99}\right]^2$$

or

$$\frac{P_1}{P_2} = = .68$$

This result indicates that the power dissipation to be met with DKDP will not be appreciably different from that of KDP for equal modulation and that the only advantage to be gained from its use is a possible simplification of the driving electronics.

2.3.4 Precautions

One important lesson that was learned during this measurement is that the absolute value of dissipated power in any operational device will increase sharply if the crystal is not properly protected from moisture absorbtion. The effective loss tangent of the material was found to range as high as 130×10^{-4} when the crystal was not polished on its edges and was in a high humidity atmosphere.

Reference to the derived equation for power dissipation will show it to increase in direct proportion to the loss tangent.

$$\frac{P_{wet}}{P_{dry}} = \frac{\tan \delta \text{ wet}}{\tan \delta \text{ dry}}$$

$$= \frac{130}{5} \cong 25$$

The crystals received here have not been polished on the edges but it is recommended that any similar crystals in the future have all surfaces polished.

2.3.5 Spectral Transmission

The spectral transmission for DKDP extends slightly farther into the infrared then does that for KDP. The transmission of the two materials is shown in figure 2.2. It was not possible to extend the measurement into the UV region since a well polished KD_2PO_4 crystal was not available and scattering becomes more severe at the shorter wavelengths.

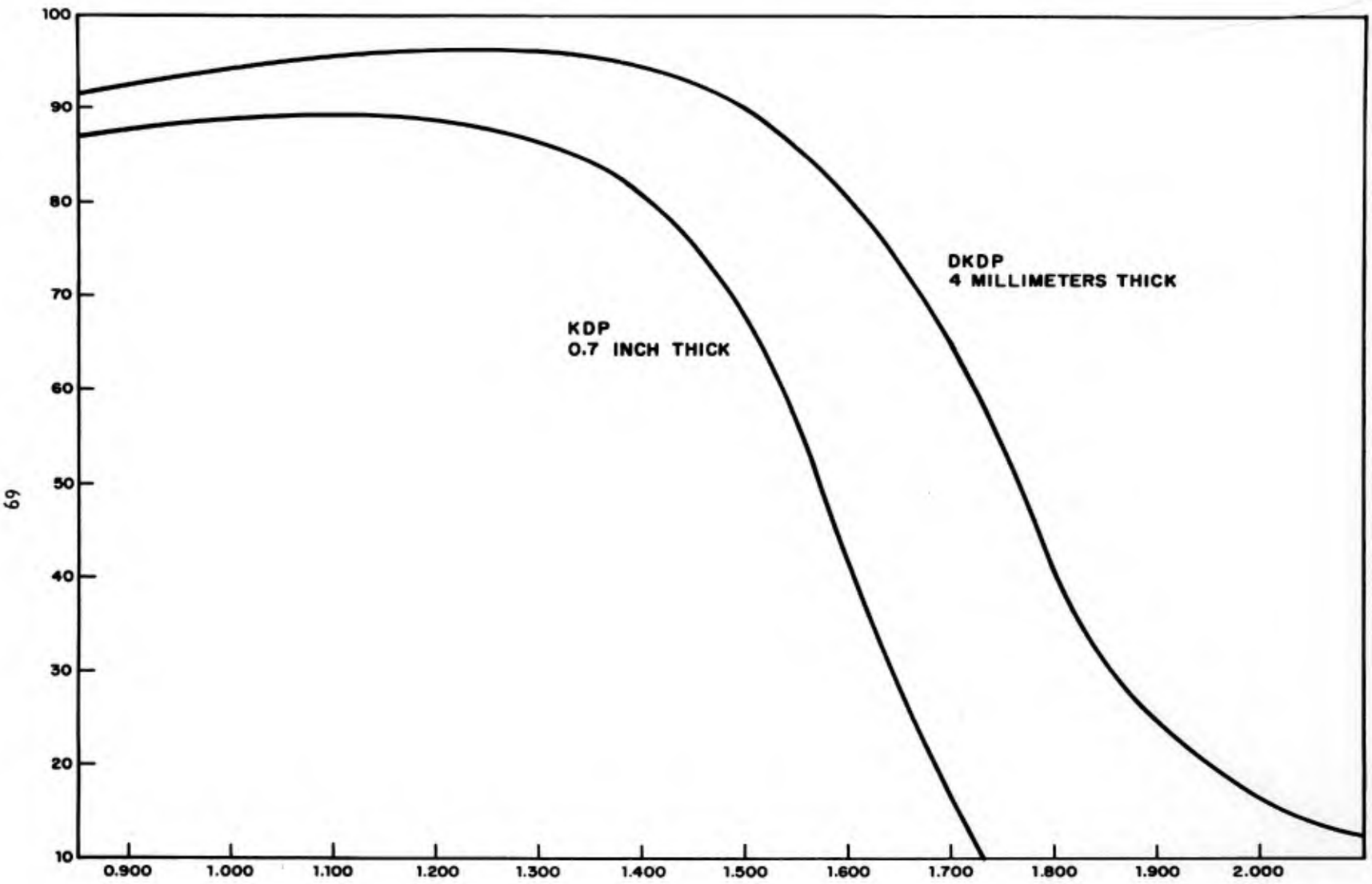

Figure 2.2 Transmission Curve, KDP Versus DKDP

2.4 Light Sources

2.4.1 Modulation Experiment with Hg^{198}

2.4.1.1 System Flatness

The system flatness figure for the plates and crystal used was found to be $\lambda/10$ ($\lambda = 5461\text{Å}$, Hg^{198}) as described in section 2.1.

2.4.1.2 Effective Finesse

The true reflectivity of the plates and the total loss introduced by the crystal were found to be 90.7 percent and 4.5 percent respectively in section 2.2. Using these values, the effective coefficient of finesse was found as follows:

$$F = 4R(1 - a) / [1 - R(1 - a)]^2$$

$$F = 190$$

$$\sqrt{F} = 13.6$$

2.4.1.3 Transmission

The predicted transmission loss attributable to the crystal can be expressed as:

$$I_t = \left(\frac{T}{T + a}\right)^2 I_o$$

$$I_t = 0.455\, I_o$$

Figure 1.8 shows that for $\bar{\Delta} = \lambda/10$ the peak transmission of the modulator would be less than $0.25\, I_o$. Introduction of the crystal loss produces the total peak transmission

$$I_t = (0.25)\, I_o - (0.45)(0.25)\, I_o$$

$$I_t < 0.13\, I_o$$

and since

$$\Delta f = c\Delta v = c\Delta\lambda/\lambda^2$$

$$\Delta f = C/2\pi d\sqrt{F}$$

is the half-bandwidth of the cavity. For d = 2 cm and F = 13.6,

$$2\Delta f = 350 \times 10^6 \text{ cps} \quad \text{(ideal)}$$

Figure 1.8 shows that the half-angle for $\bar{\Delta} = \lambda/10$ is 25 degrees, so the half wavelength is:

$$\frac{\lambda}{360^\circ}\ (25^\circ) = \frac{\lambda}{14}$$

The practical bandwidth of our modulator is therefore:

$$2\Delta f = 2\left|\frac{C}{2\pi d.14}\right|$$

$$= 330 \times 10^6 \text{ cps}$$

The nominal bandwidth of the Hg^{198} discharge is about 0.002Å or 200×10^6 cps. This is chiefly Doppler broadening:

$$\Delta\lambda_{\text{Doppler}} = 1.67\frac{\lambda_o}{C}\sqrt{\frac{2RT}{M}}\ \text{Å}$$

and is directly proportional to the square root of T (°Absolute). This effect forced us to run the lamp at low power for minimum bandwidth, which made the experiment very difficult to perform. An independent measurement of our source bandwidth is described in the remainder os section 2.4.1.

2.4.1.4 Source Bandwidth and Interferometer Bandwidth

The bandwidth of the F.P. cavity can be derived in the following way:

$$\sin\frac{\delta}{2} = \frac{1}{\sqrt{F}} = \text{half angle}$$

$$\frac{\lambda}{2\pi\sqrt{F}} = \text{half wavelength}$$

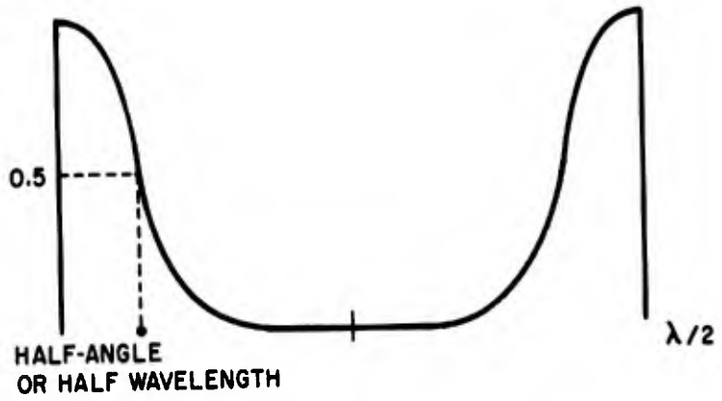

If there are N waves in the cavity then $N\Delta\lambda$'s sum to the half wavelength

$$N\Delta\lambda = \lambda/2\pi\sqrt{F}$$

or

$$d\Delta\lambda/\lambda = \lambda/2\pi\sqrt{F}$$

where

d = the plate separation

so that

$$\Delta\lambda/\lambda^2 = 1/2\pi d\sqrt{F}$$

Plates giving 90.7 percent reflectivity were assembled with a 1.5 mm spacer to form a Fabry-Perot etalon. The ring structure was photographed and the finesse was measured directly. The finesse is a measure of the ratio of fringe separation to fringe width and is expressed as

$$= \frac{\pi \sqrt{F}}{2}$$

For

$$R = 90.7 \text{ and } \sqrt{F} = 20.5$$

$$= 32$$

The measured finesse was 26 indicating 18.5 percent broadening. The free spectral range of the interferometer is defined as the change in wave number (Δv) required to shift the mth order fringe of wavelength $\lambda_o + \Delta\lambda$ into coincidence with the mth + 1 order fringe of wavelength λ_o.

$$\Delta\eta = \frac{1}{2d}$$

or

$$\Delta\eta = 3.333 \text{ cm}^{-1} \quad (d = 0.15 \text{ cm})$$

The measured fringe width was 0.15 mm giving a theoretical width of 0.125 mm.

The separation was 4 mm so:

$$\frac{0.025}{4} \Delta\eta = 0.021 \text{ cm}^{-1}$$

and

$$\Delta f = 625 \times 10^6 \text{ cps.}$$

2.4.1.5 Beam Divergence

The divergence of the collimated Hg^{198} light beam was measured and was found to be 0.003 radians.

2.4.1.6 Experimental Setup

Figure 2.3 is a schematic representation of the optical system and figure 2.4 is a block diagram of the associated electronics.

A 600 cps signal was used in the first modulation experiment in conjunction with a 600 cps bandpass amplifier (Δf = 630). The low power level of the Hg^{198} lamp proved to be a major difficulty and great pains were necessary to keep the noise level to a minimum. The d-c S/N ratio was only 10 and the a-c S/N ratio was 4. As a result the accuracy of the measurements was poor.

The interferometer and crystal were tuned following the procedure outlined in section 2.4.1.1. The modulated signal was measured on a Ballantine rms meter and the waveform was monitored on the C.R.O. The percent modulation was found to be approximately 15 percent of the d-c level with a 150 vrms driving signal. Rotation of the polarizer produced two well defined peaks when the direction of polarization was parallel to one or the other of the induced axes.

One of these peaks was slightly greater than the other. We attributed this effect to piezoelectric modulation. Such modulation would be in phase with only one of the axes and thus would add or subtract according to the direction of polarization. The piezoelectroc rolloff is close to 200 kc so it should not have any effect on the response from 1 to 30 mc.

The peak transmission of the modulator was measured by comparing the d-c output levels with the d-c input measured with the P.M. This was done with the crystal both in and out of the cavity. The transmission of the interferometer alone was 16 percent but dropped to 8 percent when the crystal was mounted in the cavity.

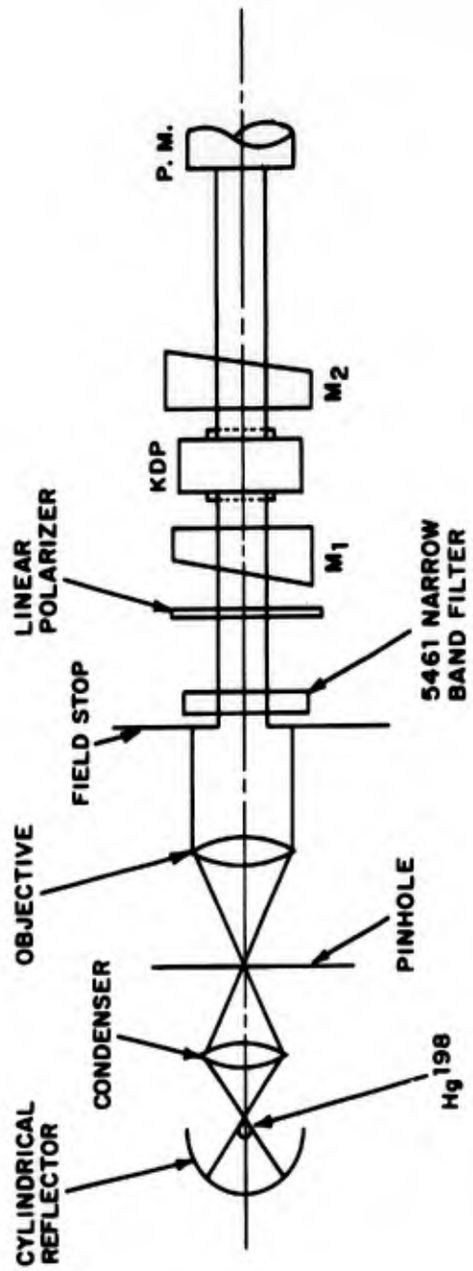

Figure 2.3 Block Diagram of the Optical System

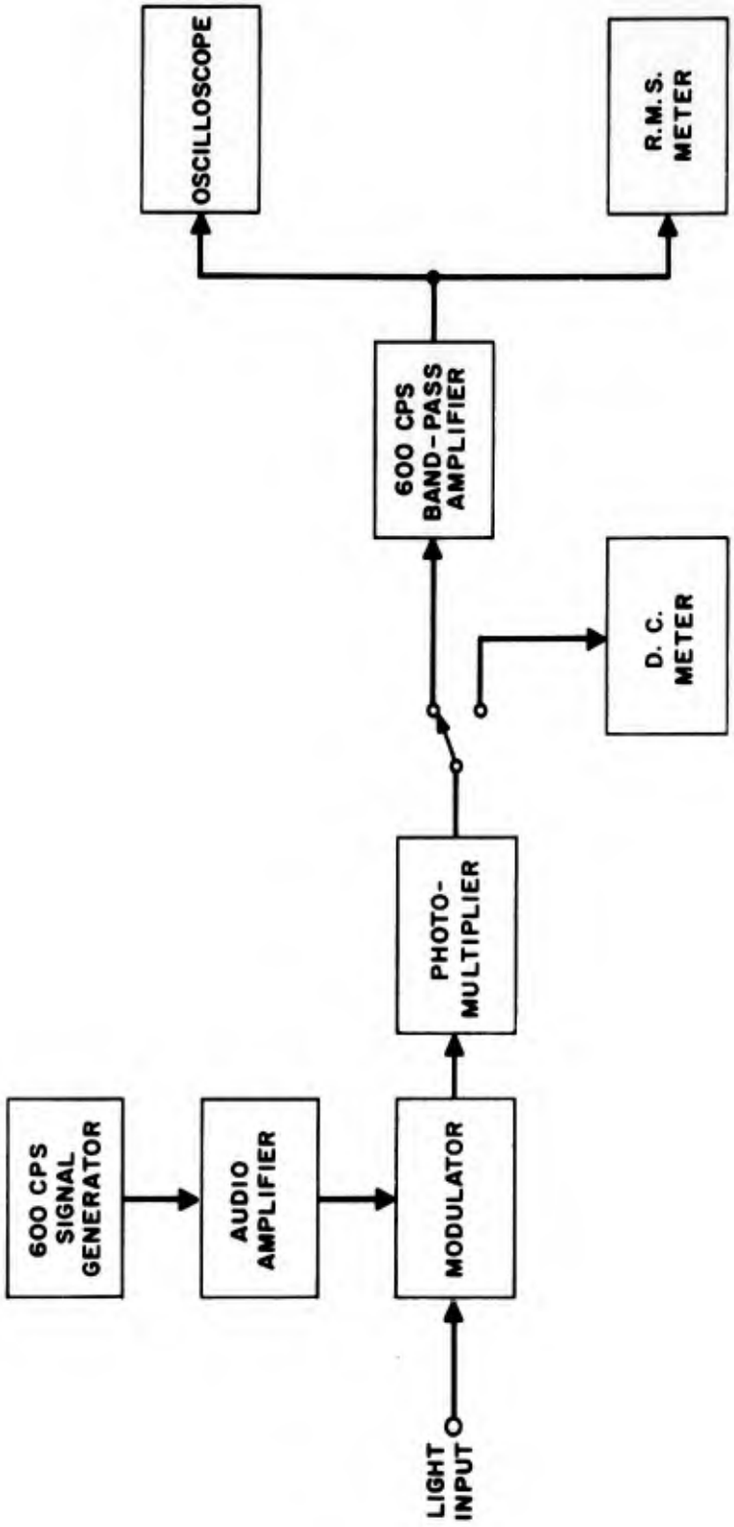

Figure 2.4 Block Diagram of the Electronic System

2.4.1.7 Correlation of Results with Theory

The large transmission loss of the interferometer alone was surprising in view of the measured flatness of the plates ($\lambda/240$) until we realized that poor plate adjustment was probably limiting the flatness figure to ~ $\lambda/8$ (see section 2.5.2). Curve d of figure 1-8 (R = 90 percent) shows that for $\overline{\Delta} \cong \lambda/14$ the peak transmission is about 17.5 percent. The 50 percent reduction in transmission caused by the introduction of the crystal was in agreement with the calculated loss of 45 percent.

Extrapolation of our measured modulating voltage indicated that ~ 350v 0 to peak would be required for 25 percent modulation. The poor modulation sensitivity was attributed chiefly to the source bandwidth, since we felt that this bandwidth should have been about 1/10 the bandwidth of the interferometer. Our calculations indicated that it was greater by a factor of two.

2.5 Modulator Measurements

2.5.1 Modulator Adjustment

Although all of the Fabry-Perot theory and equations are applicable to the present modulator configuration, it should be emphasized that it is not being used in the classical manner for the resolution of spectral components by fringes of equal inclination. Divergent light rays passing through the interferometer require the use of a lens at the output to focus then on the receiving screen to form the interference patterns. See figure 1-1.

Since we are using a very well collimated beam and therefore depend on direct interference of the emergent rays, optical alignment is highly important and requires the use of several unusual techniques. It is vital that the transmitted and reflected ray components be exactly superimposed to insure maximum interference.

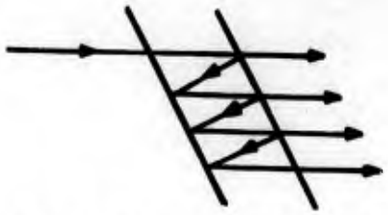

NO DIRECT INTERFERENCE

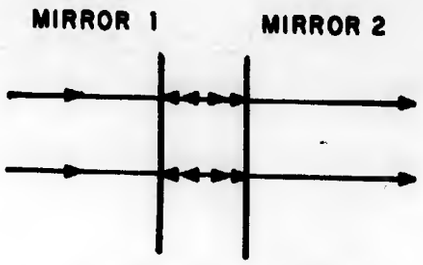

DIRECT INTERFERENCE

2.5.1.1 Mirror Adjustment

The interferometer has been provided with a precision adjustment to set mirror I exactly perpendicular to the input beam. After this adjustment has been made, mirror 2 must be made parallel with mirror 1. These two adjustments are accomplished as follows:

Mirror 1.

A thin plate is placed in the laser beam at least 50 cm away from the interferometer and is arranged so that the laser beam passes through a small aperture in its center. The image of the reflected beam should then be adjusted so that it is centered on the aperture. This procedure will apply even if optics are present between the aperture and the interferometer.

Mirror 2.

Mirror 2 can be made roughly parallel to mirror 1 by making the following adjustment. The source as viewed through the interferometer will appear as a series of images diminishing in brightness and extending in the direction of the open end of the wedge between the plates.

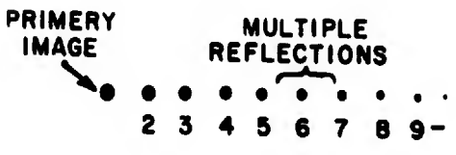

OBSERVED PATTERN

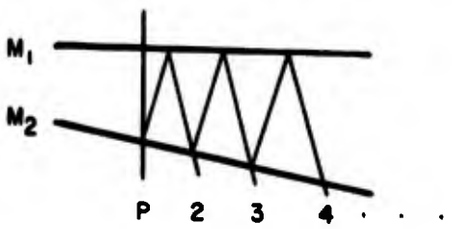

Mirror 2 is adjusted to bring all of these images into coincidence. The interference fringes should be directly observable by focusing the eye on a point in the center of the reflecting surface of mirror 2. An eye piece will greatly facilitate this observation. If the source is of sufficient strength the fringes will appear on a ground glass screen held at the exit side of mirror 2. The remaining small wedge between mirror 1 and mirror 2 is now eliminated by adjusting mirror 2 so that the number of fringes visible is reduced to a minimum (zero, if possible).

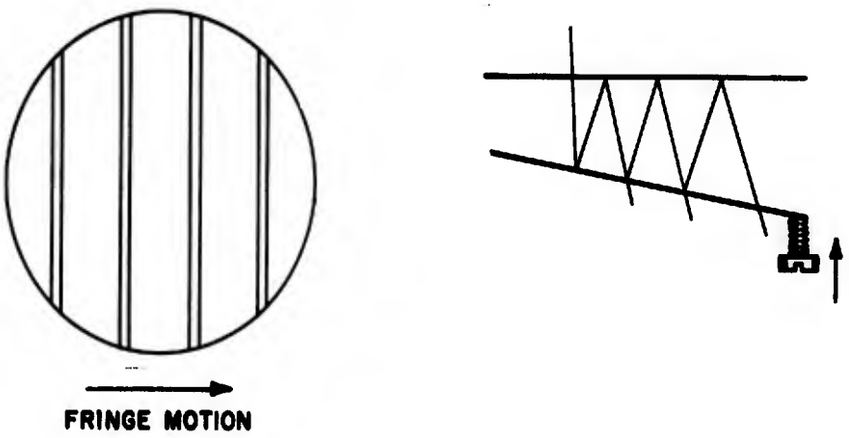

A very slight pressure on any part of the mirror mount should affect the intensity.

2.5.1.2 Crystal Adjustment

Finally the optical axis of the crystal is lined up with the optical axis of the interferometer. The angular aperture of the crystal when placed in the cavity is zero. As mentioned previously we depend on direct interference of the reflected and transmitted ray components and the KDP is birefringent for all rays that are off axis. If the input is linearly polarized then the birefringence has the effect of reducing the amplitude of the interfering components of successive transmitted rays. This is equivalent to a reduction in cavity Q and thus a reduced modulation index. The following procedure may be used to line up the optical axis.

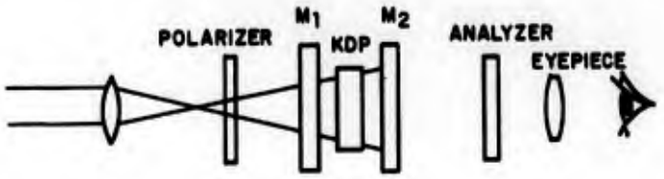

The input is diverged with suitable optics and polarized. The characteristic pattern of principal isogyres and rings is observable directly by rotating the analyzer. (This may be easier if an eyepiece is used.)

If the axis of the crystal is parallel to the cavity axis the pattern will be connected at all points and the center will consist of a well defined cross.

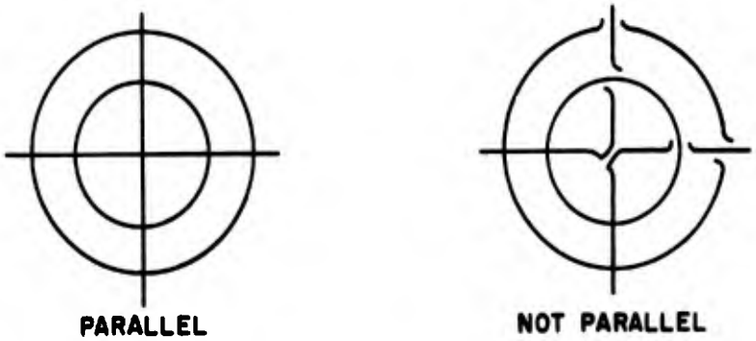

If the cross is broken at the first ring and distorted at the center, the axis is not parallel. The crystal is gimbal mounted and can therefore be adjusted to correct its orientation. After this final adjustment has been performed step (2) should be repeated for the crystal has probably lessened the degree of parallelism slightly.

2.5.1.3 Input Beam Polarization Adjustment

The input must be polarized in the direction of one of the induced optic axes (x' or y'). Since it is usually inconvenient to rotate the entire laser assembly the following procedure can be used to rotate the beam polarization. A quarter wave

plate placed with one of its axes parallel to the laser polarization produces circularly polarized light. A linear polarizer will now produce linearly polarized light that may be rotated through 360 degrees by rotating the polarizer. This combination will introduce about a 50 percent loss in input intensity. With the modulator in operation a slight rotation of the polarizer will peak the modulation index when the input is exactly parallel to the x' or y' axis.

2.5.1.4 Operating Point Adjustment

The optical length of the cavity will usually have to be adjusted to set the modulator at the proper operating point. Mirror 1 can be moved about ± one wavelength and can be easily adjusted to within $\lambda/20$ of the proper point without affecting the mirror parallelism.

2.5.2 Modulator Design

The curvatures of the mirror and crystal surfaces that determine the system flatness figure can be represented just as well by plane surfaces that deviate from parallelism by an amount equal to the flatness figure.

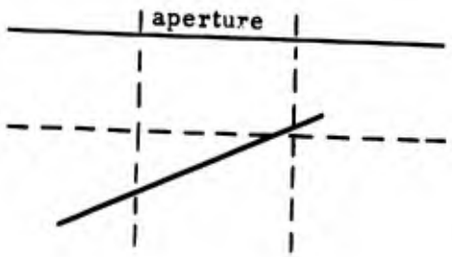

It is useful to represent the flatness in this way for it makes it possible to show that mirror alignment will limit the system flatness to relatively poor values.

Section 2.5.1 describes the optical technique developed to align the mirrors. The 1.0 inch aperture of the crystal limits the visually observable alignment that can be achieved to:

$$\theta = \frac{\lambda/2 \text{ cm}}{2.5 \text{ cm}} = \frac{3 \times 10^{-5}}{2.5} \text{ rad}$$

$$= 12 \times 10^{-6} \text{ rad}$$

$$= 2.4 \text{ sec}$$

The central 1/4 inch aperture has the same wedge angle but Δd is now $\lambda/8$. The plates may be made more parallel by adjusting them until no fringes are visible but the magnitude of Δd cannot be determined.

2.5.2.1 Mechanical Design of the Interferometer

Most of the specifications of the mechanical section of the interferometer were determined by trial prior to the confirmation of their validity in theory. The first interferometer tried was an etalon with the crystal mounted in a fixed position inside the etalon spacer. This system had two major disadvantages. The crystal's optic axis could not be adjusted with any facility and it was found that the faces of the spacer were not sufficiently parallel for use in a modulator, although the spacer produced good quality ring structures. Moreover the pressure exerted on the mirrors distorted them considerably from their nonstressed flatness figure. The most objectionable limitation imposed by a spacer is that the operating point (separation) cannot be adjusted. It is not desirable that the operating point be determined by the d-c bias on the crystal since the required voltage could be as high as 9 kv. ($1/4\lambda$ voltage.)

To eliminate these difficulties an interferometer was designed with the plates on movable platforms so that no forces are transmitted directly to them. This interferometer consists of one section that adjusts the cavity spacing axially and another that adjusts the angle between the plates.

The first plate of the interferometer is mounted on a precision tool slide which is mounted so that it is as close to parallel to the optical axis as possible. The small axial movement required for operating point adjustment thus contains practically no lateral component. When one of the plates of an interferometer is moved with respect to the other, the degree of parallelism must not be changed. The extreme straightness of the tool slide ways insures this. To set the angular adjustment of the second plate to within two seconds of arc an adjusting mechanism with a mechanical advantage linkage was designed to give 8 seconds of angular motion per turn of the adjusting screw. This is accomplished by a 48 thread/inch screw which pushes a wedge with a slope of 0.01. The movable plate rides on top of this wedge and the lever arm is 5 inches long. Two of these wedges are used and are arranged together with a pivot point to serve as a kinematic mount.

The KDP crystal is mounted in a gimbal that sits on the base of the interferometer between the two mirror plates.

2.5.2.2 Results

This interferometer was used in the first 600 cps modulation experiment and the adjustment precision seemed fully adequate.

It was found that the wedge surface wore vary rapidly and that the component of force in the direction of wedge motion was great enough to move the plate slightly in a lateral direction. Because of this the prototype interferometer was designed with a different mechanical linkage. The adjustment specification of 8 seconds per turn was retained for it was found to be adequate.

2.6 Electronic Measurements

A preliminary check of the unloaded amplifier showed it to have a reasonably flat response over its bandpass of 100 cps to 30 mc. This check was made before adjustment of the plate and grid line trimmer capacitors. The maximum output voltage as measured on a Tektronix 581 oscilloscope was 282 volts P-P (equivalent to 100 vrms for a pure sine wave) with an estimated distortion of 5 to 10%.

The amplifier was driven by an Hewlett-Packard 606A signal generator, which is capable of producing 3 vrms (8.5 v P-P) across the 50 ohm input impedance. The

amplifier output was measured with an Hewlett-Packard 410B VTVM, a Tektronix 545A oscilloscope with a type D differential preamplifier, and a Tektronix 481 oscilloscope. A differential voltmeter with RF response was not available.

The Hewlett-Packard 410B VTVM is very sensitive to distortion of RF sine waves. It was noted that the voltmeter was reading 10% low on a sine wave with about 5% distortion.

Since the crystal is voltage sensitive and not power sensitive, all measurements should be based on peak to peak, not RMS volts. Of course for pure sine waves peak to peak volts equal 2.828 RMS volts.

The full output of the amplifier was observable on the 545A oscilloscope with a type D differential preamplifier. However, the frequency limit of this setup was 1 mc, so most measurements had to be made on each differential half of the amplifier separately. However, it should be noted that the distortion of the full differential amplifier is less than the distortion of each of separate halves. Frequencies to 65 mc were measured with the 581 oscilloscope.

The unloaded frequency response of each amplifier differential half is shown in figure 2-5. The response is reasonably flat except for a sharp 6db dip at 17 mc. The midband voltage gain is approximately 50 and the response is down 3db at 86 cps and 45 mc.

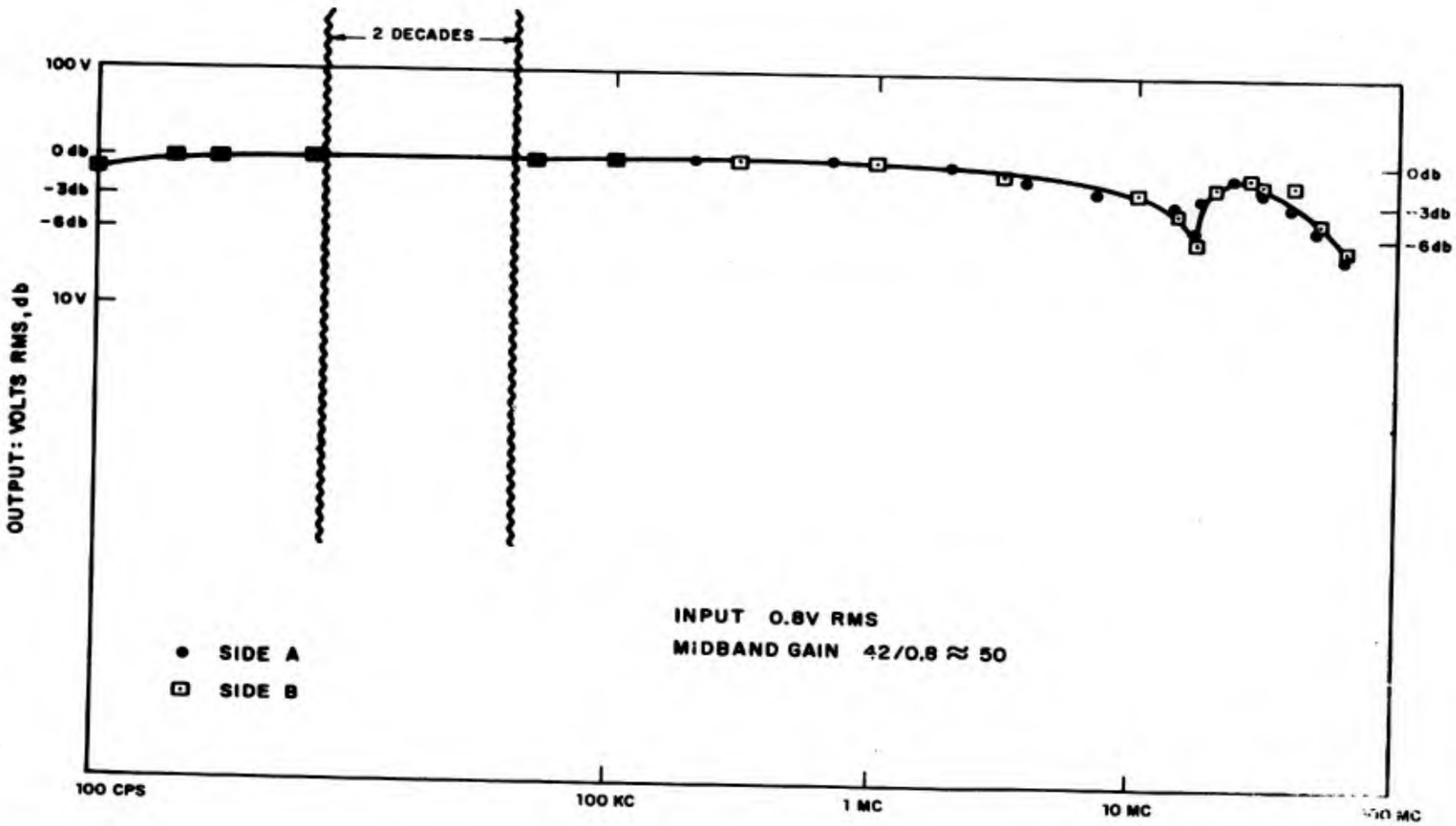

Figure 2-5. Frequency Response of Individual Differential Halves of Amplifier

3.0 FINAL MODULATOR DESIGN AND MEASUREMENTS

3.1 Description and Specifications of Final Modulator

The mechanical framework of the final Fabry-Perot interferometer holds the modulator crystal and interferometer mirrors in position in the light beam and supplies the means to make the adjustments that are necessary for proper modulator operation. The base of the framework mounts on a standard optical bench and can be moved along it parallel to the optical axis which is 6 inches above the bench. The base includes adjustments for making the first interferometer mirror perpendicular to the optical axis. Mounted on the base are the second mirror adjustment assembly, the operating point adjustment assembly and the crystal gimbal assembly. The second mirror adjustment assembly supplies a fine adjustment for making the second mirror parallel to the first, the operating point adjustment permits the first mirror to be moved about 1/4 wavelength with respect to the second while keeping the mirrors parallel and the crystal gimbal assembly permits the crystal to be tilted about two mutually perpendicular axes, each normal to the optical axis.

3.1.1 Second Mirror Adjustment

Figure 3-1 is a simplified illustration of this adjustment. The support angle is fastened to the base, while the mirror is held by the plate carrier. A line X-X through screw A and tiepoint C (a flexible column) forms a right angle with a line Y-Y through screw B and tiepoint C. Adjustment of screw A will cause the plate carrier to pivot or tilt about axis Y-Y, while adjustment of screw B will tilt the plate carrier about axis X-X.

The actual second mirror adjustment contains both coarse and fine adjustments for each pivot. Figure 3-2 shows one of these pivot adjustments. The other is exactly the same. A steel ball is trapped between the support angle and plate carrier at three corners (A, B, and C in figure 3-1) with each ball resting in a fine pitch cup-point screw threaded through the plate carrier. The axial position screw is used along with the two coarse adjustment screws to adjust mirror 2 along the optical axis. The coarse adjustment screws are primarily used to set the mirrors roughly parallel to each other.

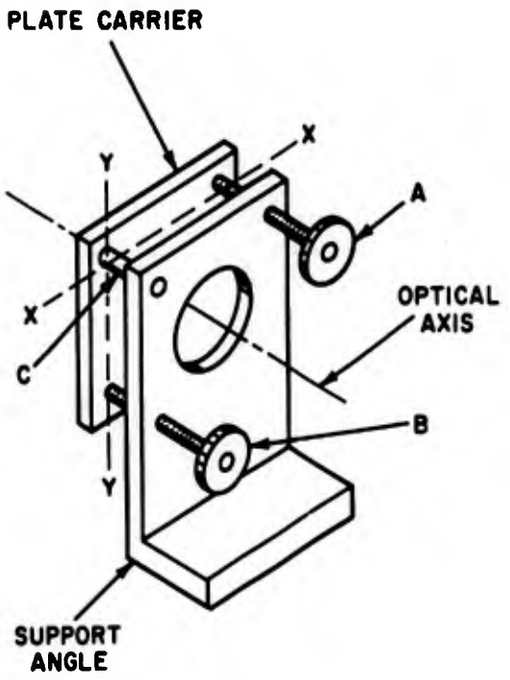

Figure 3-1. Simplified Illustration of Second Mirror Adjustment

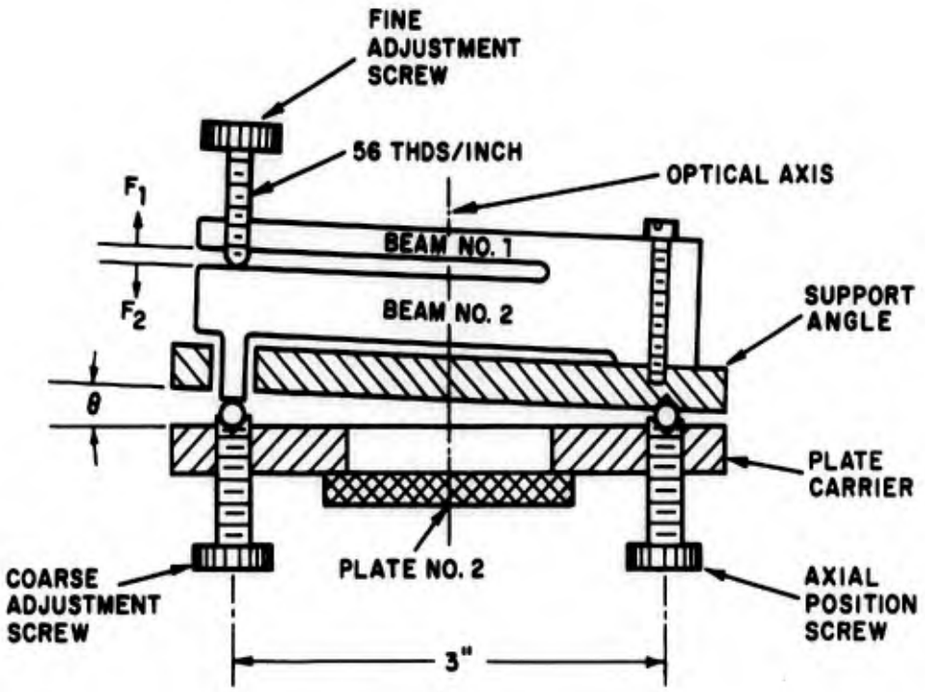

Figure 3-2. Coarse and Fine Pivot Adjustment for Second Mirror

3.1.2 Description of Fine Adjustment

A compound spring is used to reduce the action of the fine adjustment screw. When this screw is turned, beam #1 will move 145 times as far as beam #2 with respect to the support angle. Beam #2 transmits its motion to the plate carrier through the ball trapped by the coarse adjustment screw.

The angular movement of the plate carrier can be derived as follows:

Stiffness ratio of beam #2 to beam #1 = 145:1.

Therefore, for one turn of the fine adjustment screw, beam #1 will deflect

$$F_1 = 145\ F_2 \qquad (3.1\text{-}1)$$

but $F_1 + F_2 = 1/56$ inch $= 0.01786$ inch. (3.1-2)

Substituting (3.1-2) in (3.1-1)

$$F_1 = 145\ (0.01786 - F_1) = 2.5897 - 145\ F_1$$

or

$$F_1 = \frac{2.5897}{146} = 0.01774$$

$$F_2 = 0.01786 - 0.01774 = 0.00012 \text{ inch/turn.}$$

Since the distance between corners is three inches, the change in angle θ per turn will be

$$\theta = \frac{s}{l} = \frac{0.00012}{3} = 0.00004 \text{ radians per turn} = 8.75 \text{ seconds/turn.}$$

The adjustment ranges of the fine adjustment screws are limited to four turns by a clamp collar. The total fine adjustment range is therefore 33 seconds. The coarse adjustment range is 0.395 degree per turn.

3.1.3 Operating Point Adjustment Assembly

This assembly (figure 3-3) consists of a support angle and a parallel plate carrier separated by a strain column. The strain column is placed under

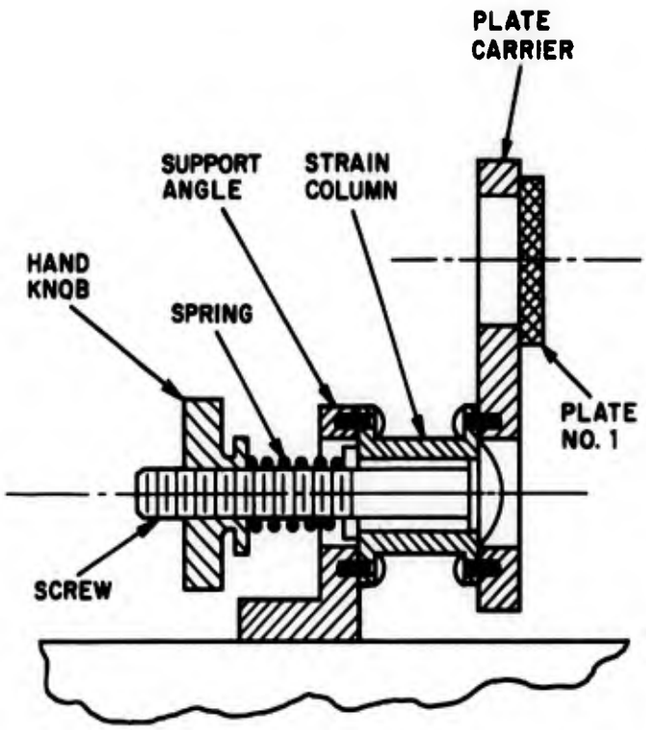

Figure 3-3. Operating Point Adjustment

compression by the combination of the screw, hand wheel and spring in figure 3-3. As shown below, 109 pounds compression force will shorten the strain column by 3/8 wavelength (3/4 wavelength for an alternate strain column supplied) while keeping the plate carrier parallel to the optical axis within the very narrow limits required by the modulator design.

The design of the strain column is based on the relationship between stress and strain expressed by Young's modulus of elasticity, E.

$$E = \frac{\text{stress}}{\text{strain}} = \frac{s}{\epsilon}$$

The strain required for the 1-1/4 inch long strain column is:

$$8.24 \times 10^{-6} \text{ inch } (3/8\lambda)$$

therefore,

$$S = \epsilon E = \frac{8.24 \times 10^{-6}}{1.25} \times 21 \times 10^{6} \text{ psi (Invar)}$$

$$= 138.6 \text{ psi.}$$

The outside diameter of the center portion of the strain column 1-1/4 inches and the inside diameter is 3/4 inch. The cross sectional area is thus 0.785 square inch, and the compressive load for 3/8λ motion is:

$$P = 138.6 \text{ lb/in}^2 \times 0.7854 \text{ in}^2 = 109 \text{ lb.}$$

A spring with a rate k = 228 lb/inch is used, while the loading screw has 32 threads to the inch.

Turns (handwheel) for 3/8λ motion =

$$\frac{109 \text{ lb}}{228 \text{ lb/in}} \times 32 \text{ threads/inch} = 15.25 \text{ turns.}$$

An alternate strain column for 3/4λ range is provided.

3.1.4 Crystal Gimbal and Base Adjustments

The crystal gimbal assembly is pictured in figure 3-4. The bearings have sufficient drag to hold any adjustment after it is made.

The adjustments on the base assembly are shown in figure 3-5. A movement of ±1.2 can be made in either plane of adjustment.

3.2 Measurements

3.2.1 Optics Adjustment

Initial testing of the modulation was carried with a gas optical maser operating at 6328 Å and with the modulator mirrors adjusted to give bar fringes. The bright areas of the bars were visibly too thick for the known reflectivities of the mirrors. This fringe broadening was finally traced to vibration of the cantilever mirror mounts on the modulator. The entire apparatus was moved from a third floor workbench to a basement lathe bed. The 12 foot lathe bed was isolated from the concrete floor by a compliant mounting consisting of 4 inflated automobile inner tubes. This successfully reduced the vibration due to conduction through the mounting structure to a level where the effects of vibrations caused by airborne sounds could be seen. Air duct vibrations, fan vibration, hand claps near the modulator, and loud talking were found to cause visible effects. Operation during the evening reduced some of these unwanted sounds.

3.2.2 D-C Modulation Sensitivity

The first measurement of modulation sensitivity was made by varying an applied d-c voltage and measuring the anode current of the photomultiplier tube used as a detector. These tests were used to select the best of the crystals and led to the decision to recoat the mirrors. A quasi-static modulation of 25% was obtained with a peak voltage change of 250 volts. The peak transmission of this configuration was 30%. Independent measurements showed that the mirror's reflectivity was 92%. Allowing for losses in the crystal, etc., the equivalent reflectivity was approximately 86%. It can be seen from figure 1-11 that curve C is a close approximation to this measured value, 180 volts peak for 86% equivalent reflectivity. This measurement indicates that the equivalent optical path variations are on the order of one twenty-fifth of a wavelength at 6328 Å.

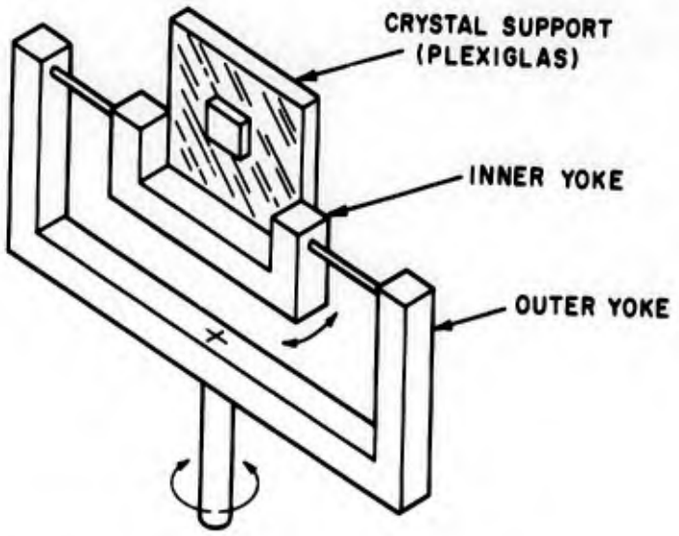

Figure 3-4. Crystal Gimbal Adjustment

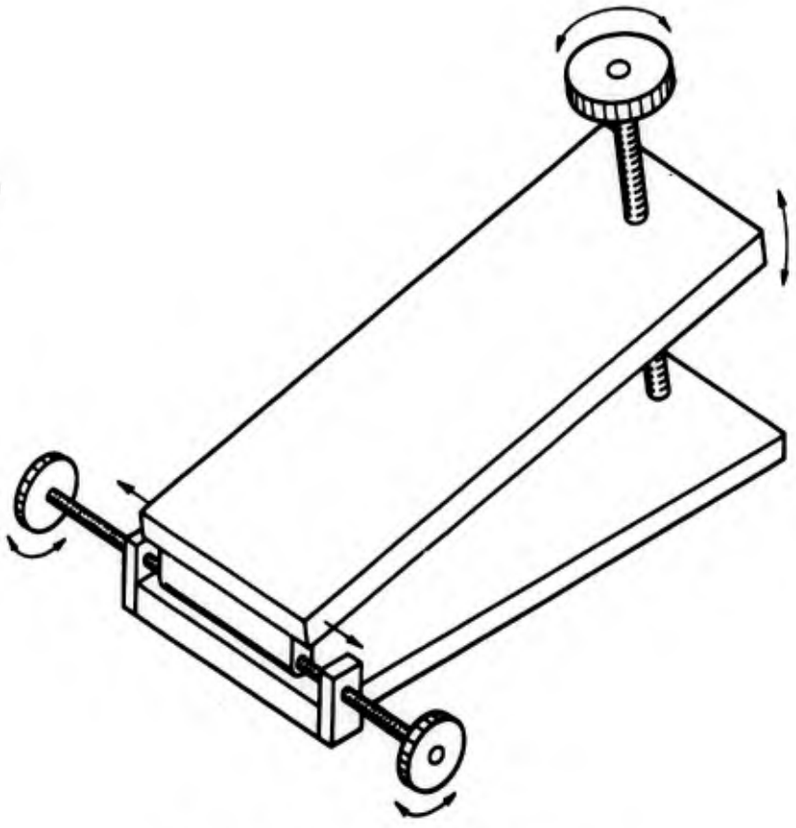

Figure 3-5. Base Adjustment

3.2.3 High Frequency Test Setup

The final modulator test setup consists of the following elements. The gas laser light source, a limiting aperture, the modulator, a narrow band filter for 6328 Å, and an RCA 7746 photomultiplier tube used as the detector are mounted on the optical bench with a common optical axis. The distributed amplifier built to drive the modulator is mounted close to the modulator crystal and is connected to it with two pieces of coaxial cable, grounded commonly to the modulator frame. An Hewlett-Packard 606A Signal Generator is used to drive the distributed amplifier. Provision is made for monitoring the voltage applied to the crystal with a Tektronix 581 oscilloscope.

The photomultiplier is energized by a variable, highly stable 1500 volt power supply. Up to three Hewlett-Packard distributed amplifiers follow the photomultiplier and drive a Tektronix 581 oscilloscope, with 185 ohm coaxial cable used for interconnections.

The RCA 7746 photomultiplier tube has a rise time of 2 nanoseconds, a maximum gain of 17×10^6, and a maximum anode current of 2 ma. This high anode current capability was important since the anode load resistor was 200 ohms. A 200 ohm load was needed for a detector bandwidth greater than 30 mc/s and was needed to match the input impedance of the wideband distributed amplifiers. The measured bandwidth of the three distributed amplifiers and scope in cascade was 65 mc/s at the 3db down point. The low frequency cutoff was approximately 100 kc/s because of the low frequency response of the amplifiers.

3.2.4 High Frequency Modulation Sensitivity

Only qualitative measurements of the modulator performance could be made because of two effects. When the photomultiplier tube was operated at low gain, the stray pickup from the 14 mc/s gas maser excitation masked the detected signal. At high gain, the noise level was excessive being 100 to 1,000 times the calculated shot noise for the measured d-c anode current. The noise level was of the same order of magnitude as the detected signal. By careful adjustment

of the scope synchronization, the waveform could be displayed. A crude estimate of the modulation index was made by estimating the scope deflection, dividing by the measured gain of the amplifiers and comparing this number with the measured d-c voltage across the 200 ohm load resistor. At 10 mc/s approximately 10% modulation was obtained with a 110 volt rms driving signal on the crystal. The modulator frequency response was tested from 100 kc/s to 30 mc/s and was found to follow the frequency response of the modulator electronics. Synchronization at frequencies above 20 mc/s was very difficult, but a 30 mc/s sine wave was displayed on several occasions.

3.2.5 Photomultiplier Tube Noise

An attempt was made to determine the cause of the excessive noise by exposing the photomultiplier tube to the straight through gas maser beam. Measurements in a fairly narrow band (approximately 1 mc/s) showed that anode currents greater than 10 μamps gave excessive noise. For example, 90 μamps anode current gave a noise level 10^3 times greater than the shot noise level calculated on the basis of 90 μamps, while at 4 μamps the noise level was only twice the calculated value. Since the light intensity was the same during these tests, it is concluded that at high current levels and high supply voltage values, the photomultiplier tube introduced excessive noise. This was probably due to ion feedback within the tube.

4.0 CONCLUSIONS

Wide band amplitude modulation of optical carriers has been demonstrated from d-c to 30 mc/s, by means of an electro-optic KDP crystal. The voltage required for 25% modulation was found to be 175 rms or about 3 times greater than the predicted value. It was found that the modulator response was flat (independent of driving characteristics) in the low pass band tested. It was not possible to perform distortion analysis of the modulated signal since the noise amplitude in the 30 megacycle band width was about 25% of the signal amplitude. It was found that interferometer vibration severely affected the modulator performance, and that the optics used do not represent the present limit of optical technology. Direct experimental verification of the transmission functions, and maximum modulation frequencies are lacking. The emperical determination of the transmission functions is felt to be extremely important, for if the experiments show the theory to be valid, future modulator design can proceed along practically achievable lines when parameters such as peak transmission, band width and signal distortion are definitely known.

Appendix A - Transmission of a Fabry-Perot Modulator

A ray picture for a Fabry-Perot interferometer can be drawn by following the procedure of Jenkins and White[1], but allowing for absorption within the cavity as well as in the mirrors. Assume an amplitude of one for the incident wave, then let t and t' be the fractions of the incident wave amplitude transmitted into and out of the cavity by the mirrors, and let r be the fraction of the amplitude that is reflected by the mirrors. Let a be the fraction of the intensity of the incident wave absorbed in the cavity so that (1-a) is the fraction transmitted. The ratio of amplitudes due to absorption within the cavity is then proportional to $\sqrt{1-a}$, since amplitude squared is proportional to intensity. With these definitions, a ray picture can be drawn. (See following page.)

The vector summation of the amplitudes shows that a $\sqrt{1-a}$ can be associated with the tt' term and a $(\sqrt{1-a})^{2n}$ can be associated with the r^{2n} term. The transmission of the interferometer can eventually be written

$$\frac{I_t}{I_i} = \frac{(tt'\sqrt{1-a})^2}{[1-r^2(1-a)]^2} \quad \frac{1}{1+\frac{4r^2(1-a)}{[1-r^2(1-a)]^2}\sin^2\frac{\theta}{2}}$$

If transmission (the fraction of the intensity of the incident wave transmitted) is defined by:

$$T = tt'$$

and reflectivity by

$$R = r^2 ,$$

---

[1] Jenkins and White, Fundamentals of Optics, Third Edition, McGraw-Hill, pp. 263,264 273 and 274.

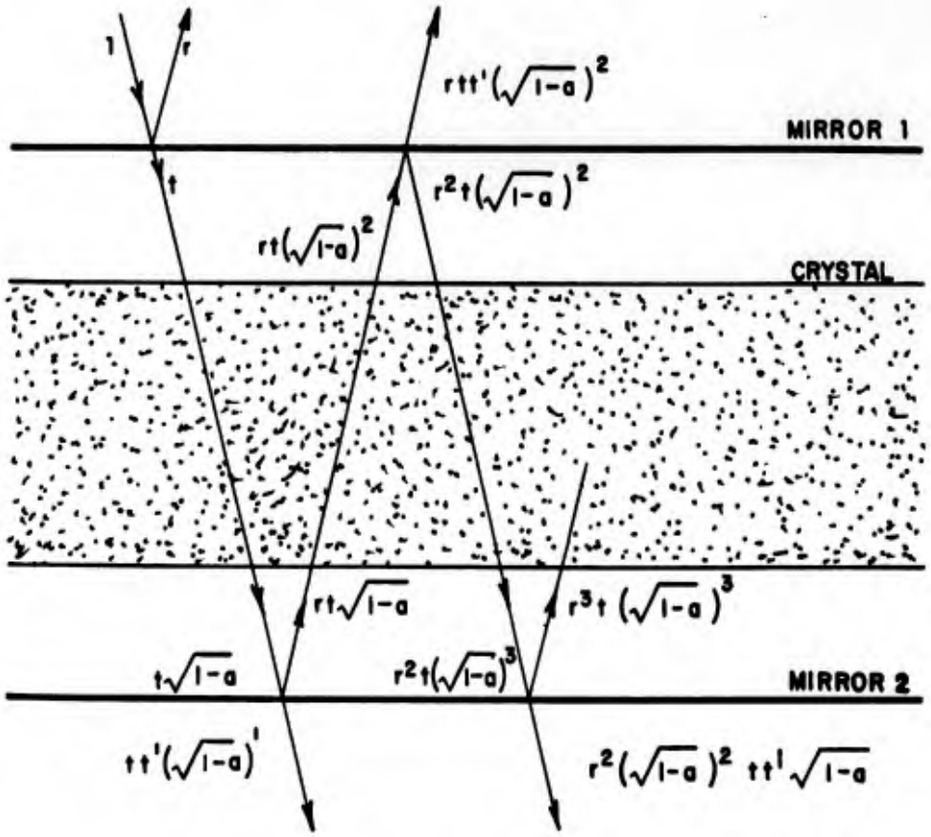

Ray Picture

the equivalent transmission T' and the equivalent reflectivity R' can be defined by

$$T' = T(\sqrt{1-a})$$

$$R' = R(1-a).$$

The effective finesse of the Fabry-Perot interferometer is then

$$F_{eff} = \frac{4\,R'}{(1-R'^2)^2} \quad .$$

The transmission expression can then be written conveniently as

$$\frac{I_t}{I_i} = \left(\frac{T'}{1 - R'}\right)^2 \frac{1}{\left(1 + F_{eff} \sin^2 \frac{\theta}{2}\right)}$$

The absorption A at the mirror surface is expressed by the usual energy balance equation

$$1 = T + R + A$$

or

$$R = 1 - (T + A)$$

Expressing R' in terms of R and substituting in the above expression:

$$R' = R(1-a) = (1-a)[1-T-A]$$

and

$$1-R' = a + T(1-a) + A(1-a)$$

The peak transmission becomes

$$\left.\frac{I_t}{I_i}\right]_{\theta=k2\pi} = \frac{T^2(1-a)}{\left[T(1-a) + A(1-a) + a\right]^2}$$

When a is small, second order terms can be neglected and the denominator becomes approximately $(T + A + a)^2$.

Appendix B - Estimation of Modulation Sensitivity

The transmission of an ideal Fabry-Perot interferometer is:

$$T_i = (1 + F \sin^2 \frac{\theta}{2})^{-1}$$

where

$$\theta = \frac{4\pi nt}{\lambda}$$

and

$$F = \frac{4R}{(1 - R)^2}$$

The rate of change of transmission with a change in phase angle is:

$$\frac{dT_i}{d\theta} = - (1 + F \sin^2 \frac{\theta}{2})^2 \; F \, d (\sin^2 \frac{\theta}{2}) = \frac{- F \sin\frac{\theta}{2} \cos \frac{\theta}{2}}{(1 + F \sin^2 \frac{\theta}{2})^2}$$

for $T_i = 1/2$,

$$\frac{1}{2} = \frac{1}{1 + F \sin^2 \frac{\theta}{2}}$$

so

$$\sin \frac{\theta}{2} = \frac{1}{\sqrt{F}}$$

Assume that $\cos \frac{\theta}{2} \approx 1$ for small values of θ. The transmission as a function of the optical path p is:

$$\frac{dT_i}{dp} = \frac{dT_i}{d\theta} \cdot \frac{d\theta}{dp}$$

where

$$p' = np \text{ (optical path length)}$$

and

$$\frac{d\theta}{dp} = \frac{4\pi}{\lambda}$$

so

$$\frac{dT_i}{dp} = - \frac{\pi \sqrt{F}\, n}{\lambda}$$

Let

$$\Delta T_i \approx \frac{\pi \sqrt{F}}{\lambda} \Delta t$$

Since

$$\Delta p' = \Delta np$$

$$\Delta T_i \approx \frac{\pi \sqrt{F}\, n_o^3\, r_{63}\, E_Z\, p}{Z \lambda}$$

or

$$\Delta T_i \approx \frac{\pi \sqrt{F}\, n_o^3\, r_{63}\, V_Z}{2\lambda}$$

Appendix C. - Probability Distribution if One of the Mirror Surfaces is Spherical

In figure C-1 mirror 1 is flat and mirror 2 is spherical with a radius of curvature R.

A circular aperture of radius a is assumed.

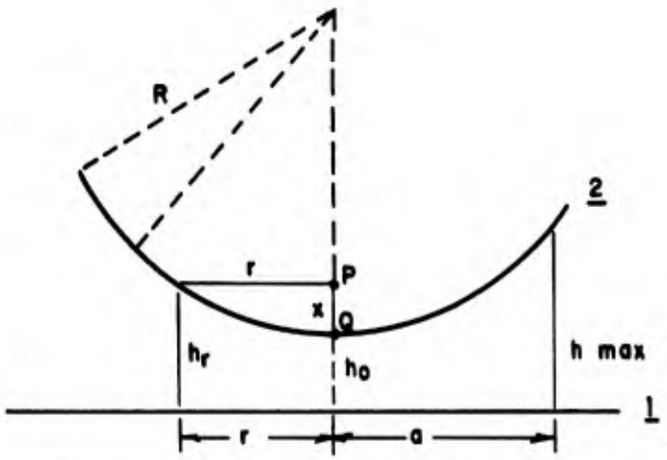

Figure C-1. Spherical Mirror Surface

Surface dA is located between the two radii r and r + dr on mirror 2. Its area is $2\pi r dr$.

This surface dA is at a distance h_r from the mirror 1 .

The probability P of this surface is expressed as:

$$P = \frac{dA}{A} = \frac{2\pi r dr}{\pi a^2} = \frac{2r dr}{a^2}$$

As shown below, rdr in figure 1 can be expressed as dh.

$$x \text{ times } (2R - x) = r^2$$

$$x = R\left[1 - \sqrt{1 - \left(\frac{r}{R}\right)^2}\right]$$

$$h_r = h_o + R\left[1 - \sqrt{1 - \left(\frac{r}{R}\right)^2}\right]$$

$$dh = \frac{rdr}{R\sqrt{1 - \left(\frac{r}{R}\right)^2}} \qquad rdr = R\sqrt{1 - \left(\frac{r}{R}\right)^2}\, dh$$

$$P = (h,\ h + dh) = \frac{2R\sqrt{1 - \left(\frac{r}{R}\right)^2}}{a^2}\, dh$$

It can be shown that:

$$a^2 = (h_{max} - h_o)\left[2R - (h_{max} - h_o)\right]$$

$$P(h,\ h + dh) = \frac{2R\sqrt{1 - (r/R)^2}}{(h_{max} - h_o)\left[2R + h_o - h_{max}\right]}\, dh$$

If $R >> r$:

$$P(h,\ h + dh) = \frac{2R\, dh}{C_1} = C_2 \times dh$$

When C_1 and C_2 are constants, $dA = P(h,\ h + dh) \times A = C_2 \times A \times dh$.

Using the symbol Δ instead of h, we get the expression for $A = S = 1$:

$$dA = dS = f(\Delta)\, d\Delta.$$

Appendix D - Rectangular Distribution of Surface Imperfections

As mentioned in 1.2.2, the total surface of mirror 2, which is at a distance of $p + \Delta$ and $p + \Delta + d\Delta$ from mirror 1, is given by the formula:

$$dS = f(\Delta)\, d\Delta \tag{D-1}$$

in which $f(\Delta)$ is the distribution of the deviation Δ on the surface of mirror 2.

A distance Δ is proportional to a phase difference $\delta\zeta$ as shown below:

$$\delta\zeta = \frac{4\pi\Delta}{\lambda} \tag{D-2}$$

(λ = wavelength)

Substituting (D-2) in (D-1) gives:

$$dS = \text{constant times } g(\delta\zeta)\, d(\delta\zeta) \tag{D-3}$$

The deformed transmission curve $J(\zeta)$ is expressed by:

$$J(\zeta) = 1/S \int I(\zeta)\, dS \tag{D-4}$$

in which $I(\zeta)$ is the Airy formula transmission curve.

We take $\delta\zeta$ as the variable instead of Δ.

$$J(\zeta) = \frac{\int I(\zeta+\delta\zeta)\, g(\delta\zeta)\, d(\delta\zeta)}{\int g(\delta\zeta)\, d(\delta\zeta)} \tag{D-5}$$

For a rectangular probability distribution:

$$g(\delta\zeta) \text{ is constant for } -\delta\zeta_{max} < \delta\zeta < \delta\zeta_{max} \tag{D-6}$$

$$g(\delta\zeta) \text{ is } 0 \quad \text{for } \delta\zeta > \left|\delta\zeta_{max}\right|$$

and for the Airy formula in (D-5)

$$J(\zeta) = \frac{1}{2\delta\zeta_M} \int_{-\delta\zeta_M}^{+\delta\zeta_M} \frac{d(\delta\zeta)}{1 + 4h \sin^2 \frac{(\zeta + \delta\zeta)}{2}} - \tag{D-7}$$

if

$$h = \frac{R}{(1 - R)^2} \tag{D-8}$$

Solution for formula (D-7):

$$J(\zeta) = \frac{1}{\sqrt{4h + 1}\,\delta\zeta_M} \left[\operatorname{arc} \left(\sqrt{4h + 1} \tan \frac{\zeta + \delta\zeta_M}{2} \right) - \operatorname{arc} \left(\sqrt{4h + 1} \tan \frac{\zeta - \delta\zeta_M}{2} \right) \right] \tag{D-9}$$

If $\zeta \to 0$:

$$4h \sin^2 \frac{\zeta + \delta\zeta}{2} = h (\zeta + \delta\zeta)^2 \tag{D-10}$$

Substituting (D-10) in (D-9):

$$J(\zeta) = \frac{1}{2\delta\zeta_M} \int_{-\delta\zeta_M}^{+\delta\zeta_M} \frac{d(\delta\zeta)}{1 + h (\zeta + \delta\zeta)^2} \tag{D-11}$$

$$J(0) = \frac{1}{\sqrt{h}\,\delta\zeta_M} \operatorname{arc\ tg} \left(\sqrt{h}\ \delta\zeta_M \right) \tag{D-12}$$

Appendix E - Gaussian Distribution of Surface Irregularities

In general the deformed transmission curve (formula (D-5) in Appendix D) is given by:

$$J_{(\phi)} = \frac{\int I(\phi + \delta\phi)\, g(\delta\phi)\, d(\delta\phi)}{\int g(\delta\phi)\, d(\delta\phi)} \qquad \text{(E-1)}$$

The Gaussian distribution curve is defined by:

$$f(x) = \int_{-\infty}^{+\infty} \sqrt{\frac{\alpha}{\pi}}\; e^{-\alpha x^2}\; dx. \qquad \text{(E-2)}$$

in which α is determined by the standard deviation:

$$\alpha = \frac{1}{2\sigma^2} \qquad \text{(E-3)}$$

It is known that $f(\sigma) \approx 0.6 \times f(0)$.

If we substitute (E-2) in (E-1) we get:

$$J_{(\phi)} = \frac{\int_{-\infty}^{+\infty} I(\phi + \delta\phi)\sqrt{\frac{\alpha}{\pi}}\; e^{-\alpha\delta\phi^2}\; d(\delta\phi)}{\int_{-\infty}^{+\infty} \sqrt{\frac{\alpha}{\pi}}\; e^{-\alpha\delta^2}\; d(\delta\phi)} \qquad \text{(E-4)}$$

With the aid of the Airy formula:

$$I(\phi + \delta\phi) = \frac{(1 - R)^2}{1 + R^2 - 2R\cos(\phi + \delta\phi)} \qquad \text{(E-5)}$$

and if we substitute (E-5) in (E-4):

$$J_{(\phi)} = \frac{(1 - R)^2 \sqrt{\frac{\alpha}{\pi}} \int_{-\infty}^{+\infty} \frac{e^{-\alpha\delta\phi^2}\, d(\delta\phi)}{1 + R^2 - 2R\cos(\phi + \delta\phi)}}{\sqrt{\frac{\alpha}{\pi}} \int_{-\infty}^{+\infty} e^{-\alpha\delta^2}\, d(\delta\phi)} \qquad \text{(E-6)}$$

The denominator of (E-6) can easily be solved with the next integral:

$$\int_0^{\infty} e^{-a^2x^2}\, dx = \frac{1}{2a}\sqrt{\pi}$$

(E-6) can now be written as follows:

$$J(\phi) = (1 - R)^2 \sqrt{\frac{a}{\pi}} \int_{-\infty}^{+\infty} \frac{e^{-a\delta\phi^2}\, d(\delta\phi)}{1 + R^2 - 2R\cos(\phi + \delta\phi)} \qquad \text{(E-7)}$$

For $|R| < 1$, the following development exists[1]

$$\frac{1 - R^2}{1 + R^2 - 2R\cos(\phi + \delta\phi)} = 1 + 2\left[R\cos(\phi + \delta\phi)\cos 2(\phi + \delta\phi) + \ldots\ldots\right.$$

$$\left. + R^n \cos n(\phi + \delta\phi) + \ldots\ldots\ldots\ldots\right]$$

$$= \sum_{n=0}^{\infty} E_n R^n \cos\theta(\phi + \delta\phi) \qquad \text{(E-8)}$$

where:

$$E = \begin{cases} 1 \text{ if } n = 0 \\ 2 \text{ in all other cases} \end{cases}$$

---

[1] T. J. Bromwich: Theory of Infinite Series, MacMilland and Co., Ltd. 186(1955)

The desired integral can now be written in the form:

$$J(\phi) = \frac{1}{1 - R^2} \sqrt{\frac{\alpha}{\pi}} \int_{-\infty}^{+\infty} e^{-\alpha \delta\phi^2} \sum_{n=0}^{\infty} E_n R_m \cos n(\phi + \delta\phi)\, d(\delta\phi) =$$

$$= \frac{1}{1 - R^2} \sqrt{\frac{\alpha}{\pi}} \sum_{n=0}^{\infty} E_n R_n \left[\cos n\phi \int_{-\infty}^{+\infty} e^{-\alpha \delta\phi^2} \cos n\, \delta\phi\, d(\delta\phi) - \right.$$

$$\left. - \sin n\phi \int_{-\infty}^{+\infty} e^{-\alpha \delta\phi^2} \sin n.\ \delta\phi\, d(\delta\phi) \right] \qquad \text{(E-9)}$$

The integrand of the second integral is an odd function which causes it to vanish. To evaluate the first integral, we recognize that:

$$I_n = \int_{-\infty}^{+\infty} e^{-\alpha \delta\phi^2} \cos n\, \delta\phi\, d(\delta\phi) = \int_{-\infty}^{+\infty} e^{-\alpha \delta\phi^2} e^{in\, \delta\phi}\, d(\delta\phi) \qquad \text{(E-10)}$$

Now:

$$I_n = \int_{-\infty}^{+\infty} e^{-\alpha \delta\phi^2 + in\, \delta\phi}\, d(\delta\phi) = e^{-\frac{n^2}{4\alpha}} \int_{-\infty}^{+\infty} e^{-\left[\sqrt{\alpha}\, \delta\phi - \frac{in}{2\sqrt{\alpha}}\right]^2} d(\delta\phi)$$

Letting:

$$Z = \sqrt{\alpha}\, \delta\phi - \frac{in}{2\sqrt{\alpha}} \quad , \text{ we find that: } I_n = \sqrt{\frac{\pi}{\alpha}}\, e^{-\frac{n^2}{4\alpha}} \qquad \text{(E-11)}$$

Consequently:

$$J(\phi) = \frac{1}{1 - R^2} \sqrt{\frac{\pi}{\alpha}} \sqrt{\frac{\alpha}{\pi}} \sum_{n=0}^{\infty} E_n R^n \cos n\phi \, e^{-\frac{n^2}{4\alpha}} =$$

$$= \frac{1}{1 - R^2} \left[1 + 2 \sum_{n=1}^{\infty} R^n \cos n\phi \, e^{-\frac{n^2}{4\alpha}} \right] \qquad \text{(E-12)}$$

For comparison of the Gaussian distribution with the rectangular curve, we must decide which values for α are to be put in formula (E-12).

For a given surface and a wavelength λ, $\sqrt{\bar{\Delta}^2}/\lambda$ can be determined. (Δ = deviation from flatness).

We now consider $\sqrt{\bar{\Delta}^2}/\lambda$ to be the standard deviation of the surface.

In the case of a Fabry-Perot interferometer the following relation exists:

$$\delta\phi = 4\pi . \frac{\Delta}{\lambda} .$$

For a rectangular distribution:

$$\delta\phi_{max} = 4\pi \times \sqrt{3} \times \frac{\sqrt{\bar{\Delta}^2}}{\lambda} = 21.766 \times \frac{\sqrt{\bar{\Delta}^2}}{\lambda} . \qquad \text{(E-13)}$$

While for a Gaussian distribution, the standard deviation of $\delta\phi$ is defined by the following equation:

$$\delta\phi = \text{standard deviation} = 4\pi \times \frac{\sqrt{\bar{\Delta}^2}}{\lambda} \qquad \text{(E-14)}$$

When we compare (E-14) with (E-13) we see that the standard deviation of $\delta\phi$ for a Gaussian distribution is $1/\sqrt{3}$ times the standard deviation for a rectangular distribution. (E-15)

If a Gaussian distribution of the surface irregularities occurs, the deformed transmission curve is given by:

$$J(\phi) = \frac{1}{1 - R^2}\left[1 + 2 \sum_{n=1}^{\infty} R^n \cos n\phi \, e^{-\frac{n^2}{16\pi^2} \times \frac{1}{\left(\frac{\sqrt{\Delta^2}}{\lambda}\right)^2}}\right] \qquad \text{(E-16)}$$

An approximation formula for J(0) has been derived by Dufour and Picca[2]:

$$J_1(0) = \sqrt{\pi} \times \mu \times e^{-\mu^2} \times \left[1 - \theta(\mu)\right] \qquad \text{(E-17)}$$

in which:

$$\theta(\mu) = \frac{2}{\pi} \int_0^{\mu} e^{-t^2} \, dt$$

and

$$\mu = \frac{1}{\sqrt{0.6667 \times h \times \delta\phi_M^2}}$$

The influence of the Doppler effect of the light source on $I_{(\phi)}$ can be compared with a Gaussian distribution of surface imperfections.

Burger and van Cittert[3] derived the next equations for fringe-broadening if the Doppler effect occurs:

ϕ_1 is defined as follows:

$$I(\phi_1) = \frac{I(0)}{2}$$

$$J(\phi_1) = \frac{J(0)}{2} \qquad \text{(E-18)}$$

---

[2] C. Dufour and R. Picca, Revue d' Optique 24, 1945, 19.

[3] Zeitschrif for Physik 1928, Vol. 51, p. 638; Vol. 79, p. 722; Vol. 81, p. 428

ϕ_1/ϕ_0 can be calculated with the aid of the following equations:

$$0 < \sqrt{h\overline{\delta\phi}^2} < 0.34; \qquad \phi_1/\phi_0 = \sqrt{1 + 3h\,\overline{\delta\phi}^2}$$

$$0.34 < \sqrt{h\,\overline{\delta\phi}^2} < 1.25; \qquad \phi_1\phi_0 = 0.8 + 0.95\sqrt{h\overline{\delta\phi}^2}$$

} if $0.7 < R < 1.$

$$1.25 < \sqrt{h\,\overline{\delta\phi}^2} < 3.40; \qquad \phi_1/\phi_0 = 0.64 + 1.15\sqrt{h\,\overline{\delta\phi}^2}, \text{ if } R = 0.9$$

$$\phi_1/\phi_0 = 0.65 + 1.16\sqrt{h\,\overline{\delta\phi}^2}, \text{ if } R = 0.8$$

$$\phi_1/\phi_0 = 0.54 + 1.22\sqrt{h\,\overline{\delta\phi}^2}, \text{ if } R = 0.7$$

Using formula (E-12) the $J_{(\phi)}$ curve has been calculated, the calculations giving $J_{(0)}$ and ϕ_{11} for which $J_{(\phi_1)} = J_{(0)}/2$.

With formulas (E-17) and (E-18): $J_1(0)$ and ϕ_1 have been calculated.

The agreement between the calculated values is high.

Appendix F - Harmonic Content of Modulator Output Beam

Consider a Fabry-Perot interferometer in which the spacer layer is an ADP or KDP crystal oriented with its optic axis (z-axis) normal to the reflecting surfaces. Application of an alternating electric field in the z-direction periodically changes the crystal from uniaxial to biaxial, having an index of refraction for plane polarized light on the proper orientation such that

$$n = n_o (1 + \epsilon \cos \omega_M t) \qquad \text{(F-1)}$$

where

n_o = index of refraction in z-direction with no field.

$\epsilon = \left(\frac{r_{63} n_o^2}{2d} \right) V$, $r_{63} = 8.2 \times 10^{-7}$ cm/Kv (for ADP**).

d = geometrical thickness of the slab.

V = amplitude of voltage applied to crystal.

Suppose at $t = t_o$ a monochromatic wave front with surfaces of constant phase parallel to the reflecting surfaces of the interferometer reaches the left hand face of the crystal which we select as our reference surface as in figure F-1. If the medium had constant properties, the electric vector of a wave front originating at A after traveling a distance s is, in the steady state, the real part of

$$E = E_o e^{i[ks - \omega(t - t_o)]} \qquad \text{(F-2a)}$$

The propagation constant for a medium of constant properties is simply $k = \omega/v$, where v is the phase velocity $= c/n = \lambda f/n = (\lambda\omega)/(2\pi n)$.

**Billings, B.H., The Electro-optic effect in uniaxial crystals of type XH_2PO_4, I, J.O.S.A., Vol. 39, No. 10 (1949).

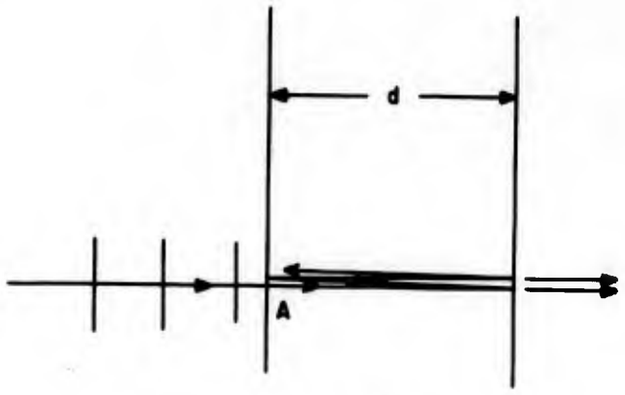

Figure F-1.
Path of Light Rays in Interferometer

Introducing this value of k in equation (F-2a) we are led to the familiar expression

$$E = E_o \, e^{i\left[\frac{2\pi ns}{\lambda} - \omega (t - t_o)\right]} \qquad \text{(F-2b)}$$

which allows us to find the instantaneous amplitude at any time and at any distance from the starting point A. The product ns can be recognized as the optical path of the ray.

If the properties of the medium are changing with time, equation (F-2b) is no longer applicable. For a medium characterized by an index of refraction n(t), the instantaneous speed of propagation of the ray is

$$v(t) = \frac{c}{n(t)} \qquad \text{(F-3)}$$

and, consequently, in a time dt the wave front advances a distance

$$ds = \frac{c}{n(t)} \, dt$$

Thus, after a time $t - t_o$ it has traveled the geometrical distance s, given by

$$s = c \int_{t_o}^{t} \frac{dt}{n_o \left[1 + \epsilon \cos \omega_M t\right]} \qquad \text{(F-4)}$$

Letting $\omega_M t = 2 \tan^{-1} u$ the integral can be transformed into an easily evaluated expression,

$$s = \frac{2c}{n_o \omega_M} \int_{u_o}^{u} \frac{du}{1 + \epsilon + (1-\epsilon) u^2} = \frac{2c}{n_o \omega_M \sqrt{1-\epsilon^2}} \tan^{-1} \left[\sqrt{\frac{1\epsilon}{1+\epsilon}}\ u\right] \Bigg|_{u_o}^{u}$$

Substituting for u its value as a function of t we have,

$$s = \frac{2c}{n_o \omega_M \sqrt{1-\epsilon^2}} \left\{ \tan^{-1} \left[\sqrt{\frac{1-\epsilon}{1+\epsilon}}\ \tan\left(\frac{\omega_M t}{2}\right)\right] - \tan^{-1} \left[\sqrt{\frac{1-\epsilon}{1+\epsilon}}\ \tan\left(\frac{\omega_M t_o}{2}\right)\right] \right\} \qquad \text{(F-5)}$$

The phase difference between the disturbance that has moved a total distance s and the instantaneous value of the disturbance at A is clearly

$$\Delta \Phi = \omega(\Delta t) \qquad \text{(F-6)}$$

where Δt denotes the time interval $t - t_o$ which results when equation (F-5) is solved for t as a function of s and t_o. Before proceeding any further, let us recognize that in all cases of practical interest the parameter ϵ is a very small number. For a slab 1 cm. thick, with an applied voltage of 1 Kilovolt, ϵ is about 10^{-6}. Then, retaining only first order terms in ϵ, we can write s in the much simpler form

$$s = \frac{2c}{n_o \omega_M} \left\{ \tan^{-1} \left[(1-\epsilon) \tan\left(\frac{\omega_M t}{2}\right)\right] - \tan^{-1} \left[(1-\epsilon) \tan\left(\frac{\omega_M t_o}{2}\right)\right] \right\} \qquad \text{(F-7)}$$

From equation (F-6) it follows immediately that in the limit $\epsilon \to 0$, s is simply $\frac{c}{n_o}(t - t_o)$. A plot of the distance which the wave front originating at A has traveled as a function of the product $\frac{c}{n_o}(t - t_o)$ is a straight line of slope 1 as shown in figure F-2.

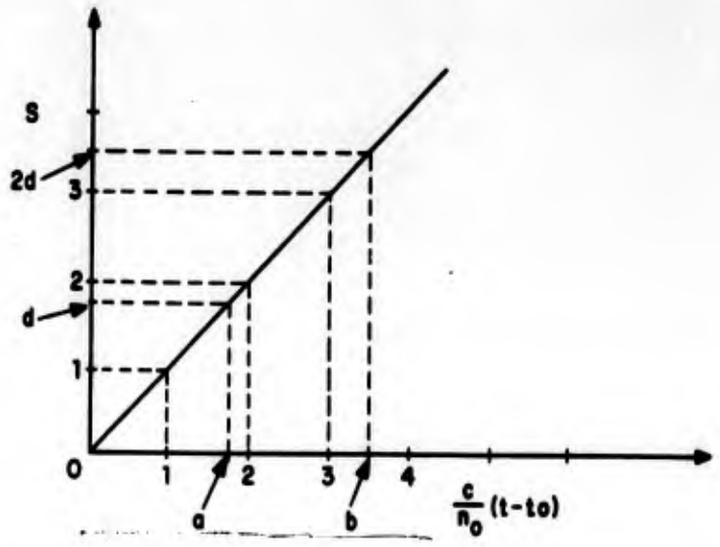

Figure F-2.
Distance of Wave Front Travel, $\epsilon \rightarrow 0$

If we wished to find the phase difference between wave fronts that have traveled distances d, 2d, 3d, ... etc. and the wave front at the origin, we could read off the corresponding values of $(t - t_o)$ and after substituting them in equation (F-6) obtain,

$$\Delta\phi_1 = 2\pi f \frac{n_o d}{c} = \frac{2\pi}{\lambda} (n_o d)$$

$$\Delta\phi_2 = 2\pi f \left(\frac{n_o 2d}{c}\right) = \frac{2\pi}{\lambda} (2\, n_o d)$$

$$\Delta\phi_3 = 2\pi f \left(\frac{n_o 3d}{c}\right) = \frac{2\pi}{\lambda} (3\, n_o d)$$

When equation (F-7) is plotted as a function of the product $\frac{c}{n_o} (t - t_o)$ we obtain a diagram which is the straight line of figure F-2 on which there are superimposed small undulations due to the periodic variations in index of refraction. Figure F-3 shows this situation.

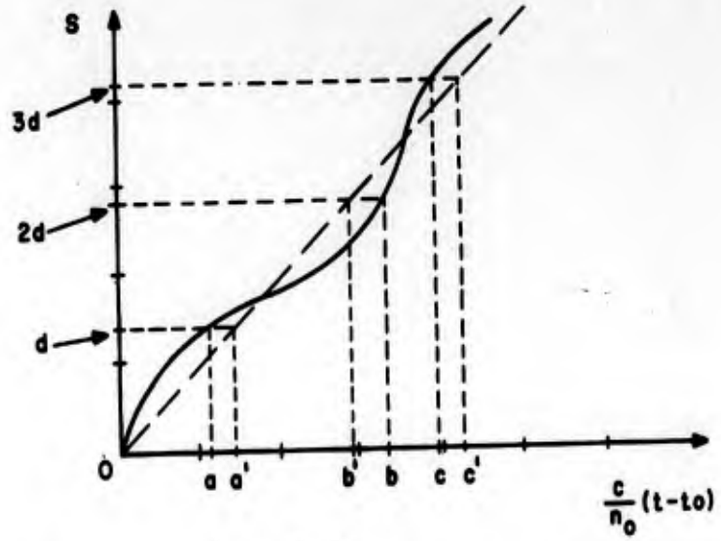

Figure F-3.
Distance of Wave Front Travel, First Order Terms of ϵ

The phase difference between a wave front at d, 2d, 3d, ... etc. and a wave front just reaching the origin could be found if the position of the points a, b, c, ... etc. on the horizontal axis were known. Such information can be obtained by solving equation (F-7) (or the exact equation F-5 for the time difference $t - t_o$. The solution for general values of ϵ is very involved and numerical answers cannot be easily extracted from it. Fortunately, we can make use of the smallness of ϵ in order to obtain a more tractable solution without sacrificing numerical accuracy.

In essence what we do is find a perturbation expansion of equation (F-7) and retain only the term independent of ϵ and the term varying linearly with ϵ. That is,

$$s = \frac{2c}{n_o \omega_M} \left\{ \frac{\omega_M}{2} (t - t_o) + \frac{\epsilon}{2} \left[\sin \omega_M t_o - \sin \omega_M t \right] \right\} \qquad \text{(F-8)}$$

Let us now write

$$t - t_o = t_s + \Delta t \qquad \text{(F-9)}$$

where $t_s = \frac{n_o s}{c}$ is the time required to travel the distance s in the absence of an applied electric field. Referring to figure F-3 we see that with a distance $s = d$, t_s is proportional to $0a'$, whereas Δt is proportional to aa'. We can then write

$$\frac{\omega_M t_s}{2} = \frac{\omega_M}{2}(t_s + \Delta t) + \frac{\epsilon}{2}\left\{\sin \omega_M t_o - \sin \omega_M [t_o + t_s + \Delta t]\right\}$$

or,

$$\frac{\epsilon}{2} \sin \omega_M (t_o + t_s\ t\ \Delta t) - \frac{\omega_M}{2} \Delta t = \frac{\epsilon}{2} \sin \omega_M t_o$$

which, to within first order terms in ϵ gives,

$$\Delta t = \frac{2\epsilon}{\omega_M} \sin\left(\frac{\omega_M n_o s}{2c}\right) \cos\left(\omega_M t_o + \frac{\omega_M n_o s}{2c}\right) \qquad \text{(F-10)}$$

Let us examine this equation in some detail.

When $\left(\frac{\omega_M n_o s}{2c}\right) \ll 1$ (low modulation frequency and moderate s) this expression approaches

$$\Delta t \rightarrow \epsilon \left(\frac{n_o s}{c}\right) \cos \omega_M t_o \qquad \text{(F-11)}$$

In this case the phase difference is

$$\Delta\phi = \frac{\omega n_o s}{c} [1 + \epsilon \cos \omega_M t] = \frac{2\pi n_o s}{\lambda} [1 + \epsilon \cos \omega_M t]$$

and the intensity of the transmitted light, for an interferometer with ideal reflecting surfaces, is very approximately,

$$\frac{I}{I_o} = \frac{1}{1 + F \sin^2\left[\frac{2\pi n_o d}{\lambda}(1 + \epsilon \cos \omega_M t)\right]} \qquad \text{(F-12)}$$

where

$$F = \frac{4r^2}{(1 - r^2)^2}$$

There is nothing very surprising about this result.

Consider now the case where the approximation F-11 is not applicable. The phase difference between the wave front which has traveled a distance s = (2k-1)d and the wave front that has traveled the distance s = d is,

$$\phi_k = \omega\left\{\frac{2n_o(k-1)d}{c} + \epsilon\left(\frac{\omega}{\omega_M}\right)\left[\sin\omega_M\left(t_o + \frac{(2k-1)\,n_o d}{c}\right) - \sin\omega_M\left(t_o + \frac{n_o d}{c}\right)\right]\right\}$$

$$= 2(k-1)\,\Phi + \delta_k \qquad \text{(F-13)}$$

where

$$\Phi_o = \frac{2\pi n_o d}{\lambda} \qquad \text{(F-13a)}$$

and

$$\delta_k = \epsilon\left(\frac{\omega}{\omega_M}\right)\left\{\sin\left[\omega_M t_o + (2k-1)\frac{\omega_M n_o d}{c}\right] - \sin\left[\omega_M t_o + \frac{\omega_M n_o d}{c}\right]\right\} \qquad \text{(F-13b)}$$

We are now in a position to calculate the intensity of the light transmitted by the interferometer. For conciseness, let us introduce the following parameters

$$\alpha = \epsilon\left(\frac{\omega}{\omega_M}\right) \qquad \text{(F-14a)}$$

$$\Omega = \left(\frac{\omega_M}{\omega}\right)\Phi_o \qquad \text{(F-14b)}$$

Then, if $|t^2|$ and $|r^2|$ are the transmission and reflection coefficients for the end surfaces of the interferometer, the resultant amplitude can be written in the form

$$A = t^2\left[1 + r^2 e^{i(2\phi_o + \delta_2)} + r^4 e^{i(4\phi_o + \delta_3)} + \ldots\right] \qquad \text{(F-15)}$$

with

$$\delta_k = \alpha \left[\sin(\psi + 2(k-1)\Omega) - \sin\psi\right]$$

$$\psi = \omega_M t_o + \Omega, \quad r' = r e^{i\phi_o}$$

In view of the identity

$$e^{i\delta_k} = e^{-i\alpha\sin\psi} \sum_{n=-\infty}^{\infty} J_n(\alpha)\, e^{i n[\psi + 2(k-1)]\Omega}$$

it follows that we can write

$$A = t^2\left\{1 + e^{-i\alpha\sin\psi} \sum_{k=1}^{\infty} (r')^{2k} \sum_{n=-\infty}^{\infty} J_n(\alpha)\, e^{in[\psi + 2k\Omega]}\right\}$$

$$= t^2\left\{1 + e^{-i\alpha\sin\psi} \sum_{-\infty}^{\infty} J_n(\alpha)\, e^{in\psi}\left[\frac{(r')^2 e^{i2n\Omega}}{1 - (r')^2 e^{i2n\Omega}}\right]\right\}$$

$$= t^2\left\{1 + e^{-i\alpha\sin\psi} \sum_{-\infty}^{\infty} J_n(\alpha)\, e^{in\psi}\left[\frac{1 - 1 + (r')^2 e^{i2n\Omega}}{1 - (r')^2 e^{i2n\Omega}}\right]\right\}$$

$$= t^2\left\{1 + e^{-i\alpha\sin\psi} \sum_{-\infty}^{\infty} J_n(\alpha)\, e^{in\psi}\left[\frac{1}{1 - (r')^2 e^{i2n\Omega}} - 1\right]\right\}$$

$$= t^2\left\{1 - 1 + e^{-i\alpha\sin\psi} \sum_{-\infty}^{\infty} \frac{J_n(\alpha)\, e^{in\psi}}{1 - (r')^2 e^{i2n\Omega}}\right\}$$

$$= t^2 e^{-i\alpha\sin\psi} \sum_{n=-\infty}^{\infty}\left[\frac{J_n(\alpha)\, e^{in\psi}}{1 - (r')^2 e^{i2n\Omega}}\right] = t^2 e^{-i\alpha\sin\psi} \sum_{n=-\infty}^{\infty} \frac{J_n(\alpha) e^{in\psi}}{1 - r^2 e^{i2(\delta + n\Omega)}} \qquad \text{(F-16)}$$

where δ is the fractional order of the interferometer in the absence of an applied field, that is,

$$\Phi_o = K\pi + \delta\,, \quad \text{where K is an integer} \qquad \text{(F-16a)}$$

Equation (F-16) can be written in the equivalent form

$$A = t^2 e^{-i\alpha \sin\psi} \sum_{n=-\infty}^{\infty} \frac{J_n(\alpha)\, e^{in\psi} \left[1 - r^2 e^{-i2(\delta+n\Omega)}\right]}{1 - 2r^2 \cos 2(\delta + n\Omega) + r^4}$$

$$= t^2 e^{-i\alpha \sin\psi} \left[S_1 - r^2 S_3\right] \qquad \text{(F-17)}$$

where

$$S_1 = \sum_{-\infty}^{\infty} \frac{J_n(\alpha)\, e^{in\psi}}{\Delta_n}$$

$$S_3 = \sum_{-\infty}^{\infty} \frac{J_n(\alpha)\, e^{-i2\delta}\, e^{in(\psi-2\Omega)}}{\Delta_n}$$

$$\Delta_n = 1 - 2r^2 \cos 2(\delta + n\Omega) + r^4$$

The intensity of the resultant beam is

$$I = AA^* = \left|t^4\right| \left[S_1 S_1^* - r^2(S_1 S_3^* + S_1^* S_3) + r^4 S_3 S_3^*\right] \qquad \text{(F-18)}$$

where the star denotes complex conjugation. From the definitions of S_1 and S_3 it follows that

$$S_1 S_1^* = \sum_{m=-\infty}^{\infty} \sum_{n=-\infty}^{\infty} \frac{J_n(\alpha)\, J_{n-m}(\alpha)\, e^{im\psi}}{\Delta_n \Delta_{n-m}} \qquad \text{(F-19a)}$$

$$S_3 S_3^* = \sum_{m=-\infty}^{\infty} \sum_{n=-\infty}^{\infty} \frac{J_n(\alpha)\, J_{n-m}(\alpha)\, e^{im(\psi-2\Omega)}}{\Delta_n \Delta_{n-m}} \qquad \text{(F-19b)}$$

$$S_1 S_3^* + S_1^* S_3 = 2 \sum_{m=-\infty}^{\infty} \sum_{n=-\infty}^{\infty} \frac{J_n(\alpha)\, J_{n-m}(\alpha)}{\Delta_n \Delta_{n-m}} \cos \left[m(\psi - 2\Omega) + 2n\Omega + 2\delta \right] \qquad \text{(F-19c)}$$

From these equations it is an easy matter to pick out the various order harmonics of the output beam.

It can be shown that the m-th harmonic has intensity

$$I_m = 2 \left| t^4 \right| \sum_{n=-\infty}^{\infty} \frac{J_n(\alpha)\, J_{n+m}(\alpha) \cos \left[m\psi + \zeta_n^m \right]}{\sqrt{\Delta_n \Delta_{n+m}}} \qquad \text{(F-20)}$$

where

$$\tan \zeta_n^m = \frac{2 \left| r^2 \right| \sin m\Omega \cos \left[(2n+m)\Omega + 2\delta \right] - \left| r^4 \right| \sin 2m\Omega}{1 - 2 \left| r^2 \right| \cos m\Omega \cos \left[(2n+m)\Omega + 2\delta \right] + \left| r^4 \right| \cos 2m\Omega}$$

For the low order harmonics equation (F-20) may be written in a simplified form provided $\Omega \ll 1$. We have

$$I_m \rightarrow - \frac{4 \left| t^4 \right| \cos m\psi}{1 - \left| r^4 \right|} \sum_{k=1}^{\infty} \left| r^{2k} \right| J_m(2\alpha \sin k\Omega) \sin k(2\delta - m\Omega)$$

In particular, the DC term is given by the expression

$$I_o = \frac{\left| t^4 \right| \sqrt{2}}{1 - \left| r^4 \right|} \sum_{k=o}^{\infty} \epsilon_k \left| r^{2k} \right| \cos \left(2k\delta + \frac{\pi}{4} \right) J_o(2\alpha \sin k\Omega) \qquad \text{(F-21a)}$$

where

$$\epsilon_o = 1, \quad \epsilon_k = 2, \quad k \neq 0.$$

and the first harmonic by the similar expression

$$I_1 = - \frac{4 \left| t^4 \right|}{1 - \left| r^4 \right|} \cos \psi \sum_{k=1}^{\infty} \left| r^{2k} \right| \sin 2k\delta\, J_1(2\alpha \sin k\Omega) \qquad \text{(F-21b)}$$

In general, it is equation (F-20) that must be used. This is not as serious as it would appear at first sight, because the higher modulation frequencies are associated with correspondingly smaller values of α, the argument of the Bessel functions in equation (F-20). For low values of the common argument, Bessel functions of increasing order decrease very rapidly and it is only necessary to take a few terms in the series (F-20) to obtain accurate numerical answers.

Appendix G - Theory of Distributed Amplifiers

The basic configuration of a distributed amplifier is shown in figures G-1 and G-2. The configuration shown in figure G-1 uses lumped delay lines consisting of constant-k T sections as a first approximation to a smooth line. Figure G-2 shows a second approximation to a smooth line using m-derived sections, and is the one used in the final amplifier.

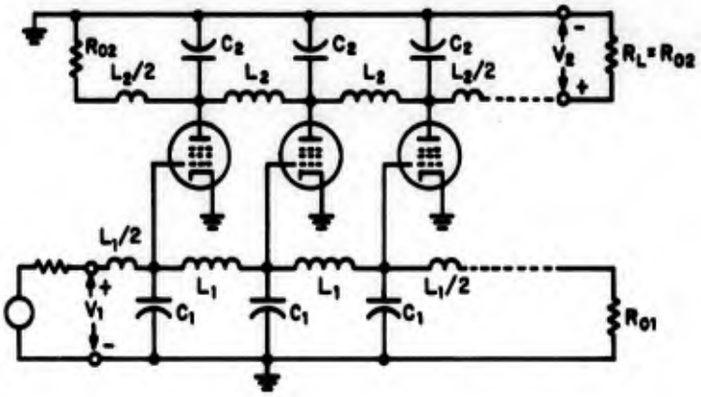

Figure G-1. Distributed Amplifier Using Constant-k Section Delay Lines.

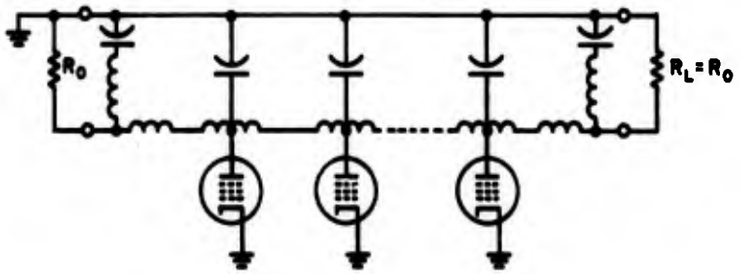

Figure G-2. Plate Line Using m-Derived Sections.

An explanation of these two lumped lines is given below.

The general form of the constant-k T section is shown in figure G-3.

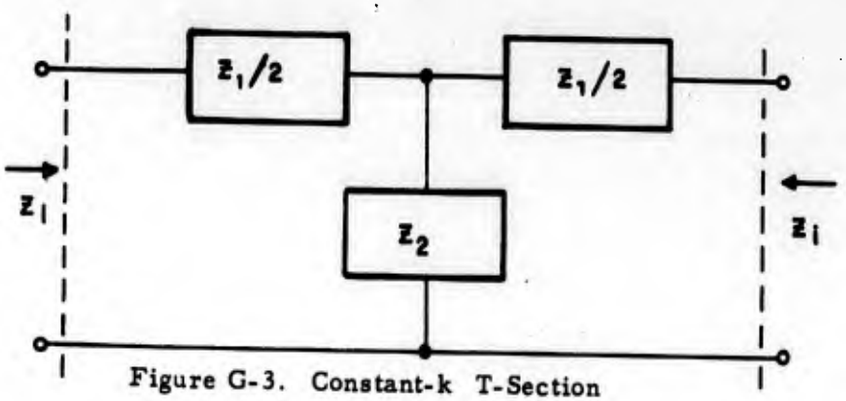

Figure G-3. Constant-k T-Section

The image impedance Z_i looking into this structure is

$$Z_i = \sqrt{Z_1 Z_2 + \frac{Z_1^2}{4}} \qquad \text{(G-1)}$$

The m-derived T section follows directly from the constant-k section as shown in figure G-4.

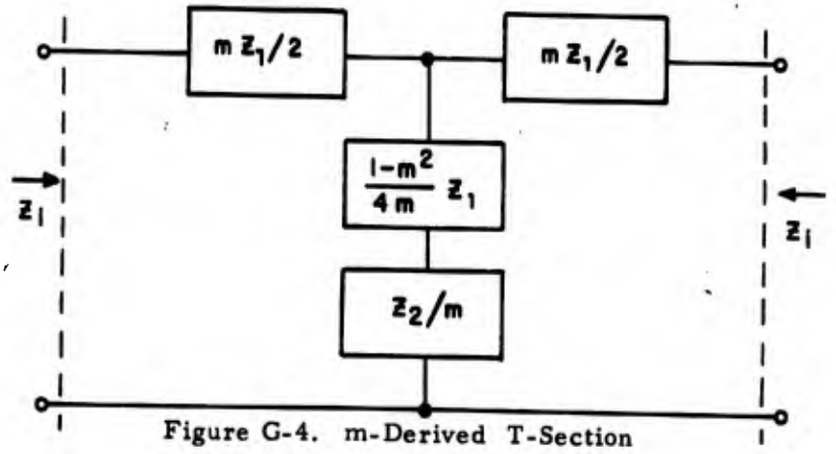

Figure G-4. m-Derived T-Section

The image impedance for this section is the same as that of the constant-k section, equation (G-1).

A distributed amplifier is made up of the above structures in the form of lowpass filters for which the respective constant-k and m-derived sections are shown in figures G-5 and G-6.

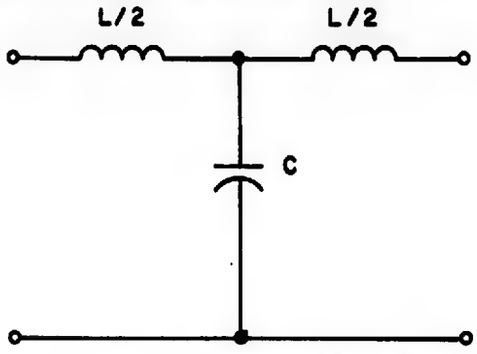

Figure G-5. Low Pass Constant-k T-Section

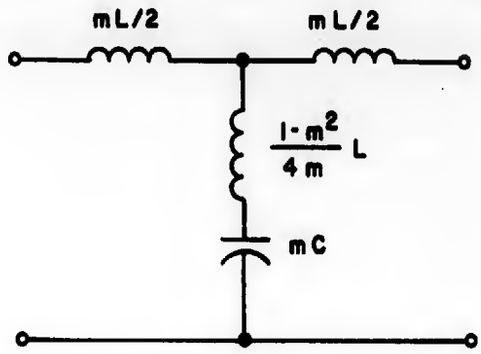

Figure G-6. Low Pass m-Derived T-Section

The image impedance for either section can be found by substitution in equation (G-1).

$$Z_i = \sqrt{L/C - \frac{\omega^2 L^2}{4}} \qquad \text{(G-2)}$$

One of the characteristics of a lumped line made up of lowpass sections is a cutoff frequency above which there is no transmission. This can be seen from equation (G-2) where the term under the radial goes to zero when $\omega = \frac{2}{LC} = \omega_c$.

$$f_c = \frac{\omega_c}{2\pi} = \frac{1}{\pi\sqrt{LC}} \qquad \text{(G-3)}$$

$$Z_i = L/C \sqrt{1 - \left(\frac{f}{f_c}\right)^2} \qquad \text{(G-4)}$$

The propagation of a signal wave down a delay line composed of lowpass sections is determined by the phase factor β, assuming no dissipative loss, and is defined by

$$\cos\beta = 1 + \frac{Z_1}{2Z_2} \qquad \text{(G-5)}$$

The above analysis, equations (G-1) through (G-5), holds for both constant-k and m-derived sections and either could be inserted interchangeably in a lumped line without affecting the image impedance. However, m-derived sections have definite advantages over constant-k sections for the approximation of a smooth line. Smooth lines can be approximated even more closely by the use of more complicated section structures such as those encountered in filter network theory.

The use of m-derived sections improves the performance of the line and the line termination near the cutoff frequency. The time delay is defined as the phase factor divided by the angular frequency:

$$t_d = \frac{\beta}{\omega} \tag{G-6}$$

Substitute the values of the m-derived filter from figures (G-5) and (G-6) in equation (G-5), expressing the frequency in terms of the cutoff frequency f_c. Hence:

$$\cos \beta = 1 - \left(\frac{2m^2 (f/f_c)^2}{1 - (1 - m^2)(f/f_c)^2} \right) \tag{G-7}$$

For comparison the constant-k expression, where m = 1, reduces to:

$$\cos \beta = 1 - 2 \left(\frac{f}{f_c}\right)^2 \tag{G-8}$$

In both cases for a low frequency normalized to the cutoff frequency (f/f_c), $\beta = 0$ and therefore produces zero time delay for a single wave propagated down the line. However, as f approaches f_c, t_d varies with frequency and produces phase distortion in the signal. This distortion can be minimized by choosing a value of m which maintains the approximation $\cos \beta = 1$ close to f_c. The optimum value for m found from equations (G-6) and (G-7) is m = 1.27.

The termination of the lumped line approximates Z_i more closely near f_c when an m-derived section is used. One should first look at half of a T-section as shown in figure G-7.

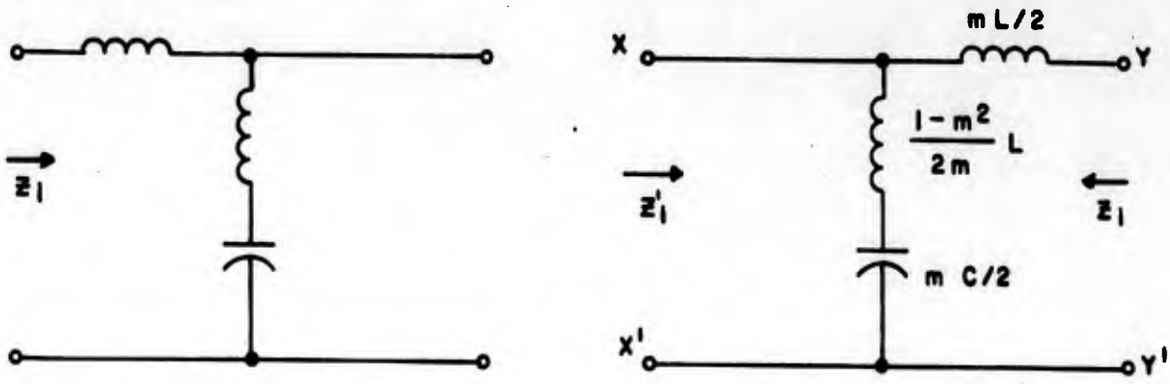

Figure G-7. 1/2 T-Section

The image impedance at terminals y - y' is Z_e as given in equation (G-4). The image impedance Z_2' at terminals x - x' is found to be:

$$Z_i' = \sqrt{L/C}\ \frac{1 - (1 - m^2)(f/f_c)^2}{\sqrt{1 - (f/f_c)^2}} \qquad \text{(G-9)}$$

For an approximation of the characteristic impedance $Z_o = L/C$ as f approaches f_c, the optimum value for m is found to be 0.6.

In the preceding discussion, we have considered the lumped delay line as being made up of an infinite number of sections extending in both directions. To terminate the line at a finite point, a resistor $R_o = L/C$ is placed at the terminals x - x' of the half section (figure G-7) so that the image impedance is matched to the approximation expressed in equation (G-9). The impedance Z_i at terminals y - y' is then the same as if a line infinitely long were connected to x - x'.

The lumped lines, both grid and plate, are built up of series inductances, shunt capacitances and resistive terminations. The inherent input (grid to ground) and output (plate to ground) capacitances form the shunt capacitances with trimmer

capacitors used for the adjustment of circuit capacitances to the desired values. The phase velocities of both the grid and plate lines must be equal, so the first design equation for the amplifier is:

$$V_p = \frac{1}{\sqrt{L_g C_g}} = \frac{1}{\sqrt{L_p C_p}} \qquad \text{(G-10)}$$

The characteristic impedances of the lines are,

$$Z_g = \sqrt{L_g / C_g} \qquad \text{(G-11)}$$

$$Z_p = \sqrt{L_p / C_p} \qquad \text{(G-12)}$$

which determine the resistance terminations,

$$R_g = \sqrt{L_g / C_g} \qquad \text{(G-13)}$$

$$R_p = \sqrt{L_p / C_p} \qquad \text{(G-14)}$$

Once the value of R_p is established, the gain of the amplifier may be determined from the low frequency equivalent circuit of n tubes in parallel with a load resistor of $R_p/2$. Hence the gain of an n section distributed amplifier is:

$$G_n = \frac{n g_m R_p}{2} \qquad \text{(G-15)}$$

The upper frequency limit of the amplifier is determined by the frequency at which the approximations of equations (G-4), (G-7) and (G-9) are still reasonable as f approaches f_c. A practical index is that the useful upper frequency limit is $0.65\, f_c$. From equations (G-3) and (G-10),

$$f_c = \frac{1}{\pi\sqrt{L_p C_p}} = \frac{1}{\pi\sqrt{L_g C_g}} = \frac{1}{\pi R_p C_p} = \frac{1}{\pi R_g C_g} \qquad \text{(G-16)}$$

Appendix H - Determination of M-Derived Sections

The m-derived section in figure H-1 is derived from the constant-k section, figure H-2, and is designed to have the same image impedance.

$$Z_i = L/C \; 1 - (f/f_c)^2 \tag{H-1}$$

where the cutoff frequency

$$f_c = \frac{1}{\pi LC} \tag{H-2}$$

For $f << f_c$

$$Z_i = L/C \tag{H-3}$$

The time delay in a lumped line is defined as the phase factor divided by the angular frequency:

$$t_d = \beta/\omega \tag{H-4}$$

where

$$\cos \beta = 1 - \frac{2 m^2 (f/f_c)^2}{1 - (1 - m^2) (f/f_c)^2} \tag{H-5}$$

Phase distortion can be minimized by choosing a value for m which maintains the approximation $\cos \beta = 1$ as f approaches f_c. Analysis of equation (H-5) shows that the optimum value for m is 1.27. The m-derived section takes the form shown in figure H-3 when the value m = 1.27 is substituted in the structure of figure H-1. The negative inductance required in the shunt arm of the section is produced by a center-tapped inductor with the proper degree of coupling between each half.

Consider the center-tapped inductor structure shown in figure H-4, where the total inductance between terminals X-Y is L'_T. If $L'/2$ is called the inductance of half the inductor coil looking at X-X' or Y-Y', the total inductance may be expressed as

$$L'_T = L' + m \tag{H-6}$$

or

$$L'_T = (L'/2 + M/2) + (L'/2 + m/2) \tag{H-7}$$

Where m is the mutual inductance of both halves of the coil. The structure can then be relabeled as in figure H-5 and an equivalent circuit drawn as in figure H-6.

The m-derived section with its negative inductance can be constructed if a center tapped coil is built to satisfy the specifications derived below.

$$\frac{0.635L}{2} = \frac{L'}{2} + \frac{m}{2} \quad \text{and} \quad -0.12L = \frac{-m}{2} \tag{H-8}$$

Solving these equations for L' and m

$$L' = 1.03L \text{ and } m = 0.24L \tag{H-9}$$

From equation (H-6):

$$L'_T = L' + m = 1.27L \tag{H-10}$$

The mutual inductance m is usually expressed in terms of a coupling coefficient K between the two coils.

$$K \equiv \frac{m/2}{\sqrt{(L'/2)(L'/2)}} = \frac{m}{L'} \tag{H-11}$$

The coupling coefficient for the two halves of the center tapped coil is

$$K = \frac{0.24L'}{1.03L'} = 0.233 \qquad \text{(H-12)}$$

After the total inductance is determined, standard formulas can be used to wind the inductors needed for the structure shown in figure H-3.

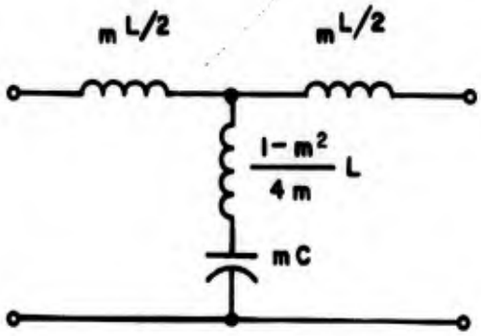

Figure H-1

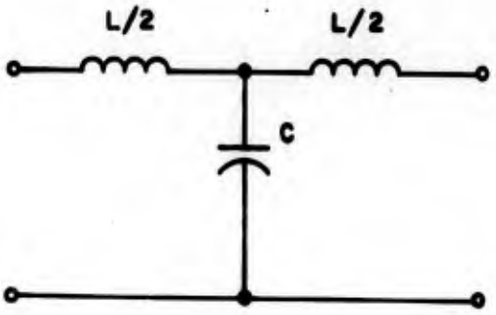

Figure H-2

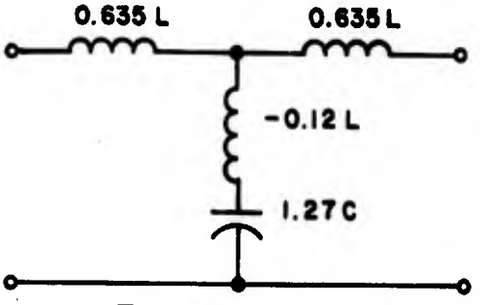

Figure H-3

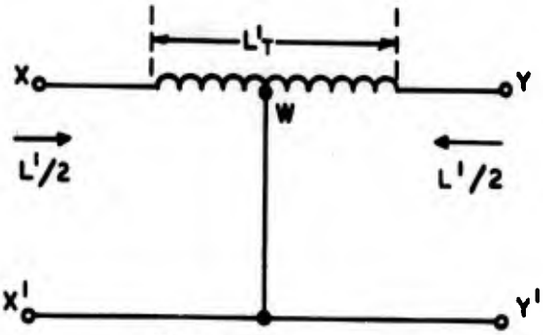

Figure H-4

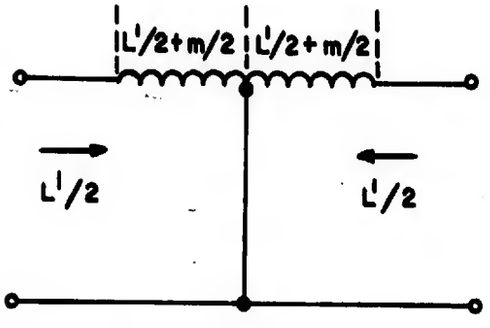

Figure H-5

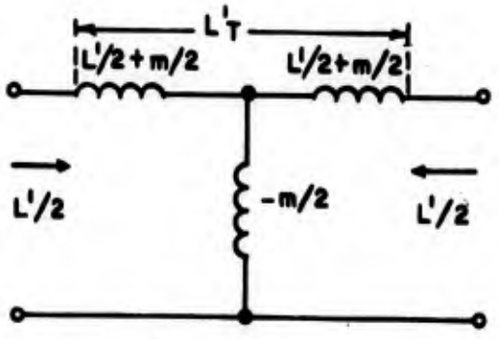

Figure H-6

Figures H-1 to H-6. Various T-Section Configurations

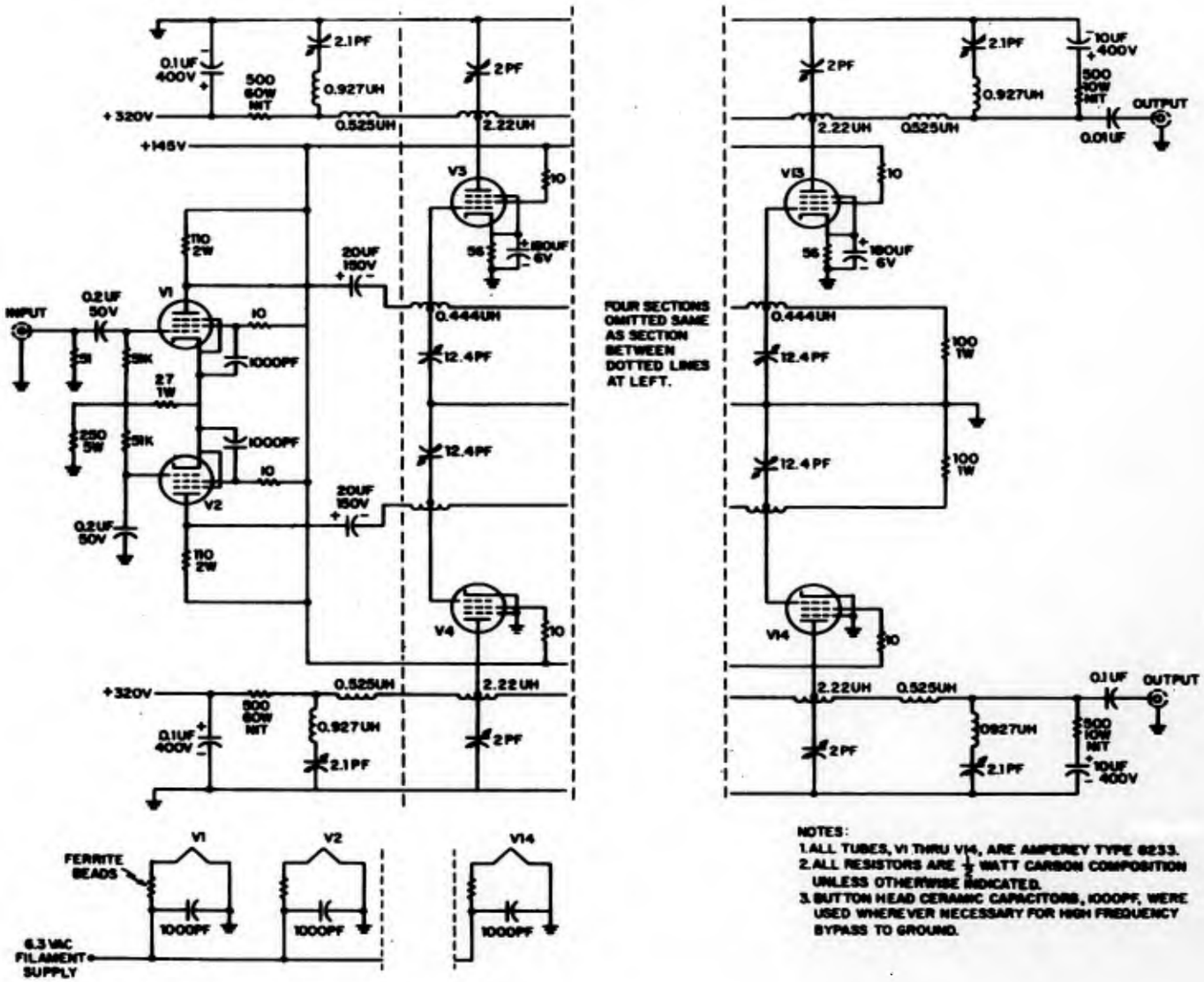

NOTES:
1. ALL TUBES, V1 THRU V14, ARE AMPEREY TYPE 6233.
2. ALL RESISTORS ARE ½ WATT CARBON COMPOSITION UNLESS OTHERWISE INDICATED.
3. BUTTON HEAD CERAMIC CAPACITORS, 1000PF, WERE USED WHEREVER NECESSARY FOR HIGH FREQUENCY BYPASS TO GROUND.

Schematic of Distributed Amplifier

UNCLASSIFIED